UNIVERSIDADE DE SÃO PAULO
INSTITUTO DE QUÍMICA

Programa de Pós-Graduação em Ciências Biológicas (Bioquímica)

PAULO NEWTON TONOLLI

Photosensitization of Lipofuscin in Skin Keratinocytes: Effects of Visible Light on Human Skin

Versão corrigida da Tese defendida

São Paulo

Data de depósito na SPG:

08/08/2018

PAULO NEWTON TONOLLI

Fotossensibilização de Lipofuscina em Queratinócitos da Pele Humana: Efeitos da Luz Visível na Pele

Tese apresentada ao Instituto de Química da Universidade de São Paulo para obtenção do Título de Doutor em Ciências (Bioquímica)

Orientador: Prof. Dr. Maurício da Silva Baptista

São Paulo
2018

Ficha Catalográfica elaborada eletronicamente pelo autor, utilizando o
programa desenvolvido pela Seção Técnica de Informática do ICMC/USP e
adaptado para a Divisão de Biblioteca e Documentação do Conjunto das Químicas da USP

Bibliotecária responsável pela orientação de catalogação da publicação:
Marlene Aparecida Vieira - CRB - 8/5562

T663p

Tonolli, Paulo Newton
Photosensitization of Lipofuscin in Skin Keratinocytes: Effects of Visible Light on Human Skin / Paulo Newton Tonolli. - São Paulo, 2018.
181 p.

Tese (doutorado) - Instituto de Química da Universidade de São Paulo. Departamento de Bioquímica.
Orientador: Baptista, Maurício da Silva

1. Visible light. 2. Lipofuscin. 3. Skin keratinocytes. 4. Lysosomes. 5. Mitochondria. I. T. II. Baptista, Maurício da Silva, orientador.

“There is no other species on the Earth that does science. It is, so far, entirely a human invention, evolved by natural selection in the cerebral cortex for one simple reason: it works. It is not perfect. It can be misused. It is only a tool. But it is by far the best tool we have, self-correcting, ongoing, and applicable to everything. It has two rules. First: there are no sacred truths; all assumptions must be critically examined; arguments from authority are worthless. Second: whatever is inconsistent with the facts must be discarded or revised. We must understand the Cosmos as it is and not confuse how it is with how we wish it to be.” (Carl Sagan, Cosmos)

Agradecimentos

Primeiramente, eu gostaria de agradecer a Deus por abençoar e proteger a minha vida, dando-me forças para superar os muitos desafios enfrentados, com sabedoria e capacidade.

Ao grande mestre e orientador, Prof. Dr. Maurício da Silva Baptista, pela oportunidade de realizar o doutorado no seu laboratório, pela confiança, ensinamentos, incentivo, e entusiasmo, além das grandes oportunidades proporcionadas nessa jornada. Sou muito grato pela evolução científica e conquistas obtidas sob sua orientação.

A todos os amigos, colegas e ex-colegas de laboratório, em especial à Dra. Helena Junqueira, Dr. Divinomar Severino, Dra. Carolina Santacruz, Prof. Dr. Orlando Chiarelli Neto, Profa. Dra. Waleska K. Martins, Ms. Aline Abrantes, Dra. Tayana Tsubone e Prof. Dr. Thiago Tasso, pelas ideias, apoios, discussões, ensinamentos, colaborações, as quais foram imprescindíveis ao trabalho e também para a minha evolução científica. Às técnicas Alessandra, Helena Junqueira, e ao Décio, bem como todos os membros (atuais e antigos) de treinamento técnico da FAPESP e auxiliares técnicos, por garantirem as melhores condições para a realização desse trabalho e ajudas diversas.

À Ms. Juliana de Carvalho Neves, amiga desde a graduação na UFSCar, pelos incentivos, apoios, e pela revisão do inglês da minha tese. Ao Dr. Jan Schlothauer pelas discussões, contribuições, e revisão do inglês desta tese.

Ao Prof. Dr. Il-Sei Watanabe, do Departamento de Anatomia, do Instituto de Ciências Biomédicas da USP, e a técnica Sônia Almeida, pela preparação e análise de amostras de microscopia eletrônica de transmissão (*Chapter 2* e *3*).

À minha mãe Miriam, pai Sebastião e irmã Joyce, pelos apoios diversos, incentivos, palavras de conforto, amor, e carinho. Por estarem sempre ao meu lado nos momentos que mais precisei. Saibam que sem vocês não estaria aqui hoje, alcançando mais esse sonho.

Aos amigos Gláucio, Vitor, e Iuri pelas inúmeras ajudas (científicas e não-científicas), pelos muitos momentos de diversão, risadas, e companhia dos almoços no bandeijão. Aos outros amigos pela companhia, auxílios, e momentos de descontração: Tiego, Joãozinho, Marcos Sulca, Paulo Pimenta, Hilário, Yuri, Leco, Giliard.

À Pamella Michetti, bem como aos seus pais, dona Rose e seu Olívio, pelo carinho, ajudas diversas, e companhia.

A todos os professores que participaram da minha formação acadêmica na Universidade Federal de São Carlos (UFSCar) e Universidade de São Paulo (USP). A todos os funcionários do IQ-USP e técnicos da Central Analítica (Ms. Adriana Matsukuma e Wilton Lima).

Às agências de financiamento de pesquisa: Conselho Nacional de Desenvolvimento Científico e Tecnológico (CNPq), Fundação de Amparo à Pesquisa do Estado de São Paulo (FAPESP), e Coordenação de Aperfeiçoamento de Pessoal de Nível Superior (Capes). Agradeço à Pró-Reitoria de Pós-Graduação da Universidade de São Paulo por financiar a minha participação como palestrante no *American Society for Photobiology Meeting 2018*.

A todos aqueles que de uma forma especial participaram da minha trajetória, científica ou não, e contribuíram para que eu chegasse até aqui.

RESUMO

Tonolli, P.N. **Fotossensibilização de Lipofuscina em Queratinócitos de Pele Humana: Efeitos da Luz Visível na Pele**. 2018. 181p. Tese – Programa de Pós-Graduação em Ciências Biológicas (Bioquímica). Instituto de Química, Universidade de São Paulo, São Paulo.

A lipofuscina é um pigmento autofluorescente acumulado progressivamente durante o envelhecimento celular em diversos tecidos, como o músculo cardíaco e retina, principalmente no período pós-mitótico. Esse fenômeno pode ocorrer em decorrência do estresse oxidativo, quando biomoléculas e organelas (principalmente mitocôndrias) sofrem danos, gerando produtos não degradáveis no interior dos lisossomos. A lipofuscina pode ser fotossensibilizada promovendo processos fotoxidativos nos componentes celulares. Muitos estudos de lipofuscina foram feitos em células do epitélio pigmentar da retina de olho humano, mas conhece-se muito pouco sobre a lipofuscina de pele humana. Neste trabalho nós investigamos a formação fotoinduzida (UVA e luz visível) de lipofuscina e as consequências da sua fotossensibilização pela luz visível. Nós também estabelecemos protocolos eficazes na indução de lipofuscinogênese, por meio de dano específico em mitocôndrias e lisossomos. Células que acumularam lipofuscina, após exposição à UVA ou luz azul, tornaram-se sensíveis à luz visível (400-750 nm). Caracterizamos as propriedades de absorção e de emissão da lipofuscina e seu tempo de vida de fluorescência, utilizando a microscopia de fluorescência resolvida no tempo (FLIM). Observamos que lipofuscina em queratinócitos tem máximo de absorção na região do azul (420-450 nm), com emissão máxima de fluorescência no vermelho. As células HaCaT carregadas com lipofuscina e

fotossensibilizadas no visível, tiveram redução da viabilidade celular, que foi relacionada com a geração de oxigênio singlete, bem como acumularam lesões pré-mutagênicas 8-oxo-dG e quebras na fita de DNA. Também, investigamos a eficiência de diferentes comprimentos de onda da luz visível (408, 466, 522 e 650 nm) em promover a formação de lipofuscina em consequência de lesões em mitocôndrias e lisossomos. Tanto a luz azul (408 e 466 nm) quanto a luz verde (522 nm), mas não vermelha (650 nm) promoveram dano em mitocôndrias (integridade de membrana e DNA) e lisossomos (integridade de membrana e atividade autofágica), induzindo eficientemente lipofuscinogênese. Logo, além de UVA, o próprio espectro do visível aumenta a sensibilidade de queratinócitos à luz visível, através da geração de lipofuscina. Por fim, testamos o potencial carcinogênico da luz azul de alta energia (408 nm), irradiando células HaCaT cronicamente. Identificamos quatro mudanças principais envolvidas com o processo de transformação maligna: instabilidade genômica, redução da expressão de proteína supressora de tumor p16INK^{4a}, aumento da taxa de proliferação, e resistência à apoptose. Além disso, a formação de dímeros de pirimidina ciclobutano (CPD) no DNA nuclear de células HaCaT logo após ou depois de vários ciclos de irradiação com 408 nm foi observada pela primeira vez na literatura.

Palavras-chave: lipofuscina, HaCaT, lisossomo, mitocôndria, transformação maligna, UVA, luz visível.

ABSTRACT

Tonolli, P.N. **Photosensitization of Lipofuscin in Skin Keratinocytes: Effect of Visible Light on Human Skin.** 2018. 181p. PhD Thesis – Graduate Program in Biochemistry. Instituto de Química, Universidade de São Paulo.

Lipofuscin is an autofluorescent pigment progressively accumulated during cellular aging, in several tissues, such as heart, muscle and retina, especially in the postmitotic period. That phenomenon may result from oxidative stress, when biomolecules and organelles (mainly mitochondria) are damaged, generating non-degradable products inside lysosomes. Lipofuscin can be photosensitized, promoting photoxidative processes in cellular components. Many studies on lipofuscin were made using the human retinal pigment epithelial cells, but very little is known about lipofuscin from human skin. In this work we investigated the photoinduced formation (UVA and visible light) of lipofuscin and the consequence of its photosensitization by visible light. We also established an efficient protocol for the induction of lipofuscinogenesis, through specific damage in mitochondria and lysosomes. Cells that accumulated lipofuscin, after exposure to UVA and blue light, became sensitive to visible light (400-750 nm). We characterized the absorption and fluorescence emission of lipofuscin, as well as its fluorescence lifetime through the time resolved fluorescence microscopy (FLIM). We observed that lipofuscin in keratinocytes has absorption maximum in the blue region of light spectrum (420-450 nm), and maximum emission in the red. When photosensitized at 466 nm, lipofuscin-loaded HaCaT cells had reduced cell viability, which was related with singlet oxygen generation, accumulated 8-oxo-dG premutagenic lesions and breaks in the DNA strand. Besides, we investigated the efficiency of different wavelengths

in visible light spectrum (408, 466, 522 and 650 nm) to promote lipofuscin formation due to damages in both mitochondria and lysosomes. Blue (408 and 466 nm) and green light (522 nm), but not red light (650 nm), promoted damage in mitochondria (membrane and DNA integrity) and lysosomes (membrane integrity and autophagic activity), effectively inducing lipofuscinogenesis. Thus, in addition to UVA, visible spectrum itself increases the sensitivity of keratinocytes to the visible light, through the generation of lipofuscin. Finally, we tested the carcinogenic potential of high-energy blue light (408 nm), by chronically irradiating HaCaT cells. For the first time in the literature, the formation of pyrimidine cyclobutane (CPD) dimers in the nuclear DNA of HaCaT cells was observed immediately or after several cycles of irradiation at 408 nm. We identified four major changes involved with the process of malignant transformation: genomic instability, decrease in the expression of tumor suppressor protein p16INK4a, increase in the proliferation rate and resistance to UVA-induced apoptosis.

Keywords: lipofuscin, HaCaT, lysosome, mitochondria, malignant transformation, UVA, visible light.

List of Acronyms and Abbreviations

ATP	Adenosine triphosphate
BrDU	5-bromo-2'-deoxyuridine
CPD	Cyclobutane pyrimidine dimers
DAPI	4',6-diamino-2-phenylindole
DCF	2',7'-dichlorofluorescein
DMEM	Dulbecco's Modified Eagle Medium
DMMB	1,9-Dimethyl methylene blue
DNA	Deoxyribonucleic acid
ELISA	Enzyme-Linked Immunosorbent Assay
HaCaT	Spontaneously immortalized human keratinocyte cell line
LED	Light Emitting Diode
FACS	Fluorescence-activated cell sorting
FCS	Forward scattering
FLIM	Fluorescence lifetime imaging microscopy
LTG	LysoTracker® Green
LTR	LysoTracker® Red
MTDR	MitoTracker® Deep Red
MTT	3-(4,5-Dimethylthiazol-2-yl)-2,5-Diphenyltetrazolium Bromide
NADH	Nicotinamide adenine dinucleotide
NADPH	Nicotinamide adenine dinucleotide phosphate
NHK	Primary normal human skin keratinocytes from neonatal foreskin
OTM	Olive Tail Moment
PBS	Phosphate-buffered saline
PCR	Polymerase chain reaction
TEM	Transmission Electron Microscopy
ROS	Reactive Oxygen Species
RPE	Retinal Pigment Epithelium cells
SBB	Sudan Black B
XL-PCR	Long extension polymerase chain reaction
$^1\Delta g\ O_2$	Singlet molecular oxygen

SUMMARY

Foreword

This PhD thesis has the generic goal of describing and elucidating the mechanisms by which visible light (400-750 nm) harms human skin keratinocytes, which are key players in the skin integrity and homeostasis, as well as, in the biological responses after the exposure of skin to sunlight. These goals demand an interdisciplinary investigative approach and the use of a relatively wide range of experimental systems, varying from the endogenous molecules that initially absorb UVA and visible light to the generation of new photosensitizing species, especially lipofuscin (the core of this work) in keratinocytes. In order to facilitate the reading of this thesis we organized it in six chapters, which are briefly described below. *Chapter 2* is published in the *Journal of Investigative Dermatology* (Tonolli et al. 2017) and the others are organized in order to facilitate their future publications as research articles in scientific journals. Below, we briefly describe each chapter:

Chapter 1 is the introduction, presenting a comprehensive review of the literature on human skin, interactions with sunlight, photosensitization reactions, photooxidative processes, generation of reactive oxygen species (ROS), lipofuscinogenesis, DNA lesions, mutations, and skin cancer.

Chapter 2 corresponds to the initial work in which this thesis was originated. The accumulation of lipofuscin, as well as its consequence to vision had been well studied in retinal pigment epithelial cells, but little was known on lipofuscinogenesis of skin cells, especially in epidermal cells. We demonstrated that UVA induces lipofuscinogenesis in HaCaT and primary normal human skin

keratinocytes, increasing the photosensivity, cytotoxicity and genotoxicity of visible light in these cells.

Chapter 3 describes an experimental model especially developed to allow efficient accumulation of lipofuscin in human keratinocytes cells. Selective and parallel damage in mitochondria and lysosomes by photosensitization of 1,9-Dimethyl-Methylene Blue (DMMB), simultaneously stimulates mitophagy and inhibits autophagy, allowing efficient accumulation of lipofuscin. By using this experimental model, we were able to characterize the important photochemical properties of epidermal lipofuscin, its sensitivity to blue light, and efficiency in inducing the DNA lesions.

Chapter 4 characterizes action spectra of visible spectrum in terms of damage in lysosomes and mitochondria, as well as to induce lipofuscinogenesis in keratinocytes. We have used classical measures of the organelles viability and level of lipofuscinogenesis and compared how these measures vary as a function of excitation wavelength (blue, green and red light).

Chapter 5 presents an experimental model of chronic exposure of HaCaT cells to blue light (408 nm) developed to evaluate the potential of this light to cause malignant transformation. Indeed, we observed several characteristics of malignant transformations in the cell populations that survived to sequential IC_{50} doses of blue light.

Chapter 6 brings the general conclusion of this thesis, gathering data from several chapters to propose a comprehensive view of the harmful effects of visible light on human skin keratinocytes. We also proposed several open questions to be answered in the future.

Chapter 1 – Introduction: Solar Radiation and Its Consequences to Human Skin

General Perspective

The sun is crucial for the existence and evolution of life on Earth. The absorption of photons by molecules naturally present in organisms and microorganisms, both in the vegetable and animal domains, makes the world the way it is today. Only one, but an important aspect, is that the human beings are progressively increasing the ability of using sun´s energy for biomass conversion, in processes such as artificial photosynthesis (House *et al.*, 2015). Another factor of equally crucial importance for life, as we know it, is the molecular oxygen (O_2). The coexistence of O_2 and excited state molecules, which are formed after light absorption, generates a powerful selective force, since the reactive oxygen species are produced and can damage the genetic information, leading to mutations – eventually permitting evolution.

On the other hand, the photoprotection – to maintain the genetic information - always had an important role for life, especially for human beings that are overexposed or even those less exposed to the sunlight. In spite of all the advances in terms of sun care technologies, still today, humans do not seem to understand the best way to interact with sunlight. Strategies are frequently imbalanced favoring either extreme avoidance or exaggerated sun exposition. This problem of people´s habits is the main justification for this work, which we hypothesize that exposure to visible light is the major factor that has been ignored in sun protection strategies. Indeed, we aim to elucidate the effects of visible light on human skin keratinocytes, mainly photooxidative

processes and carcinogenic potential. Besides, we studied a visible-light photosensitizer, the lipofuscin, which is generated after blockade of the autophagic flux induced by exposure to UVA and/or blue and green light (*Chapter 2* and *4*). This pigment has been further studied in the context of blindness diseases in eye tissues, but is poorly investigated in skin. This work exactly explores this gap, investigating the photochemical properties and photodamage promoted by photosensitization of human skin lipofuscin.

1.1. Solar Electromagnetic Radiation

The sunlight spectrum is divided into three main ranges: ultraviolet (100-400 nm), visible light (400-750 nm) and infrared (>800 nm). Ultraviolet is subdivided in UVC (100-280 nm), UVB (200-300 nm), and UVA (300-400 nm) (Figure 1.1). The portion of the electromagnetic spectrum capable of sensitizing the human eyes corresponds to the fraction called visible light. The classification of this range is solely based on eye photoreceptors, having little connection with other property of our body, such as skin.

Each one of the sunlight ranges has different contributions to total solar energy that reaches the Earth's surface (~ 1,000 W/m^2): 5% ultraviolet (only UVA and UVB, since the UVC is largely absorbed by ozone layer), 43% visible light, and 52% near-infrared (750-2500 nm) (Gunther, 2011).

Despite of the visible light and infrared representing the strongest output ranges of sun's total irradiance on the Earth's surface, few studies have been made regarding its effects on human skin cells (see section 1.3.2). In contrast, there is a lot of knowledge about the dangerous effects of UV range on the skin cells, which the sun care policies have prioritized (see section 1.3.2).

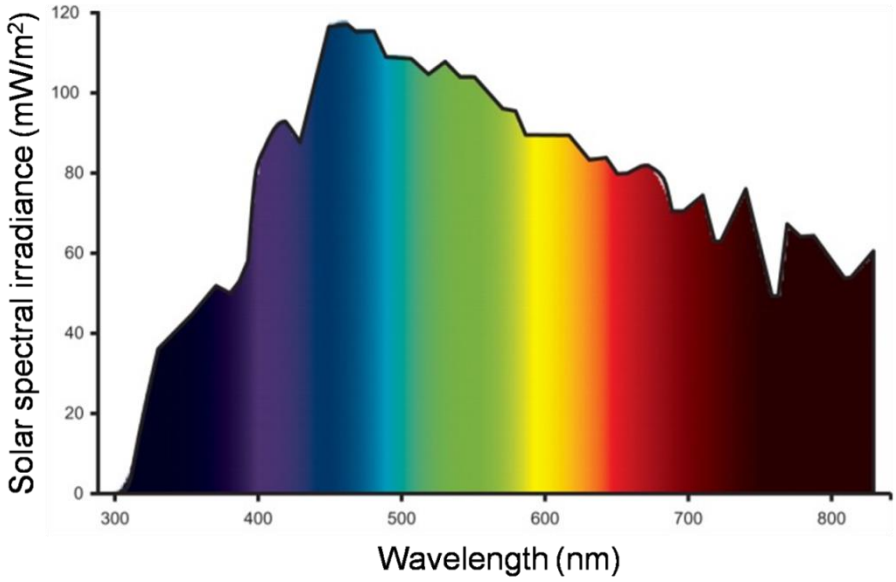

Figure 1.1. Sunlight spectrum measured at twelve noon, at 40ºN latitude, 20º incidence angle compared with zenith, 0.305 cm thickness of ozone layer. Image taken from Behar-Cohen et al. (2014).

1.2. Photosensitizers and Photosensitization Reactions

When a molecule is raised to its excited state it becomes unstable in relation to the initial (fundamental) state. If the excited molecule does not undergo a rearrangement or fragmentation, it will lose the absorbed energy, returning to its ground state. There are different ways for the molecule to return to the ground state: (i) the radiative processes, in which the excited state decays with the emission of electromagnetic radiation (phosphorescence or fluorescence) or (ii) the non-radiative processes, such as a loss of energy in the form of heat or suppression, which occurs when an excited molecule loses energy by interacting with another molecule (accepting part of the energy).

The Jablonski diagram (Figure 1.2) illustrates these radiative and non-radiative processes, as well as possible changes of spin multiplicity between the states and mechanisms of photosensitization (Noomnarm and Clegg, 2009). The ground, first and second electronic excited states are represented by S_0,

S_1, S_2, respectively. Among these electronic states there are sub-levels that represent vibrational and rotational states. For the triplet states (pair of electrons with parallel spin) the description is T_n, where n = 0 (only for molecules with a triplet ground state, such as oxygen), 1, 2, and so on. After the excitation of a molecule to the first excited singlet state (n > 1), the tendency is for it to undergo internal conversion de-excitation to the first excited singlet state. From this state there are three main possibilities: non-radiative decay (heat is released in the environment), fluorescence emission, and intersystem crossing, which allows its conversion to the triplet excited state. Unlike in internal conversion, in this route, there is a change of spin multiplicity, that is, from a singlet state to a triplet. In the triplet state with n > 1, the excited species tends to lose the excess energy by internal conversion, until it reaches T_1, and from there, it is deactivated by phosphorescence or by other energy transfer reactions.

Photosensitization is a process by which the excited molecule transfers its excitation energy to a neighboring molecule, thereby returning to the ground state. The molecule that absorbs the light and transfers its energy to others molecules is called the photosensitizer. In the context of biological systems, photosensitizers may be considered endogenous (porphyrins, bilirubin, chlorophyll, melanin) (Baier *et al.*, 2006) or exogenous (i.e., either from others organisms or synthetically developed) (Neumann *et al.*, 2005). During the photosensitization reaction, the photosensitizers can react with other molecules of their surroundings, through two main types of mechanisms: type I and type II (Abrahamse *et al.*, 2016).

In the type I reaction, the photosensitizer interacts directly with the substrate in an electron transfer reaction, producing radicals or radical-ions both in the photosensitizer and in the substrate (Agnez-Lima *et al.*, 2012). Although the electron transfer reaction can occur in any direction, most of the time the electron is transferred from the substrate to the photosensitizer, resulting in a cation radical substrate and an anion or semi-reduced radical of the photosensitizer. In the presence of oxygen, both radicals can react, generating oxidized products, or transferring electron to the molecular oxygen, forming the superoxide anion radical ($O_2^{\bullet-}$), regenerating the original photosensitizer in the ground state. Type I reactions are favored in some biological systems by the high concentration of possible target substrates, as well as by low oxygen concentration, disfavoring energy transfer from the triplet to the oxygen, which is called type II mechanism.

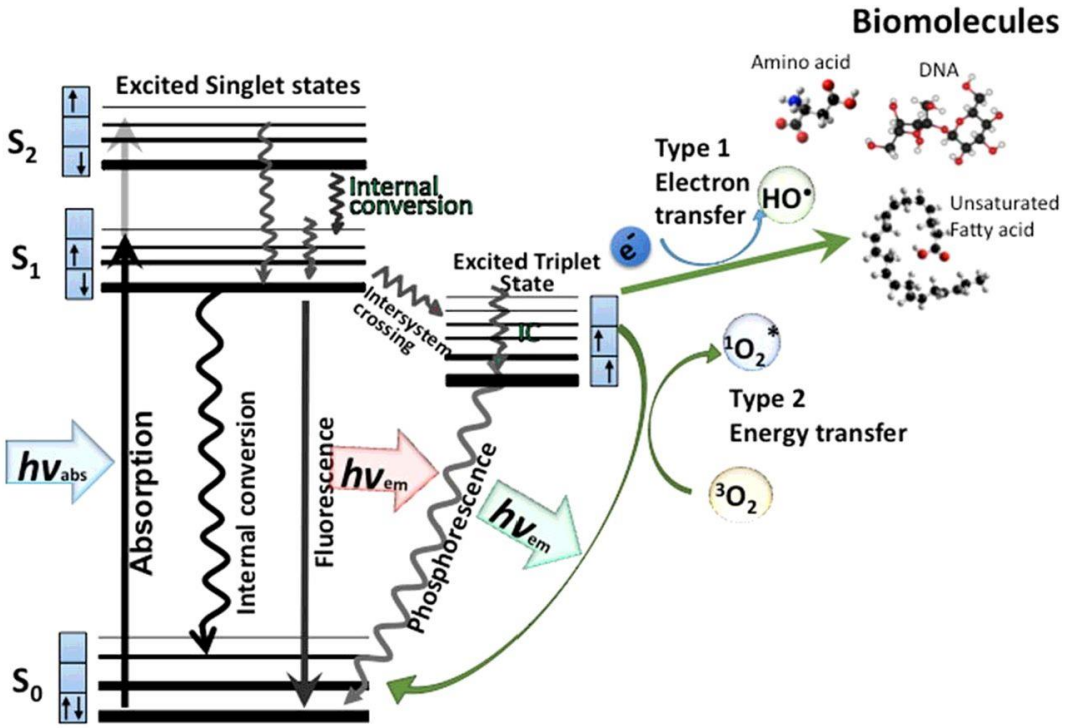

Figure 1.2. Jablonski diagram. Image taken from Abrahamse et al. (2016).

In the type II reaction, the photosensitizer reacts directly with the molecular oxygen (which has a triplet ground state) by energy transfer, raising the ground state to the singlet state of the molecular oxygen. While the photosensitizer is regenerated, returning to its ground state, the oxygen becomes highly reactive. In contrast to the triplet ground state, the excited singlet state offers an empty orbital, allowing oxygen addition to the double bond and, consequently, causing oxidation. In biological systems in oxygenated environments, the type II photosensitization reactions produce singlet oxygen, which reacts with biological substrates, such as proteins and lipids, located near the photosensitizer.

Singlet oxygen (the $^1\Delta g$ O_2 state, the singlet oxygen present in biological systems) is often generated from photosensitization reactions (type II mechanism), in which molecules (photosensitizers) absorb light energy raising into excited state, transferring the energy to adjacent O_2, and finally return to ground state (Halliwell & Gutteridge 2015). Recent works suggest that the singlet oxygen lifetime, inside the cell, is probably 0.5 µs or less, having a small diffusion distance within the cell (Kanofsky 2011; Hackbarth et al. 2010). The $^1\Delta g$ O_2 readily reacts with electron rich double bounds, attacking unsaturated lipids (as phospholipids in membranes), proteins, and DNA. Particularly in DNA, singlet oxygen attacks guanosine due to lower redox potential among all four bases, being the 8-oxodG the main product between singlet oxygen and DNA (Steenken and Jovanovic, 1997).

Human skin has an abundance of natural chromophores with high absorption in the UV and visible light spectrum: melanin and melanin precursors; flavin; NADH; NAPH; porphyrins; tryptophan in proteins;

carotenoids; lipofuscin; extracellular matrix proteins (keratin, collagen, elastin); hemoglobin (Besaratinia et al. 2007; Wondrak et al. 2006) (Figure 1.3). It has been proposed that photosensitization of endogenous chromophores in skin is involved with photoaging, DNA damage, mutations and skin cancer, through generation of reactive oxygen species, such as singlet oxygen, superoxide anion and hydroxyl radical (Liebel *et al.*, 2012).

However, this knowledge has been only partly used in new strategies of sun care products. For example, although the flavin compounds are well known to absorb UVA and visible light photons (Marian *et al.*, 2014), only protection against the UVA is being considered, ignoring the other ranges of the sunlight spectrum.

The disregard of the knowledge already available for sun care strategies is probably bringing disastrous consequences to society and individuals. For example, in spite of the massive campaigns to encourage the use of sunscreen in Australia, the rates of melanoma in this country continue to raise (Czarnecki, 2016).

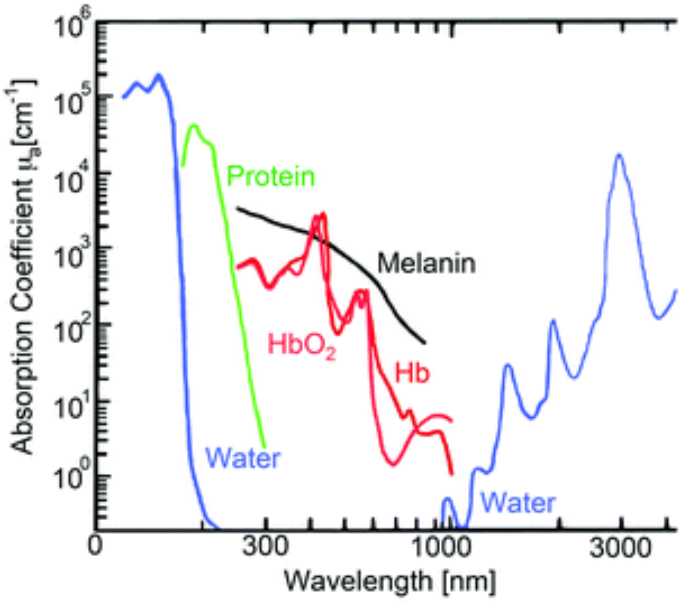

Figure 1.3. Absorption of typical components of human skin cells. Image taken from Shrestha et al. (2012).

1.3. Human Skin: Structure and Interactions with Solar Radiation

1.3.1. Structure of human skin

The skin is the largest organ of the human body and serves both physical and chemical barriers, protecting the organism from the external environment, being important for thermoregulation, preventing dehydration; vitamin D synthesis, and having both sensory and immunological surveillance function. The skin is composed of three layers: epidermis, dermis, and subcutaneous tissue.

The epidermis is the outermost layer of epithelial tissue, being stratified and composed by three major resident populations of cells: keratinocytes, melanocytes, and Langerhans cells (Eckert & Rorke 1989; Fuchs 1998). The organization of the epidermis comprises four layers, following the order from the innermost to the outermost layer: *stratum basale* (or *germinativum*), *stratum spinosum* (or *malpighii*), *stratum granulosum*, and *stratum corneum* (Figure 1.4).

The *stratum basale* is a single layer composed of proliferative columnar or cubical keratinocytes, which undergoes a continuous process of differentiation, migrating towards to outer layers (Eckert and Rorke, 1989). Keratinocytes in *stratum basale* express keratin K5 and K14, which cease to be expressed when these cells leave this layer (Eichner, Sun and Aebi, 1986). The keratinocyte differentiation is a sequential process dependent on a calcium gradient in epidermis (concentration increasing from *basal* to *granulosum* layer) (Bikle, Xie and Tu, 2012).

Melanocytes are located between cells of the basal layer, producing melanin and through their cytoplasmic prolongations (dendritic processes)

distributing the melanosomes (organelles that accumulate melanin granules) to the adjacent keratinocytes (Cichorek *et al.*, 2013).

The keratinocytes begin to differentiate in the *stratum spinosum*, synthesizing news sets of keratins (K1 and K10) and involucrin, establishing intercellular bridges (desmosomes), which connect one to another, and give a prickly appearance under the optic microscope (Eichner, Sun and Aebi, 1986). In the middle of this layer, there are the Langerhans cells, which are dendritic cells derived from brown bone marrow and with important role in immune protection of the skin and specialized in antigen presentation (Romani, Brunner and Stingl, 2012).

During maturation towards to the surface of the skin, the keratinocytes are continuously flattened, and their nuclei and cytoplasm are lost, acquiring a granular appearance due to the presence of electrondense keratohyalin granules, forming the layer called *stratum granulosum* (Steven *et al.*, 1990).

The last stage of keratinocyte maturation is in the *stratum corneum*, formed by non-viable hexagonal horn cells, called corneocytes, which are enveloped and filled by keratin. In the extracellular space of the corneocytes there are stacked lipid bilayers interspersed with layers of water (Ishida-Yamamoto and Iizuka, 1998). The function of the *stratum corneum* is to provide a physiologic barrier to chemical penetration and microbiologic invasion from environment, also preventing fluid and solute loss from epidermis (Elias and Choi, 2005).

Below the epidermis is the dermis, which consists of two layers: the papillary layer and the reticular layer. The papillary layer is connected to the epidermis, containing freely disposed thin collagen fibers, while in the reticular

layer, thick collagen fibers lie parallel to the epidermis. In addition, the dermis is composed of fibroblasts (which produce collagen), elastin and proteoglycans, as well as mast cells and macrophages. The dermis is vascularized, presenting cells and nerve fibers, lymphatic vessels, sweat glands, hair roots and a small amount of striated muscle. Located below the dermis is the hypodermis, or subcutaneous layer, composed of connective and adipose tissue, supporting epidermis and dermis, and important to body temperature regulation.

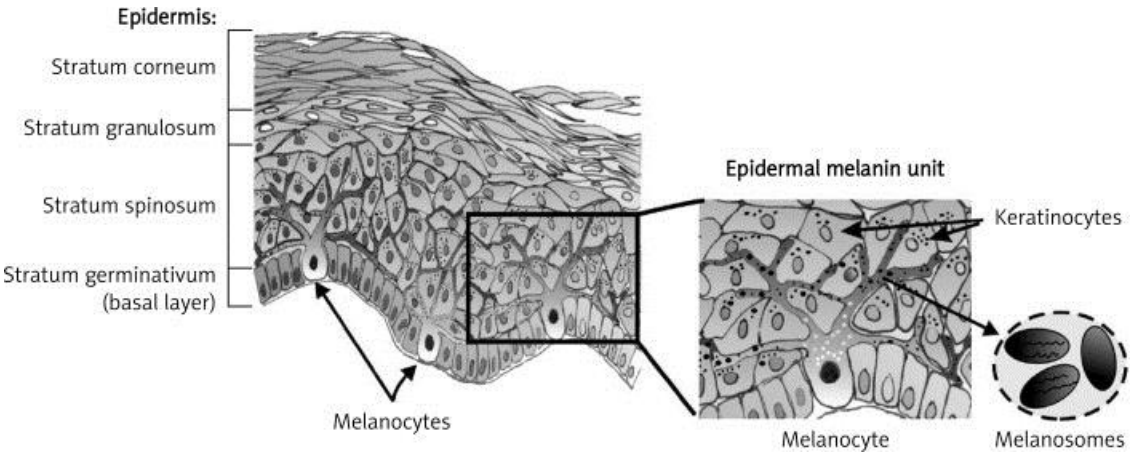

Figure 1.4. Diagram of the epidermis structure. Image taken from Cichorek et al. (2013).

1.3.2. Interaction of light with the skin and its cells

Light strikes and penetrates the skin daily, influencing its physiology in both beneficial and harmful ways, as has been extensively demonstrated for ultraviolet radiation (Pfeifer, 1997; Douki *et al.*, 2003; Mouret *et al.*, 2010; Pfeifer and Besaratinia, 2012). When the light reaches the skin, it can be absorbed, reflected, dispersed, and transmitted. Approximately 4-6% of the light incident on the epithelial tissue is reflected, due to the difference in the refractive index between the air and the surface of the skin, in the layer called the *stratum corneum* (Figure 1.5). The effect of dispersion is the scattering of light, limiting

the depth of tissue penetration. Dermal collagen is suggested as the main responsible for the dispersion of light in the skin. In relation to light transmission, this corresponds to a very small amount of the path light travels, depending on the type of skin (Everett *et al.*, 1966). Most of the photons cross the first layers of the epithelium and are absorbed by chromophores: carotenoids, oxy-/deoxyhemoglobin and, more significantly, by different types of melanin (Stamatas *et al.*, 2004).

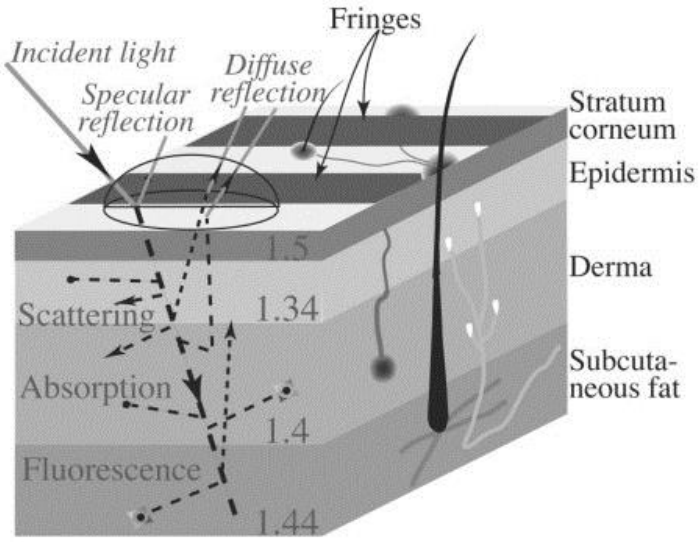

Figure 1.5. Interaction between skin and light. Image taken from Hanafi et al. (2005).

Human skin provides a physical barrier against the influences of the environment being essential for the maintenance and protection of the body. Humans and other animals protect themselves from the effects of UVB, mainly through the production of melanin, which are pigments that absorb light in the fraction of UV, visible and infrared in the electromagnetic spectrum.

An important benefit of interaction between sunlight and human skin is the vitamin D synthesis, performed mainly by the UVB radiation exposure (290-315 nm) (Holick, 2016). The vitamin D has multiple positive effects to human

health: calcium metabolism; bone health (Thacher, Fischer and Pettifor, 2014); regulation of gene expression involved in metabolic processes, DNA repair, cellular proliferation and differentiation (Montecino *et al.*, 2008).

Few studies have concerned the effect of the visible component of light on the skin. Recently, it is becoming evident that various wavelength ranges of visible light are capable of exerting biological effects on the skin, such as pigmentation, thermal damage, alteration in epithelial cell proliferation, oxidative damage triggered by the production of free radicals, causing indirect DNA damage through the generation of reactive oxygen species (Mahmoud *et al.*, 2008).

Experiments have shown that cancer cells (melanomas), containing increased amounts of melanin, accumulated twice as much DNA damage after irradiation with UVA as compared to those with low melanin content (Wood *et al.*, 2006). In a similar line of research, our group demonstrated that the DNA of these high melanin content cells also undergo oxidative damage when exposed to visible solar light, and that it was caused via the reactive oxygen species generated by melanin (Chiarelli-Neto *et al.*, 2014). Indeed, melanin clearly generates singlet oxygen after excitation with visible light and this generation is responsible for damages in the skin and hair irradiated with visible light (Chiarelli-Neto *et al.*, 2011).

These effects are largely due to absorption of radiation by photosensitizer molecules in the epithelial tissue. DNA damage can lead to mutations if the oxidative lesions are not corrected by the repair pathways. The accumulation of mutations may alter cell proliferation, triggering a tumor phenotype (Loeb, Loeb and Anderson, 2003). Otherwise, the use of visible light

components as in photodynamic therapy has proved to be very useful for treating skin diseases and skin tumors (Kim et al. 2015; Cohen & Lee 2016).

The visible range of the sunlight is the one that penetrates most deeply in the skin layers (Figure 1.6), thus, presenting a wide network of interactions with this tissue. Therefore, further studies are required to provide understandable data on the effects of visible light components on the skin.

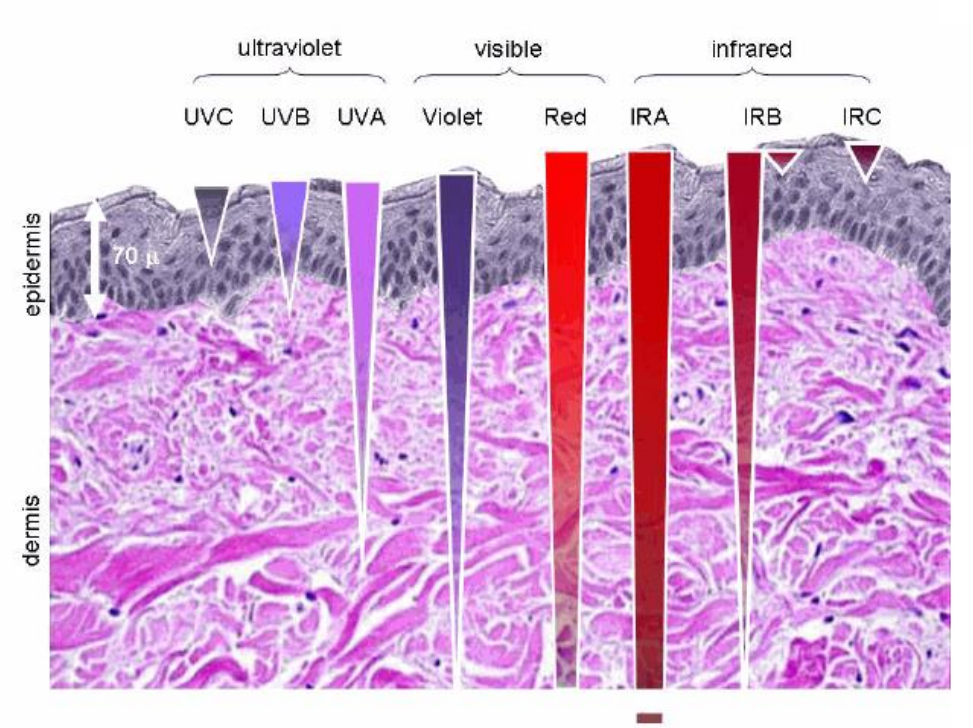

Figure 1.6. Penetration of different fractions of sunlight in human skin. Image taken from Scientific Commitee on Emerging and Newly Identified Health Risks. Health effects of artificial light. European Comission, 19th March 2012.

The skin undergoes daily exposure to oxidizing agents (cosmetics, industrial chemicals, air pollutants, UV radiation and visible light, among others). Particularly, the sunlight exposure is the major contributor to oxidative damage in skin cells, leading to photoaging and skin cancer.

Eukaryotic cells continuously produce reactive oxygen species (ROS) as a byproduct of electron transfer in the mitochondrial respiratory chain

(Kowaltowski *et al.*, 2009). The main ROS produced in the mitochondria is the superoxide radical ($O_2^{\bullet -}$), resulted from the monoeletronic reduction of O_2 at level of NADH dehydrogenase or coenzyme Q, during formation of semiquinone radical ($UQ^{\bullet -}$) (Turrens & Boveris 1980; Cadenas et al. 1977). $O_2^{\bullet -}$ shows low reactivity in aqueous solutions, unlike in hydrophobic environments, such as inside membranes, where $O_2^{\bullet -}$ can initiate the lipid peroxidation (topic 1.3.1), forming different types of radicals, including hydroxyl radical in presence of metals (see below).

Superoxide dismutase enzymes (SODs) are present in cytosol and intermembrane space as CuZnSOD, and in mitochondrial matrix as MnSOD. SODs efficiently remove $O_2^{\bullet -}$ reducing it to hydrogen peroxide (H_2O_2), which is a reactive specie with poor reactivity, but high diffusion within and between cells (Halliwell & Gutteridge 2015). Although, at high concentrations H_2O_2 can be cytotoxic, inhibiting, for example, glycolytic enzyme glyceraldehyde 3-phosphate dehydrogenase (Brodie and Reed, 1987). The most damaging effects of H_2O_2 occur when it reacts with iron, or other transition metal, such as copper, generating the hydroxyl radical ($OH^{\bullet}$) in the process called Fenton reaction (Weisiger & Fridovich 1973; Halliwell & Gutteridge 2015). Additionally, in skin exposed to sunlight, $OH^{\bullet}$ can be generated from homolytic fission of the O-O bond in H_2O_2 by UVB (Nishigori, Hattori and Toyokuni, 2004). The $OH^{\bullet}$ radical is highly reactive, reacting in a diffusion-controlled rate, and is responsible for most DNA damage (Cadet & Wagner, 2013; Dizdaroglu 2005). The main mechanism of $OH^{\bullet}$ reaction is its addition into a double bond in lipids, proteins, or DNA bases.

Under normal physiological conditions, the toxic effects of ROS can be avoided by the cellular antioxidant system, which involves enzymes (*e.g.*, superoxide dismutase, glutathione peroxidase, and catalase) or non-enzymatic antioxidants (*e.g.*, vitamin A, C, and E, glutathione). However, when ROS production becomes excessive and the balance between ROS production and antioxidant defense is disturbed, there is the so-called oxidative stress condition (Betteridge, 2000).

The DNA can undergo damage during oxidative stress condition, which may be measured as strand breakage and/or chemical modifications in bases and deoxyribose (Halliwell & Gutteridge 2015).

Cyclobutane pyrimidine dimers (CPD) and (6-4) pyrimidone photoproducts are the two major classes of DNA lesions induced by UVB (290 – 320 nm and UVC (190 – 290 nm) *via* direct absorption by DNA (Pfeifer, 1997; Rochette *et al.*, 2003). Besides, UVA (320 – 400 nm) also has been reported to induce CPD in rodent cells (Rochette *et al.*, 2003), HaCaT cells (Delinasios *et al.*, 2018), and murine and human melanocytes (Premi et al. 2015). However, UVA induces less direct damage to DNA than UVB and UVC (Agar *et al.*, 2004). The CPDs formed by UVA were reported by Douki et al. (2003) to occur more frequently between TT sites.

Studies have reported both direct and indirect mechanisms of CPD induction in skin cells by UVA (Kuluncsics et al. 1999; Premi et al. 2015; Mouret et al. 2010; Jiang et al. 2009; Schuch et al. 2009). According to Mouret et al. (2010) the direct absorption of UVA photons by DNA is dependent on the double-strand structure, increasing the capacity of absorbs this radiation. Still, the mechanism involved in the formation of CPDs by UVA is controversial.

CPD is a lesion formed by cyclobutane ring connecting 5,6 positions of two adjacent pyrimidine bases (Figure 1.7) and the most common lesion induced by sunlight, and formed at levels considerably higher than (6-4)PPs (Pfeifer & Besaratinia 2012; Pfeifer et al. 2005). (6-4)PPs are formed between 6 and 4 positions of two neighboring pyrimidines (Figure 1.7), especially at 5'-TC and 5'-CC sequence (Pfeifer et al. 2005).

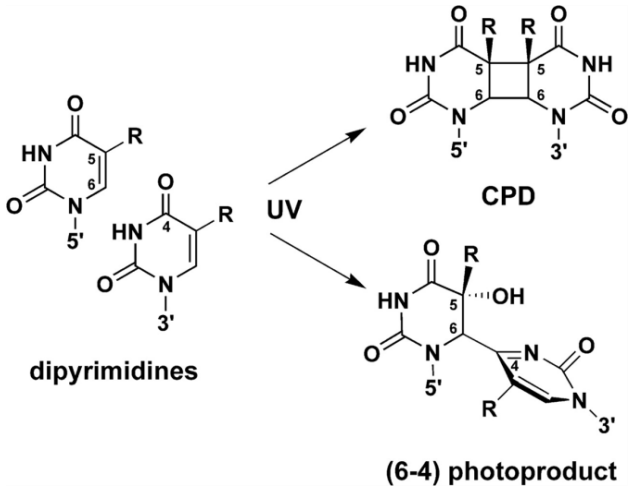

Figure 1.7. Structure of pyrimidine lesions induced by UV. Image from Li et al. (2006).

Others DNA lesions are those induced by oxidation reactions, initiated by photosensitization of molecules inside the cell (flavins, riboflavins, melanin, among others), which absorb the photon energy, reaching an excited state that can donate an electron (type I) or energy (type II) to others molecules and/or to molecular oxygen (O_2), generating singlet oxygen, which attack biomolecules, such as DNA (Besaratinia *et al.*, 2007).

The major product of DNA oxidation in cells is 8-oxo-dG (8-oxo-7-hydro-deoxyguanosine), which is a premutagenic modification, result of singlet oxygen insertion at C8 position in guanine (Figure 1.8), and accumulates during cell aging and oxidative stress (Agnez-Lima et al. 2012; Sies & Menck 1992).

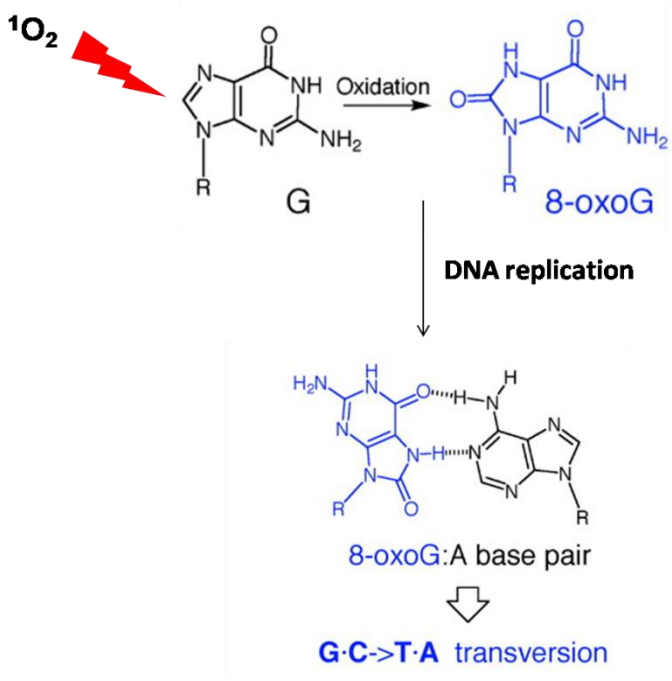

Figure 1.8. Generation of 8-oxo-dG after attacks of singlet oxygen on double bound involving carbon 8 in deoxyadenine. The consequence of this insertion, if do not repaired, is a transversion mutation G → T (see section 1.4). This image was adapted from Kino & Sugiyama (2001).

Hydroxyl radical (OH•), generated from the Fenton reaction, adds to double bounds in DNA bases and/or abstract a H atom from the methyl group and C-H bonds of 2'-deoxyribose (Evans, Dizdaroglu and Cooke, 2004). Besides the mismatch pairing, such as the FapyGua formed by hydroxyl radical insertion in guanine, which can lead to transversion GC→CG, the OH• can break the DNA strands. Strand breaks in DNA are highly mutagenic lesions, due to loss of genomic sequence, translocations, and chromosome rearrangements, which are formed when not repaired by non-homologous end joining or homologous recombination mechanisms (Rodgers and Mcvey, 2016).

1.4. Mutations and malignant transformation

Mutation is a change in one or more bases in the sequence of DNA, resulted from alterations in the DNA, as occurring due to oxidative stress, or rearrangement of the bonds between atoms, as photoproducts generated by exposure to UV radiation (Figure 1.9) (Brash, 2015). Insertions or deletions in DNA bases are also mutations, resulting in changes in the genetic sequence.

In the context of mutations induced by sunlight, the substitution mutations are most common (Pfeifer et al. 2005). The substitution mutations are of two types: (i) transition, interchanging purines (adenine to guanine, vice versa) or pyrimidines (cytosine to thymine, vice versa); or (ii) transversion, interchanging a purine for a pyrimidine base, or vice versa (Figure 1.9) (Guo *et al.*, 2017).

The major mutation generated by UV radiation, especially by UVC and UVB, is a transition mutation at dipyrimidine sequences containing cytosine, mainly at 5'-TCG and 5'-CCG. These mutations occur more frequently in some regions of genome (the hotspots), such as the CpG islands, methylated CpG sequences (where 5-methylcytosine is deaminated to thymine), forming transition mutations C to T (Figure 1.9), 5-methylcitosine to T, and CC to TT (Pfeifer & Besaratinia 2012; Pfeifer et al. 2005). The CpG islands (sequences with 1kb, on average, and rich in G+C composition) are usually found at the promoter region in housekeeping genes, especially in some tumor suppressor genes, such as P53, showing why these mutations are commonly associated with skin cancer (Deaton and Bird, 2011). According to Pfeifer et al. (2005), in human skin cancers, about 35% of all mutations in the p53 gene are transitions at 5'-TCG and 5'-CCG.

Besides, the UV radiation, mainly the UVA radiation, also forms transversion mutations: G to T, C to T, and T to G, occurring frequently under oxidative stress, where 8-oxo-dG is generated and can wrongly pair with adenine (A:T → C:G) (Figure 1.8) (Rochette et al. 2003; Pfeifer et al. 2005).

The mutations promoted by sunlight, even though including visible light, are usually assigned to UV spectrum. Unfortunately, the visible light is still considered innocuous to skin by a lot of professionals and companies working in sun care. In this thesis we will show that this is a big mistake. The transversion mutations can occur after exposure to visible light – according to we will show in *Chapters 2*, *3*, and *4* -, especially after exposition to blue light, due to excitation of endogenous photosensitizers (flavins, riboflavins, melanin, lipofuscin), generation of singlet oxygen, and formation of oxidative lesions in DNA, such as 8-oxo-dG.

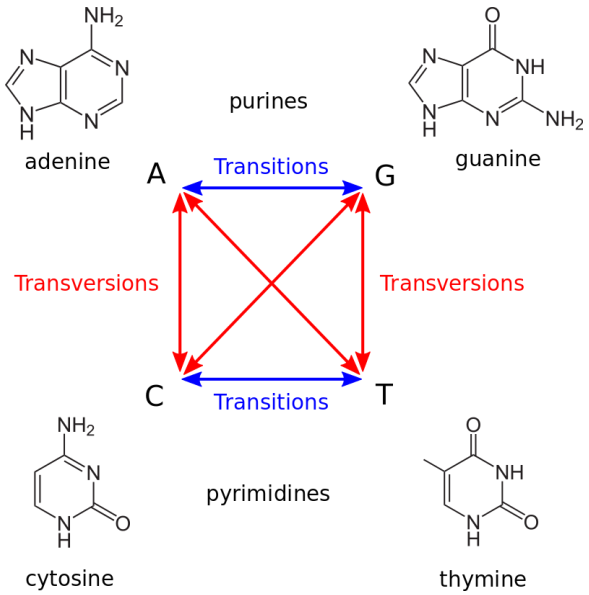

Figure 1.9. Types of substitution mutations: transition (blue line), which involves interchanging of one purine to another (A→ G or G → A) or one pyrimidine to another (C → T or T → C); and tranversion (red line) which involves the interchange between one purine to pyrimidine, and vice versa.

The malignant transformation is the process in which normal cells acquire properties of cancer cell (Stepanenko and Kavsan, 2012). Cancer cells have several distinct characteristics compared to normal cells, such as: immortalization (senescence deviation); evasion of apoptosis and growth suppression; reprogramming of energy metabolism; resistance to contact inhibition; genomic instability, angiogenesis; migration, invasion activation and metastasis (Lleonart, Artero-Castro and Kondoh, 2009; Hanahan and Weinberg, 2011).

Hanahan & Weinberg (2011) proposed the ten cancer hallmarks, revising and adding four new hallmarks to the six proposed in Hanahan & Weinberg (2000). These principles are fundamental to malignant transformation and are supposed to be the common traits to all types of cancer. They are as follows: self-sufficiency in the production of growth factors; insensitivity to anti-growth signaling; evasion of apoptosis; unlimited replicative potential; induction of angiogenesis; genomic instability and mutation; cellular energy deregulation; preventing immune destruction; tumor-inducing inflammation; activation of invasion and metastasis.

On the other hand, Hanahan & Weinberg's publications on hallmarks of cancer have been questioned by some authors (Floor *et al.*, 2012; Sonnenschein and Soto, 2013). Some of the critiques are:

- conclusions about hallmarks are made supposing equivalence on carcinogenesis process among cells in culture, genetically modified mice, and humans;
- the phenomenon called "transformation" has been considered indiscriminately in literature, considering some artifacts in cell culture

that mimic the expression of oncogenes, such as changes in serum concentration in the medium (Rubin, 2011);

- evasion of apoptosis as a hallmark of cancer should be revisited, since apoptosis, in an opposite way of its anti-cancer activity, could play a selective pressure on cells, eliminating less-fit clones and benefiting better clones, favoring the cancer progression (Labi and Erlacher, 2015);
- energy metabolism in carcinogenesis is historically defined as glycolytic. However, the Warburg effect is not always present in cancer cells. According to Sonnenschein & Soto (2011), cancer and normal cells have quantitative differences, not qualitative, metabolizing more of a substrate or increasing the signaling pathway in cancer cells compared to normal cells. Besides, these quantitative differences show plasticity (can change), which are not exclusive of cancer cells;
- the absence of one fundamental characteristic of cancer cells among the hallmarks: the loss of cell differentiation (structural organization and specialized function) (Floor *et al.*, 2012);

Still, the hallmarks of cancer can be an useful framework to organize the wide knowledge of cancer biology, synthesizing the characteristics to be acquired by cells to be considered cancerous within a population of cells.

The incidence of skin cancer, both melanoma and non-melanoma (NMSC), has been increasing worldwide, showing an epidemiological trend, mainly in white population (Apalla *et al.*, 2017).

Non-melanoma skin cancer, which involves the keratinocytes, represents one-third of all cancer occurrences in the United States, 80% of which are basal cell carcinoma (BCC) and 20% are squamous cell carcinoma (SCC), having an incidence even twenty times higher than melanoma, which is a skin cancer developed from melanocytes, the cells that synthesize melanin (Eide *et al.*, 2010).

The ultraviolet radiation exposure is the major environmental factor related to skin cancer (de Gruijl, 1999). Historically, UVB was considered the biggest villain for skin health, gathering the wide attention for the sun care industry, due to UVB photons that are absorbed directly by DNA, forming pyrimidine dimers. However, UVA can also be directly absorbed by DNA (Mouret *et al.*, 2010), or even indirectly, generating high mutagenic CPDs lesions. So, both UVA and UVB are involved with skin carcinogenesis. As showed above, UVA penetrates deeper in skin than UVB, reaching the melanocytes layer, being the main radiation involved with induction of melanoma. UVB is important for development for NMSC and melanoma in a lower scale compared to UVA (Rigel, 2008).

Besides, the action mechanism of UVA is different from UVB, where UVA is able to photosensitizing endogenous molecules inside the cells, resulting in oxidative stress, reaching the dermis and destroying collagen, leading to skin aging (Battie *et al.*, 2014).

Here, we studied the potential of visible light to induce transformation in skin cells, since the recent evidences that visible light has similar photooxidative mechanisms to UVA, damaging nuclear DNA in skin cells (Chiarelli-Neto *et al.*, 2014).

1.5. Autophagy and the mitochondrial-lysosomal axis: Theory of Aging

Autophagy is an important lysosomal mechanism for maintenance of cell homeostasis, as well for cell survival and degradation/recycling of cytoplasmic components, such as proteins and organelles. Autophagy is a conserved process, present in all cells at low level in basal conditions, being upregulated during starvation, hypoxia or oxidative stress (Filomeni, De Zio and Cecconi, 2015).

There are three types of autophagic mechanisms: chaperone-mediated autophagy, microautophagy and macroautophagy, which is the most common autophagic mechanism of cells (Figure 1.10).

The chaperone-mediated autophagy involves the direct translocation of proteins, in cytoplasm, across the lysosome membrane complexed with chaperones, which recognize the lysosomal membrane receptor LAMP-2A (lysosomal-associated membrane protein 2A), leading to unfolding and degradation of damaged protein (Cuervo and Wong, 2014).

Microautophagy is the direct engulfment of cytoplasmic content into lysosomes by invagination of lysosome membrane, showing important role in degradation promoted by lysosomes (Li, Li and Bao, 2012).

Macroautophagy involves the isolation and encompassing of cytoplasmic content to be degraded (damaged biomolecules and organelles) in a phagophore, a flat double-membrane structure, which expands through the incorporation of lipids and finally seals, forming the vesicles called autophagosomes, which fuse with lysosome to form autolysosome (or autophagolysosome) (Bernard and Klionsky, 2013). After degradation, breakdown products are released into the cytosol for recycling of the

biomolecules, generating energy under starvation, and protecting cells against oxidative stress (Feng *et al.*, 2014).

When the autophagosome is being formed, the cytoplasmic LC3-I (microtubule-associated protein light chain 3) is converted to isoform LC3-II (or LC3-PE), which is covalently bound to phosphatidylethanolamine (PE), and considered as a marker of autophagic process, since LC3-II is associated to membranes of autophagic vesicles and autophagosomes (Klionsky *et al.*, 2008).

Brunk & Terman (2002a) proposed a theory of aging based on involvement of mitochondria and lysosomes, which show alterations and misfunctions in senescent cells and cells under oxidative stress.

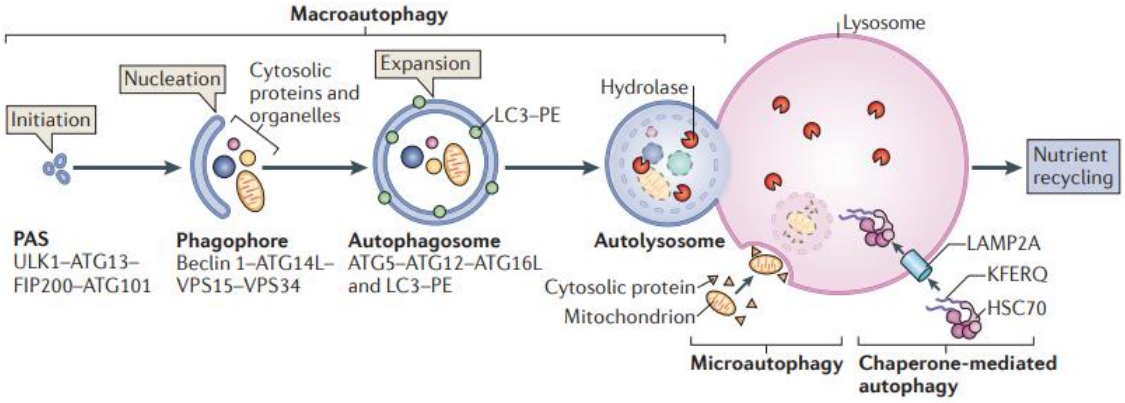

Figure 1.10. Autophagy pathways. Macroautophagy initiates with phagophore (PAS) formation, nucleation, elongation and conjugation of phosphatidylethanolamine (PE) to LC3, forming LC3-PE (or LC3-II). Autophagosome fuse to lysosome, forming autolysosome. Microautophagy is directly engulfed by lysosomes membranes. In chaperone-mediated autophagy substrates are labeled with KFERQ peptide (lysine-phenylalanine-glutamate-arginin-glutamine), recognized by heat shock cognate 70kDa (HSC70) chaperone and across the membrane, dependently of LAMP2A. Image taken from Kaur & Debnath (2015).

Mitochondria are the major source of ROS and the main target for the attack by free radicals, accumulating damage during aging. In aged cells, specifically in postmitotic cells, aged mitochondria show low production of ATP

and elevated generation of superoxide and hydrogen peroxide, establishing an oxidative stress condition (Brunk and Terman, 2002b).

Additionally, the lysosomes are involved in the autophagy mechanism, digesting damaged biomolecules and organelles inside the cells, as well the endocytosed material (from outside the cell), having an important role in turnover of biomolecules and organelles. However, during aging and oxidative stress, many oxidized molecules and damaged organelles accumulate inside the cells, and consequently in lysosomes. In these circumstances, lipofuscin ends up accumulating inside the lysosomes (Figure 1.11), preventing normal lysosomal activity, increasing the generation of ROS, decreasing ATP production of the cells, and limiting recycling of mitochondria and organelles. Therefore, damage in lysosomes and mitochondria can lead to a functional decay and cell death, mainly in postmitotic cells.

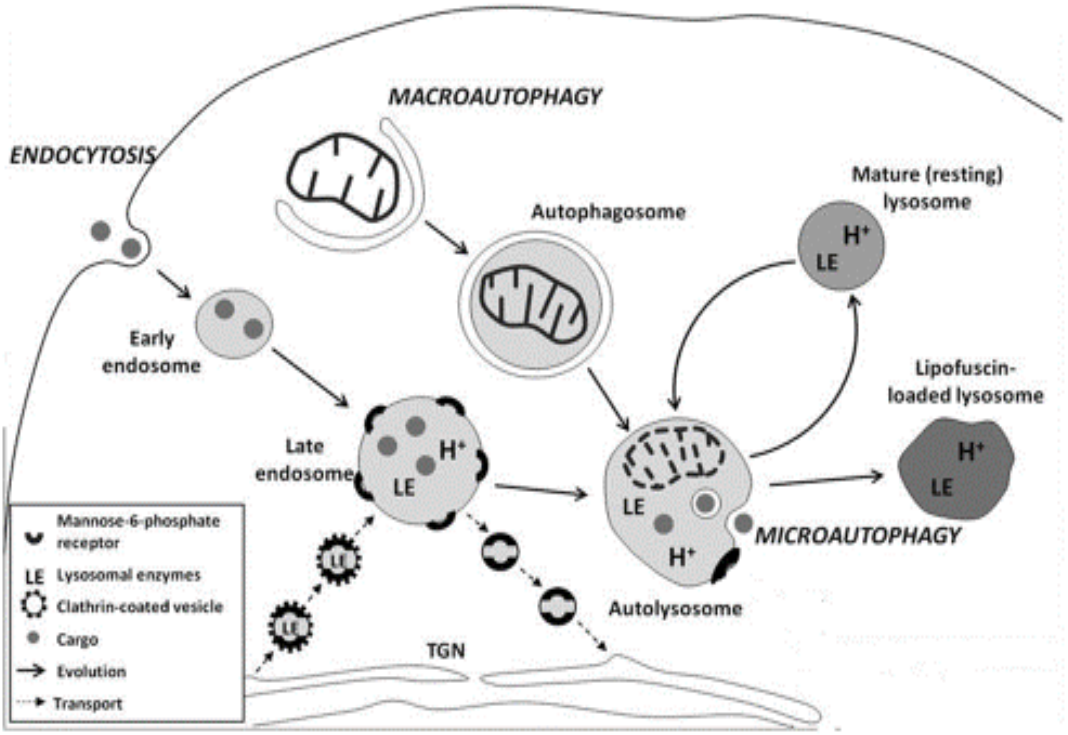

Figure 1.11. Diagram summarizing the formation of lipofuscin in lysosomes. The damaged biomolecules and organelles, especially mitochondria, accumulate inside the lysosomes forming lipofuscin, during aging in postmitotic cells. Lysosomal enzymes (LE) cannot digest lipofuscin Image taken from Brunk & Terman (2002).

1.6. Lipofuscin and Lipofuscinogenesis

The term lipofuscin (from Greek, *lipo* = fat, from Latin, *fucus* = dark) was coined by Borst (1922), although the pigment was first described by Hannover (1842) in nerve cells, which reported the accumulation of a granular material in cytoplasm. Koneff (1886) observed the relation between this pigment and aging in the nervous system.

Lipofuscin is a yellowish-brown, fluorescent (Figure 1.11), and strongly oxidized pigment with different structure and composition for each cell type, usually consisting of damaged membranes, proteins (30-70%) and lipids (20-50%), also containing carbohydrates (7%) and metals (2%), including transition metals (Fe, Cu, Zn, Mn) (Jung et al. 2010; Höhn et al. 2010; Skoczyńska et al. 2017; Brunk & Terman 2002; Terman et al. 2006).

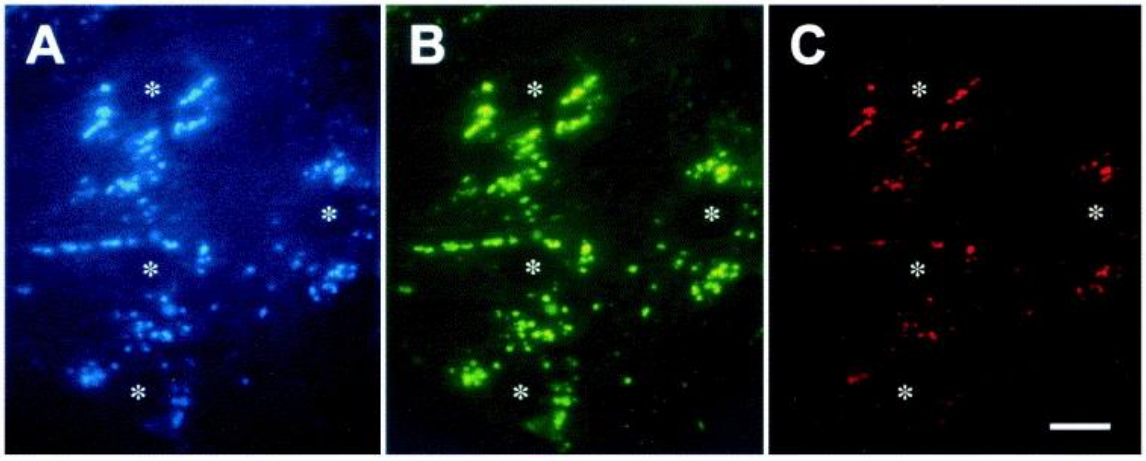

Figure 1.12. Autofluorescence from lipofuscin granules in neonatal rat cardiac myocytes (3 months). (A) excitation in UV (330–380 nm), emission LP 420 nm; (B) excitation in blue (450–490 nm), emission LP 520 nm; (C) excitation in green (510–560 nm), emission 590 nm. Asterisks = nuclei. Scale bar = 10 μm. Image taken from Brunk & Terman (2002).

The fluorescent properties of lipofuscin, when excited with ultraviolet or blue light are suggested to occur due to the Schiff bases in its structure, generated from reaction between carbonyls (aldehydes formed from lipid

peroxidation) and amino compounds from proteins (Figure 1.13) (Boulton *et al.*, 1990; Santos *et al.*, 2011).

Thus, lipofuscinogenesis is a process that occurs mainly through lipid peroxidation, resulted from the attack of hydroxyl radical or other oxidizing species on lipids. The generation of this radical occurs in the lysosome lumen, through the Fenton reaction that takes place between the hydrogen peroxide and the iron accumulated inside the lysosomes (Brunk et al. 1992).

The accumulation of lipofuscin occurs progressively with age in post-mitotic cells of humans and animals. The rate of lipofuscinogenesis is subject to functional characteristics of cells and lysosomes, depending on the rate of autophagocytosis and/or endocytosis of materials rich in phospholipids and proteins; of the degradation efficiency of this material; of the degree of lipid peroxidation in the lysosome; and the cellular capacity of exocytosis of non-degradable residues (Brunk et al. 1992).

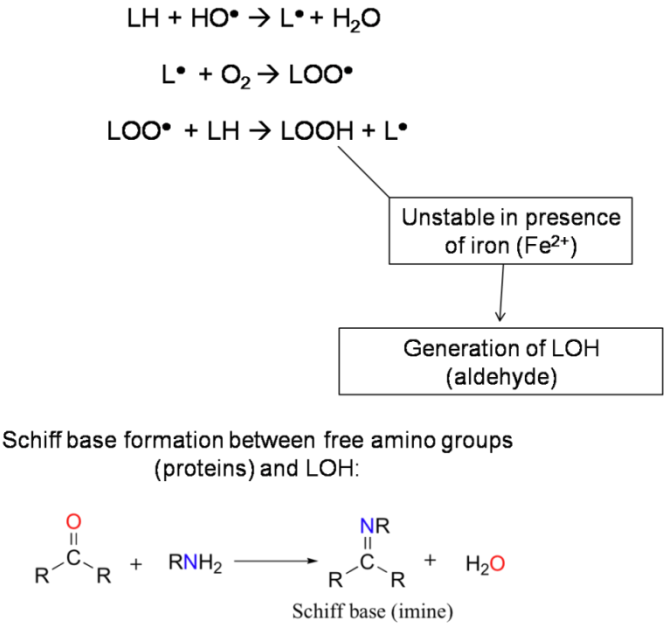

Figure 1.13. Formation of Schiff bases between aldehydes and amino groups of proteins. Hydroperoxides (LOOH), generated by propagation of HO• attack in lipids (LH), is quite unstable in presence of iron, resulting in formation of aldehydes (LOH). LOH reacts with free amino groups within proteins, forming Schiff bases.

Lysosomal hydrolases cannot digest lipofuscin which, then, progressively accumulates inside the secondary lysosomes as electrondense granules around the nucleus (Terman, Abrahamsson and Brunk, 1999). Moreover, the main characteristic of lipofuscin is its ability to inhibit the degradation of oxidized proteins by competitive binding to proteolytic enzymes, including 20S proteasome and lysosomal proteases, and thus, autocatalyzing its formation (Höhn, König and Grune, 2013).

Lipofuscin granules can incorporate transition metals, such as iron and copper, catalyzing the Fenton reaction, which generates the hydroxyl radical, a highly reactive oxygen species that attack DNA, protein and lipids (Hohn et al., 2010).

The main source of iron in the lipofuscin composition comes from damaged mitochondria, which have many iron-sulfur centers in their enzymatic complexes. Iron in the lysosomes, in presence of hydrogen peroxide, generated by dismutation of superoxide anion, leads to the peroxidation of cargo in autophagosomes, accelerating the generation the lipofuscin (Figure 1.14).

It is supposed that differences in fluorescence of lipofuscin from different cell types are due to variances in bio-amines (Yin, 1996). The cellular composition of the lipids and the protein change among the different cell types assigns different photochemical properties to the lipofuscin.

Many studies have investigated the properties and photochemistry of lipofuscin in retinal pigment epithelium (RPE) cells (Boulton et al., 1990; Reszka et al., 1995; Eldred and Katz, 1988; Eldred et al., 1982; Rózanowska et al., 1998). RPE is a tissue known to accumulate brown and autofluorescent granules, which lead to macular degeneration and loss of vision during old age

(Crouch et al., 2015). The main cause of macular degeneration is an increasing oxidative stress induced by photosensitization of these lipofuscin granules, since lipofuscin of RPE cells has absorption peaks in the ultraviolet range (280-330 nm) with emission in 570-605 nm (Eldred and Katz, 1988; Eldred et al., 1982) and also absorbs blue light (λ= 420 nm), generating singlet oxygen (Rózanowska et al., 1998).

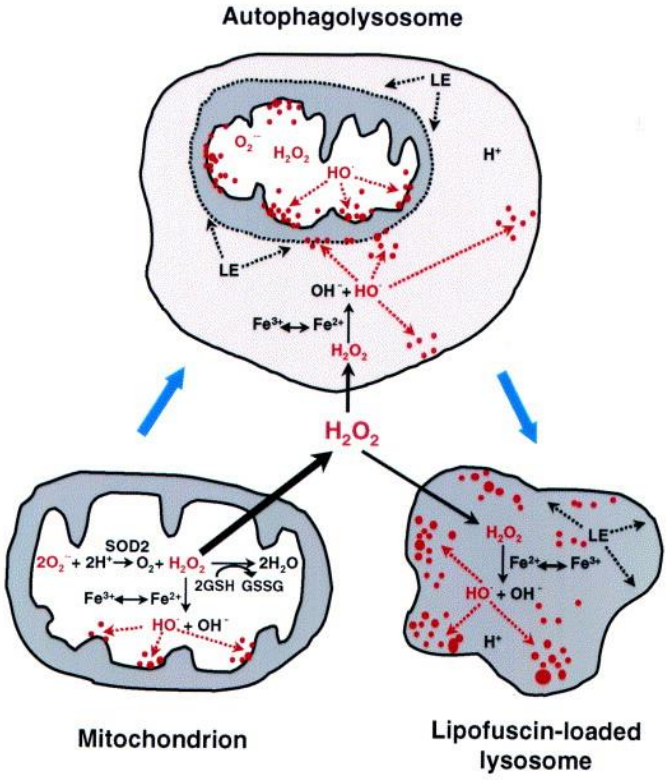

Figure 1.14. Damaged mitochondria accumulated inside the lysosomes during cell aging and oxidative stress, increases the iron concentration in the lysosomal lumen. Hydrogen peroxide, formed by dismutation of superoxide anion in mitochondrial matrix, can cross the biological membranes, and inside the lysosomes in the presence of iron, promote lipid peroxidation through attack of hydroxyl radical, forming lipofuscin.

Some studies have reported that lipofuscin can also be photosensitized by visible light, in fibroblasts and keratinocytes, inducing phototoxic processes through the generation of reactive oxygen species, such as superoxide radical,

hydroxyl radical (HO•), and singlet oxygen (Godley et al., 2005; Tonolli et al. 2017).

Objectives

General objective

This work aims to explore on how visible light can be dangerous to human skin cells, particularly to keratinocytes, via photosensitization of endogenous biomolecules, inducing the oxidative processes, the premutagenic lesions in nuclear DNA, and establishing a potential to malignant transformation in these cells. The target photosensitizer studied in this thesis is the lipofuscin, which is a powerful visible-photosensitizer and a subproduct of the oxidative stress, such as the induced under exposure to UVA radiation and, probably, to the visible light.

Specific objectives of each chapter

- **Chapter 2 - Lipofuscin Generated by UVA Radiation Turns Keratinocytes Sensitive to Visible Light**: Human skin keratinocytes (HaCaT and NHK cells) exposed to UVA accumulated lipofuscin, a powerful visible-photosensitizer, increasing the photosensitivity of these cells to visible light.

- **Chapter 3 - An Experimental Model for Studying Lipofuscin from Human Skin Keratinocytes:** Using photosensitization of DMMB, a phenothiazine dye that accumulates specifically in mitochondria and lysosomes, we induced parallel damage in those organelles, leading to the

lipofuscinogenesis in HaCaT cells, and establishing an experimental model to investigate properties of keratinocyte lipofuscin.

- **Chapter 4 - Visible Light (408 - 650 nm) and Level of the Damage on Lysosomes and Mitochondria:** Using LED arrays with peak emission wavelengths at 408, 466, 522, and 650 nm, we investigated the effects of different regions of the visible spectrum on mitochondria and lysosomes of HaCaT cells, and then evaluated the ability of these wavelengths to induce lipofuscinogenesis.

- **Chapter 5 – HaCaT Cells Chronically Irradiated with Blue-light Acquired Resistance to UVA Radiation:** Here, we intended to test the potential carcinogenic effect of high-energy blue light (peak at 408 nm), irradiating HaCaT cells chronically (three times a week) with a significant physiological dose of this light. Several characteristic properties of cancer cells were tested to evaluate the level of cellular transformation.

Chapter 2 - Lipofuscin Generated by UVA Radiation Turns Keratinocytes Sensitive to Visible Light

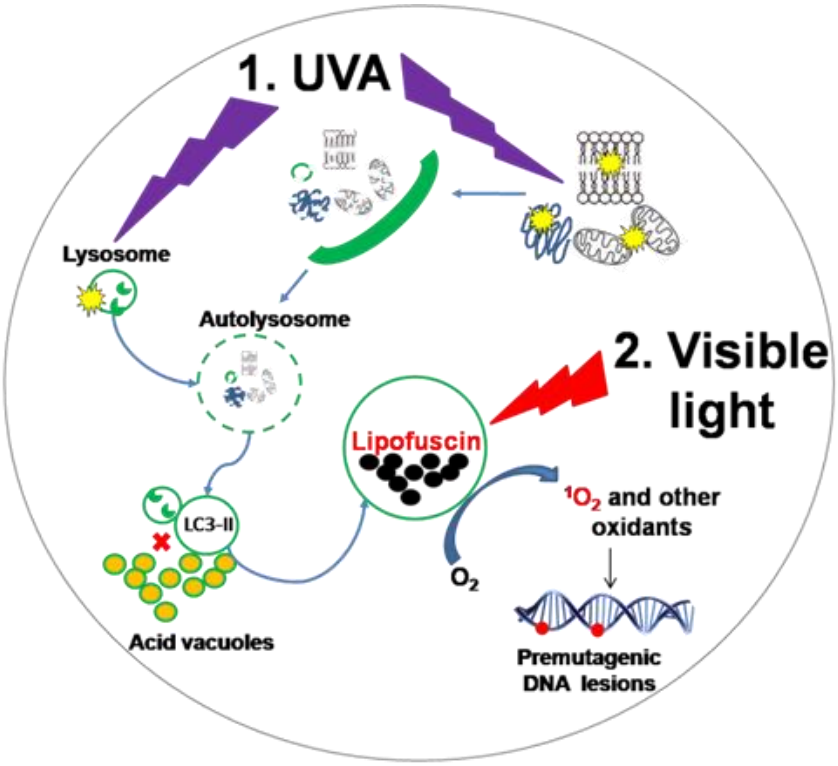

Human skin keratinocytes exposed to UVA radiation, at relevant physiological dose, accumulate lipofuscin, a subproduct of oxidative damage and a hallmark of cell aging, turning cells sensitive to visible light, decreasing cell viability and damaging DNA. It is a clear evidence of a synergic effect between UVA radiation and visible light in induction of skin aging and, probably, in carcinogenesis.

This chapter was published in the *Journal of Investigative Dermatology* (Tonolli et al. 2017) and reprinted here with minor changes. The co-authors of this paper were *Dr. Orlando Chiarelli-Neto, Dr. Carolina Santacruz-Perez, Dr. Helena Couto Junqueira, Prof. Dr. Ii-Sei Watanabe, Dr. Felipe Ravagnani, Prof. Dr. Waleska Kerllen Martins, and Prof. Dr. Mauricio S Baptista.*

Our society still faces challenges in the field of sun care. For instance, despite the massive campaign to promote the use of sunscreen in Australia, the rates of melanoma of Australians continue to raise (Czarnecki, 2016). Some studies point to the fact that exposition to solar wavelengths other than ultraviolet (UV) also affects human skin (Schieke, Schroeder and Krutmann, 2003; Mahmoud *et al.*, 2010; Chiarelli-Neto *et al.*, 2014). We report here the combined damaging effects of UVA and visible light in immortalized human epidermal keratinocytes (HaCaT) and in Normal Human Primary Epidermal Keratinocytes isolated from Neonatal Foreskin (NHK). We aim to prove that UVA stimulates the accumulation of the age-pigment lipofuscin, which then acts as a potent visible-light photosensitizer.

Harmful effects caused by UV radiation to eukaryotic cells have been thoroughly described (Ziegler *et al.*, 1994). Both tested cell lines experienced decrease in cell viability under increasing UVA doses, with NHK being more susceptible than HaCaT (Figure S2.1). Besides the usual mechanisms of cell death, UVA causes lysosomal damage and inhibits autophagy (Lamore & Wondrak 2012; Lamore & Wondrak 2013).

Autophagy inhibition results in accumulation of lipofuscin (Brunk and Terman, 2002b; Terman *et al.*, 2010), which is a heterogeneous polymer made of oxidized biomolecules and traces of metals. Lipofuscin has intense light absorption extending to the red portion of the visible spectrum (up to ~550 nm). Its presence has been correlated with deleterious effects of solar exposition in the eyes, but its role in skin phototoxicity has not been described (Haralampus-Grynaviski *et al.*, 2003; Gray and Woulfe, 2005; Schweitzer, Hammer and Schweitzer, 2005a).

Transmission electron microscopy (TEM), Sudan black B staining and time-resolved fluorescence measurements (Figure 2.1 a-h) (Figure S2.2-S2.6) show a considerable lipofuscin accumulation in both NHK and HaCaT cell lines 48 hours after irradiation with UVA. The percentage of cells presenting fluorescence above 640 nm increased from 6% in the control to 38% in cells pretreated with UVA (Figure S2.2). The fluorescence lifetime obtained from lipofuscin granules was around 1.7 ns (Figure 2.1 f), which is in agreement with previous reports (Schweitzer, Hammer and Schweitzer, 2005b). The lipofuscinogenesis pattern was also observed in HaCaT cells upon addition of chloroquine (Figure 2.1 h), which is a classical autophagy inhibitor. This pattern was successfully inhibited by deferiprone (Figure 2.1 g), an iron chelator known to prevent formation of lipofuscin (Brunk and Terman, 2002b). There is also a clear dose-dependent increase in lipofuscin accumulation in HaCaT and NHK cells treated with UVA (Figure S2.4, S2.5).

Lipofuscin acts as a photosensitizer, absorbing visible light and generating considerable amounts of triplet species and singlet oxygen (Rózanowska *et al.*, 1998), which can in turn induce photooxidation (Chiarelli-Neto *et al.*, 2011, 2014). In fact, we observed an increase in DCF oxidation after exposing UVA-irradiated HaCaT (Figure 2.1 i) and NHK (Figure S2.7) cells to visible light. HaCaT cells that received a 12 $J.cm^{-2}$ UVA dose showed the characteristic singlet oxygen emission (centered in 1270 nm), which was present neither in the dark control nor in visible light-irradiated cells (Figure 2.1 j). The emission at 1270 nm has decay within the expected range of singlet oxygen lifetime (~1µs) (Chiarelli-Neto *et al.*, 2011).

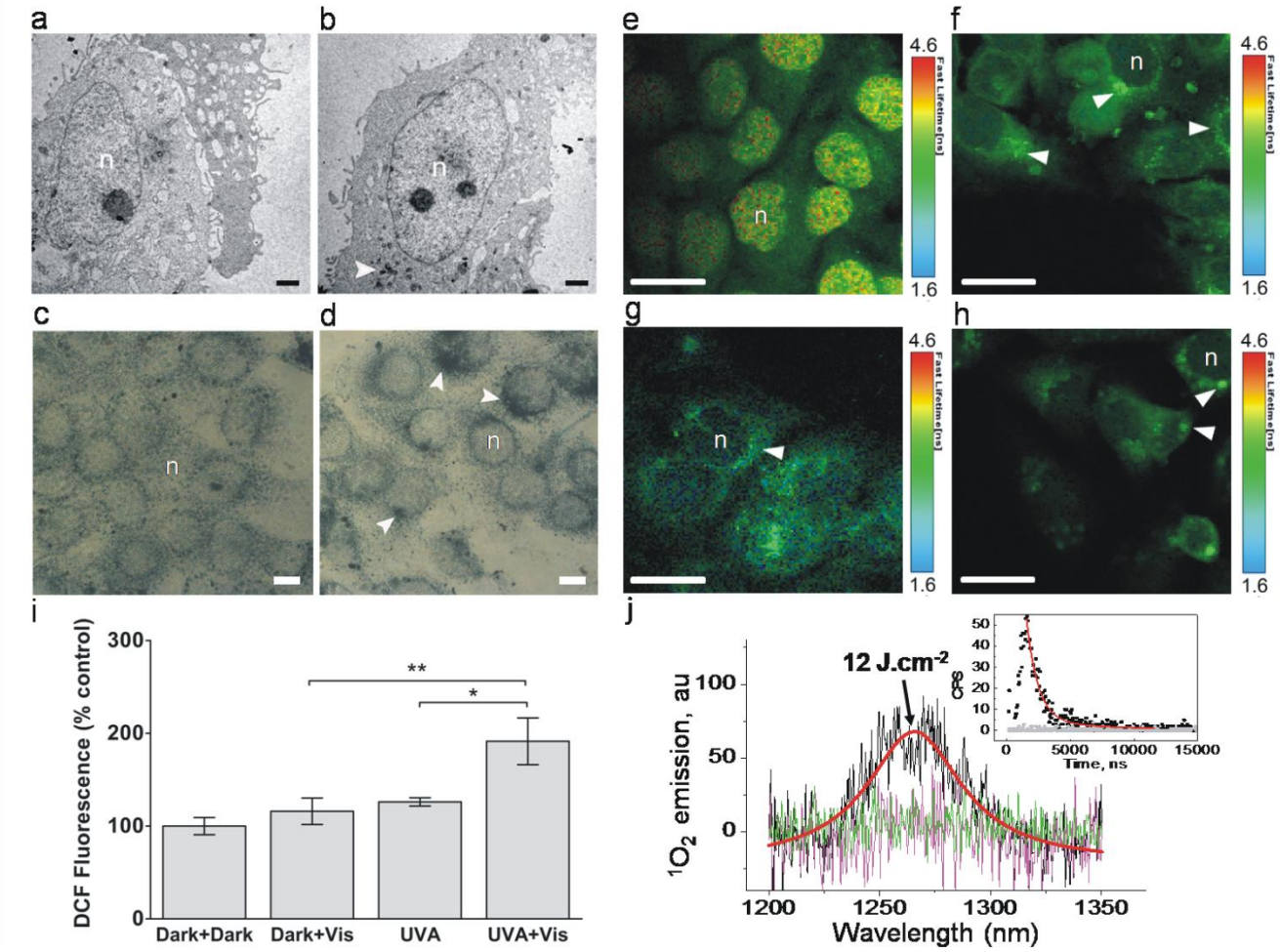

Figure 2.1. UVA (12 J.cm^{-2}) induces the accumulation of lipofuscin that acts as a visible-light photosensitizer in HaCaT cells. Transmission electron microscopy of cells left in the Dark **(a)** and 48 hours after UVA **(b);** arrow shows lipofuscin granules around nucleus (n). Sudan Black B staining of dark control **(c)** after UVA **(d)**. Fluorescence Lifetime Images of dark control **(e),** after UVA **(f)**, after UVA in the presence of 30 µM deferiprone **(g)**, 48 hours after treatment with 60 µM of chloroquine **(h).** Dichlorofluorescein (DCF) emission (λ_{exc}= 485 nm and λ_{emi}> 510 nm) in cells treated with 2′,7′-Dichlorofluorescin diacetate (DCFDA) after protocols mentioned in the picture **(i)**.$^1O_2$ emission at 1270 nm by control cells (green), irradiated with visible light (pink) and with UVA (black) **(h)**.

Both NHK and HaCaT cells were irradiated with 36 J.cm^{-2} of visible light 48 h after UVA (12 J.cm^{-2}). Note that visible light becomes a lot more toxic to cells previously treated with UVA (Figure 2.2 a-b). Consequently, keratinocytes become photosensitive to visible light when they are pre-exposed to UVA. Additional controls prove the role of lipofuscin in this increased toxicity with respect to visible light.

As shown in Figure 2.1 g and Figure 2.1 h, respectively, formation of lipofuscin is avoided by chelating intracellular iron or, alternatively, can be induced by chloroquine treatment. Indeed, the toxicity of visible light increased for cells previously treated with chloroquine (even though they had not been previously exposed to UVA), while cells treated with deferiprone no longer showed increased visible light phototoxicity (even though they had been previously exposed to UVA) (Figure S2.8).

In addition to the substantial decrease in cell viability, a considerable increasing in DNA strand break was observed in HaCaT cells that were treated with both UVA and visible light (Figure 2.2 c). Although photodamage can have multiple intracellular targets, we selected for this study direct oxidation of nuclear DNA in lipofuscin-accumulating cells exposed to visible light. After treating double-irradiated cells (subdoses of UVA and visible light were used) with enzymes that recognize oxidation DNA lesions (Figure 2.2 d-g), a clear increase in the Olive Tail Moment was observed, indicating the presence of premutagenic Fpg and Endo III-sensitive DNA lesions (Figure 2.2 h-i). Consequently, cell death *per se* is not the only consequence of the synergistic action of UVA and visible light. A more dangerous consequence is the accumulation of premutagenic DNA lesions. The observed Fpg/Endo III ratio was close to 1:1 (compare Figure 2.2 h with 2.2 i). Fpg recognizes mainly singlet oxygen oxidation products, i.e. 8-oxo-7,8-dihydroguanine, while Endo III recognizes strand breaks, abasic sites and additional oxidative pyrimidine modifications (Hatahet *et al.*, 1994). An oxidation process driven only by singlet oxygen should provide a larger ratio of Fpg- to Endo III-sensitive modifications. Therefore, our results suggest that the oxidative damage in DNA is likely to

involve not only singlet oxygen but also radical-based reactions (Chiarelli-Neto *et al.*, 2014).

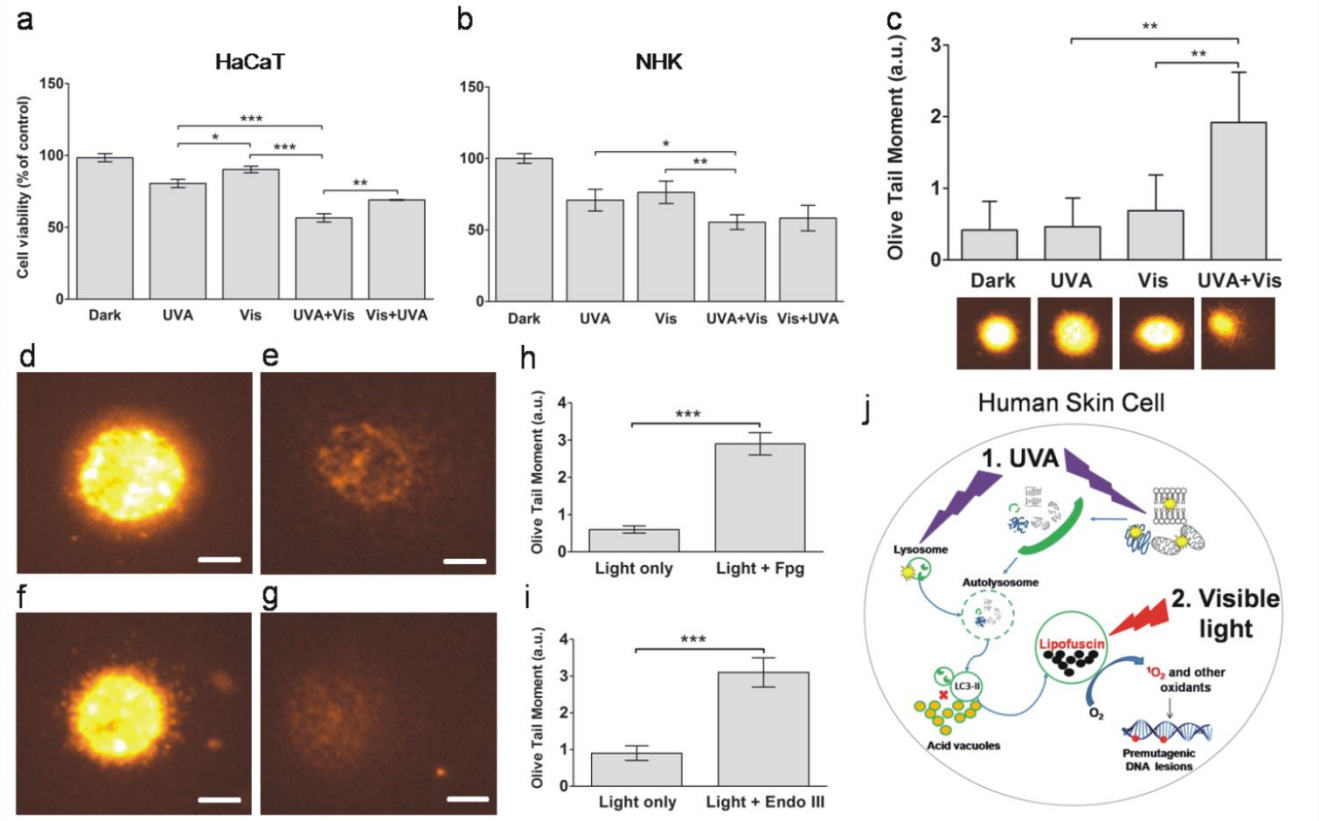

Figure 2.2. Visible light is phototoxic to lipofuscin-accumulating keratinocytes and causes oxidative DNA damage. Viability of HaCaT **(a)** and NHK **(b)** cells after different light treatments based on MTT reduction (Visible= 36 J.cm^{-2}, UVA=12 J.cm^{-2}).**(c)** DNA fragmentation (comet assay) after irradiation protocols in HaCaT cells with light doses as above. **(d-i)** Comet assays performed after the light treatment (UVA 6 J.cm^{-2} and visible 8 J.cm^{-2}) in the absence (**d,f**) and presence of FPG **(e)** and EndoIII **(g)** enzymes. Right: Quantification of Olive Tail Moment – OTM in the experimental conditions showed above. **(h)** shows quantification of (**d,e**) and **(i)** quantification of (**f,g**). **(j)** Schematic representation of our working hypothesis: UVA is absorbed by natural photosensitizers causing oxidative damage and hurting key organelles such as lysosome, inhibiting autophagy flux and favoring lipofuscin accumulation, which acts as a photosensitizer in the visible, releasing singlet oxygen and damaging nuclear DNA.

Photoprotection is traditionally centered on the prevention of skin damage caused by exposure to UV (Ziegler *et al.*, 1994; Schieke, Schroeder and Krutmann, 2003; Mahmoud *et al.*, 2010; Chiarelli-Neto *et al.*, 2014; Czarnecki, 2016). However, visible light can also act as an etiologic factor for skin photodamage (Mahmoud *et al.*, 2010; Chiarelli-Neto *et al.*, 2014). After

exposition to UVA, skin cells such as keratinocytes can generate lipofuscin, which can in turn act as a potent visible-light photosensitizer, causing premutagenic lesions in nuclear DNA (Figure 2.2 j). We hope our work will stimulate new mechanistic investigations to understand the role of key regulatory proteins, such as p53, in the combined effects of UVA and visible light (Ziegler *et al.*, 1994).

It is evident that this effect of UVA plus visible light has the potential for an undesirable amplification of the effects of solar radiation and urgently demands the development of novel strategies for sun protection. At the same time, regulatory agencies should reconsider their current sun-protection policies in order to take into account the necessity for protection against a wider spectral range of sunlight.

MATERIALS AND METHODS

Materials. The reagents 3-(4,5-dimethylthiazol-2-yl)-2,5-diphenyltetrazolium bromide (MTT), agarose, BSA (A4161), chloroquine diphosphate salt (*Sigma-Aldrich*, C6628), deferiprone, digitonin, endonuclease-III from E. coli (Endo III) (*Sigma-Aldrich*, E0526), formaldehyde, formamidopyrimidine[fapy]-DNA glycosylase (Fpg) from *E. coli* (*Sigma-Aldrich*, F3174) glutamine, HEPES, 2′,7′-Dichlorofluorescin diacetate (DCFDA) (*Sigma-Aldrich*, D6883), KCl, Na-EDTA, penicillin, streptomycin, Triton X-100 and Sudan Black B (SBB) were purchased from *Sigma-Aldrich* (USA or Germany). Fetal bovine serum (FBS), DMEM (Dulbecco's Modified Eagle Medium) and Keratinocyte-SFM (with L-glutamine), human recombinant Epidermal Growth Factor 1-53 (EGF 1-53) and Bovine Pituitary Extract (BPE) were acquired from *Gibco* (Thermo Fisher Scientific, USA). Trypan blue is from *Molecular Probes* (Thermo Fisher Scientific, USA). Water was distilled from an all-glass apparatus and further purified via a Millipore Milli-Q system. Ethanol, acetic acid and phosphoric acid were from the *Labsynth* (Brazil). *ProLong® Gold Antifade* was purchased from *Qiagen* (Brazil). All other materials were of the best analytical grade available. All reagents were prepared according to manufacturer´s instructions.

UVA and visible light sources and doses - The UVA source (*Novatecnica* Campinas, Brazil) was built in our lab with sensors for temperature and humidity. Inside the equipment, there are six UVA lamps 15W (*NARVA GLE*, Berlin, Germany) with maximum intensity at 369 nm and bandwidth at half height of 18 nm (Fig. S2.9 a, supplementary material). In order to guarantee light dose homogeneity, irradiator was divided in eight areas for an irradiance (2

mW.cm^{-2}) using a UVA dosimeter VLX-3.W (France) (Rodrigues et al., 2016). The average of irradiance was 2 mW.cm^{-2} following distribution of spectral percentage: less than 0.01 % at 345 nm; 99% at 369 nm; 0.05 % at 405 nm and less than 0.01% at 430 nm (Figure S2.9 a). The irradiation system for visible light was also constructed in own laboratory, consisting of six compact fluorescent lamps *Osram DULUX* L55W/840 (Italy), 40 mW.cm^{-2} mounted on a support that allows light dose homogeneity, with spectral irradiation ranging from 400 nm to 700 nm, with less than 0.01% in the UVA (Fig. S9b). Irradiance was adjusted to be the same of UVA light (~2 mW.cm^{-2}). Times of exposures were 0, 15, 30, 60, 90 and 180 minutes which correspond to doses of 0, 3, 6, 12, 18 and 36 J.cm^{-2}, respectively, for both UVA and visible lights. Cells were irradiated in phosphate buffer solution (pH 7.4). Both spectrum characterization (UVA and visible) were performed employing spectrophotometer USB2000+UV-VIS-ES and optical fiber QP50-2-UV-VIS (*Ocean Optics*, USA). The light doses used in this work are equivalent of typical regimens of sunlight exposition. For example, 12 J.cm^{-2} of UVA is equivalent to approximately half hour exposure to sunlight, between 11 a.m. and 13 p.m. at 48° North latitude (Jeanmougin and Civatte, 1987). In terms of having a reality check of our hypothesis, we can think of a person exposing to the sun having only protection against UVB (and not UVA).

Cell culture - Immortalized human keratinocyte cell line (HaCaT) (Boukamp *et al.*, 1988) was cultivated in Dulbecco's Modified Eagle Medium (DMEM) culture medium supplemented with 10% (v/v) fetal bovine serum (FBS), 4 mM L-glutamine, 100 U/mL penicillin and 100 µg/mL of streptomycin and incubated at

37°C and 5% CO_2, and cultivated in passages 8 to 18. Normal Human Primary Epidermal Keratinocytes isolated from Neonatal Foreskin (NHK) were gently donated by Prof. Dr. Silvya Stuchi Maria-Engler (School of Pharmaceutical Sciences, at USP) and cultivated in Keratinocyte-SFM (with L-glutamine), 0.2 ng/mL human recombinant Epidermal Growth Factor 1-53 (EGF 1-53), 30 µg/mL Bovine Pituitary Extract (BPE), in presence of 5 µg/mL gentamicin (*Gibco Life Technologies*), in 100 mm plate coated with collagen IV (0.5 mg/mL in 0.5 M acetic acid solution) (*Sigma*). NHK cells were maintained in passages 2 to 4, and medium was exchanged every 2-3 days until the cells reach 60-80% confluence. Subculture was made as recommended for this cell line. The use of NHK was approved by *Ethics Committee in Research* from University Hospital (HU) at University of São Paulo (Permit numbers: 943/09, HU/USP and SISNEP CAAE: 0062.0.198.000-09).

Cell Viability – HaCaT and NHK (passage number 2 to 4) cells were plated ($2x10^5$ cells/well) in 48-well cell culture plates (*Corning Costar*, cod. 3548). After 24 hours, cells were washed in PBS and irradiated with UVA at doses of 3, 6, 12, 18 and 36 $J.cm^{-2}$. Forty-eight hours after irradiation, colorimetric assays of cellular viability based on reduction of MTT were performed. In quadruplicate and in three independent experiments. Cells were washed in PBS and irradiated with UVA (6, 12, 18 and 36 $J.cm^{-2}$). Twenty-four hours after irradiation, cells were washed and live-cells were analyzed in epifluorescence microscope using filter set 9 from *Zeiss* (excitation band pass from 450-490 nm and emission above 515 nm). In order to analyze the phototoxicity triggered by lipofuscin using visible light excitation, just 48 hours after UVA irradiation (12

J.cm^{-2} for HaCaT and 6 J.cm^{-2} for NHK), cells were washed and refreshed with culture medium, then returned to the 5% CO_2 incubator at 37°C, for 48 hours. Forty-eight hours after initial photodamage, cells were again washed and submitted to irradiation under visible light (36 J.cm^{-2}) in the presence of PBS. Cell viability was evaluated by MTT assay.

Oxidation of 2',7'-Dichlorofluorescin diacetate to dichlorofluorescein - Twenty-four hours after being seeded 1x10^4 cells/well in 96-well plates (black clear flat bottom, *Greiner-BioOne*, Austria), HaCaT and NHK cells were irradiated with UVA, 12 and 6 J.cm^{-2}, respectively, immediately after irradiation, 200 µL of 10 µg/mL DCFDA (2′,7′-dichlorofluorescin diacetate) solution (prepared in PBS from a 5 mg/mL stock in ethanol) were added to each well, and fluorescence was monitored during 30 minutes in microplate reader *Spectramax i3* (*Molecular Devices*, USA), using excitation at 485 nm and detecting emission at 535 nm. The slope of the curve was used to calculate the oxidation rate of DCFDA to DCF (dichlorofluorescein), with increasing percentage in fluorescence/well calculated by [(Ft_{30}-Ft_0)/Ft_0*100], where Ft_{30} is fluorescence at 30 minutes, Ft_0 is fluorescence at 0 minutes (Wang and Joseph, 1999a).

Lipofuscin detection by flow cytometry (FACS) - HaCaT cells were plated in 6-well plates (2x10^5 cells/well). Twenty-four hours after seeding, cells were irradiated with UVA (18 J.cm^{-2}). Cytofluorimetric analysis of live cells were performed 48 hours after irradiation to quantify lipofuscin autofluorescence

using the FL1 (excitation with blue light at 488 nm) and FL3 (excitation with red light at 640 nm) filter sets.

Sudan Black B staining – HaCaT and NHK cells (2 x 10^5 cells/well) were seeded over a coverslip in 6-well plates, irradiated with different UVA doses. After 48 hours, cells were washed twice with PBS, fixed with 4% formaldehyde (w/v) for 15 minutes, washed again with PBS. Then, cells were stained with Sudan Black B solution (0.7% in ethanol 70%) for 30 minutes, washed in distilled water, and coverslips were visualized in transmission microscopy *Zeiss Axiovert 200* inverted microscope equipped with Plan-APOCHROMAT 100X DIC M27. Images were quantified by *ImageJ* software (NIH, Bethesda, MA, USA), converting TIF images to grayscale 8-bit and after adjusting threshold. SBB-stained area was delimited drawing region of interest with polygonal selection, obtaining data about area, mean gray value, and integrated density from different images for each sample. Graph values were obtained by dividing the integrated intensity by the area, calculating mean ± standard deviation.

Quantification of lipofuscin by fluorescence microscopy - Cells (2 x 10^5 cells/well) were seeded on coverslips in 6-well plates, and lipofuscinogenesis was induced by different doses of UVA (6 and 12 J.cm^{-2} for HaCaT, and 3 and 6 J.cm^{-2} for NHK). After 48 hours, cells were washed twice with PBS and analyzed in vivo in a *Zeiss Axiovert 200* inverted microscope (Carl Zeiss, Göttingen, Germany), with filter set 09 (excitation: BP 450-490 nm; emission: LP 515 nm). Using *ImageJ* software, cell fluorescence was measured from TIF images, converted to 16-bit, and delimiting fluorescent area with polygon

selection, obtaining data about area, mean gray value, and integrated density from different images for each sample. Total cell fluorescence (TCF) was corrected using the following formula: TCF = integrated density - (area selected x mean fluorescence of background readings). Graph values were obtained calculating mean of TCF ± standard deviation.

Fluorescence Lifetime Imaging (FLIM) - Cells (2 x 10^5 cells/well) were seeded on coverslips in 6-well plates, and lipofuscinogenesis was induced by UVA irradiation (12 J.cm^{-2} for HaCaT and 6 J.cm^{-2} for NHK). For the negative control, twenty-four hours previous to UVA irradiation, cells were incubated for 24 hours (37ºC and 5% CO_2) with deferiprone (30 µM in DMEM 1%FBS), an iron-chelator that decreases Fenton reaction and lipofuscinogenesis (Figure 2.1). Chloroquine treatment was used as positive control for lipofuscinogenesis. HaCaT cells were incubated with 60 µM of chloroquine in DMEM 1% FBS (v/v) for 24 hours at 37ºC and 5% CO_2. After washing with PBS, cells returned to CO_2 incubator for 48 hours in the presence of DMEM 10% FBS (v/v). After a second washing in PBS and fixing with 4% (w/v) paraformaldehyde in PBS solution, HaCaT coverslips were washed once more and mounted in *ProLong*® *Gold Antifade* reagent without any further staining. Slides were analyzed under fluorescence confocal microscope (*Olympus* IX 73) *FluoView* FV1000 with a piezo-driven objective scanning coupled to *MicroTime 200* system (*PicoQuant*, Berlin, Germany) for detection of fluorescence lifetime. To detect lipofuscin granules a filter set that provides excitation at 509 nm with emission long pass at 550 nm was used. Time decays were fitted using *SymphoTime* 64 (version

2.1) and by using *TimeHarp* plataform, with which single-photon-counting decays were transformed in FLIM images.

Transmission electron microscopy (TEM) analysis - Cells were seeded on coverslips in 6-well plates (4 x 10^5 cells/well) and irradiated with UVA (12 J.cm^{-2}) to induce lipofuscinogenesis. Forty-eight hours after initial photodamage, lipofuscin-loaded cells were collected and fixed for 8 hours at 4ºC in modified Karnovsky's solution (2.5% (v/v) glutaraldehyde and 2% (v/v) formalin in 0.1M sodium phosphate buffer, pH 7.4 (Watanabe and Yamada, 1983). A post-fixation with 1% (v/v) osmium tetroxide solution was employed for 2 hours at 4ºC. After dehydration in a series of graded ethanol baths 70–100% (v/v) and in propylene oxide, cells were embedded in synthetic resin. Cell sections (90 nm) were obtained using a *Reichert Ultracut E* microtome and mounted on *Formvar* films (200 mesh). After counterstaining with uranyl acetate and lead citrate (Watanabe and Yamada, 1983), ultrathin samples were analyzed under transmission electron microscopy by using a *Jeol 1010* 80 KV at electron microscope (Tokyo, Japan).

Singlet oxygen generation by lipofuscin photosensitization in cells – Cells (2 x 10^6 cells) were seeded in 100 mm plates (*Corning Falcon*). Lipofuscinogenesis was induced by UVA radiation (12 J.cm^{-2} for HaCaT and 6 J.cm^{-2} for NHK). After 48 hours from irradiation, cells were washed in PBS, removed from the plates by trypsinization, neutralized with DMEM 10% FBS. Cells were counted, adding 2 x 10^6 cells in a microcentrifuge tube, and collected by centrifugation (3000 rpm, for 5 min, 25 ºC), washed with PBS, and re-

suspended in 2 mL of 0.9% NaCl solution in deuterated water (D_2O) (*Sigma-Aldrich*). The $^1O_2$ measurements were performed in a especially-designed home-made instrument (Chiarelli-Neto *et al.*, 2011) consisting of a Nd:YAG-OPOsystem-Rainbow (355 nm and 532 nm, 5-ns pulses, 20 pulses/s, 1 mJ/pulse; *Quantel Lasers*, France), cuvette holder, silicon filter, monochromator, liquid-nitrogen-cooled near infrared photomultiplier tube (NIR-PMT R5509) from *Hamamatsu* (Hamamatsu Co., Bridgewater, NJ, USA) and a fast multiscaler analyzer card with a resolution of 5 ns/channel (MSA-300; *Becker & Hickl*, Berlin, Germany). Signals were acquired from a cell cuvette adding 2 mL of cell suspension in 0.9% NaCl solution in D_2O and subtracted from the signal obtained from dark-control cells. Emission spectra was obtained by measuring signal intensities as a function of the wavelength from 1200 to 1350 nm and $^1O_2$ decays were obtained by measuring emission at 1270 nm as a function of time.

Comet assay (photodamage in DNA) - Comet assays, assays to detect breaks in DNA strand, were performed according to optimized protocols previously described (Chiarelli-Neto et al., 2014), after lipofuscinogenesis induction and visible-light irradiation of HaCaT cells (see above). Cells were collected (30 µL of a 1 x 10^5 cells/mL), mixed with 100 µL of 0.5% (w/v) agarose in PBS, distributed in agarose pre-coated (1.5% w/v) slides and incubated on ice. After solidifying, HaCaT cells were lysed in the dark using a high-salt alkaline buffer - 0.5 M NaCl, 0.1 M EDTA, 0.01 M Tris, and 1% (v/v) Triton X-100, pH 10. Slides were placed in electrophoresis buffer (0.3 M NaOH and 1 mM EDTA, pH 13), cooled in a refrigerator for 30 min protected from light.

Electrophoresis was performed in a cold-storage room, protected from light, using a power supply (ESP 301, *General Electric*, USA) for 30 min at 25 V. After electrophoresis, slides were neutralized using 0.4 M Tris at pH 7.5 and fixed in ethanol. DNA was stained with ethidium bromide (10 mg/mL), excited at 515 nm and observed using a fluorescence microscope. Comet assays combined with enzymatic recognition were used to identify premutagenic lesions. Cells were treated with UVA and visible sub-dose irradiation protocols (UVA 6 $J.cm^{-2}$ and visible 8 $J.cm^{-2}$), and before electrophoresis, slides were treated with 0.2 U of Fpg (formamidopyrimidinen[fapy]-DNAglycosylase) or Endo III (endonuclease III) enzymes in buffer (0.1 M KCl, 0.5 mM Na-EDTA, 40 mM HEPES and 0.2 mg/mL BSA at pH 8.0) for 30 minutes at 37ºC. Comet assays were performed as described above. All images from comet assays were obtained employing *Olympus* fluorescence microscope equipped with Comet software for analysis version 6 (*Olympus* BH-2, USA).

Statistical analysis - All experiments were performed with at least three independent repetitions. The statistical analyses were performed using one-way analysis of variance (ANOVA), followed by Holm-Sidak´s post-test, employing *Sigma Stat* (version 3.5, 2006, Germany) and *OriginLab* software (version 7.0 or 8.0, Origin Lab Corp., MA, USA); p-value <0.05 was considered statistically significant.

SUPPLEMENTARY MATERIAL

CELL VIABILITY

Figure S2.1

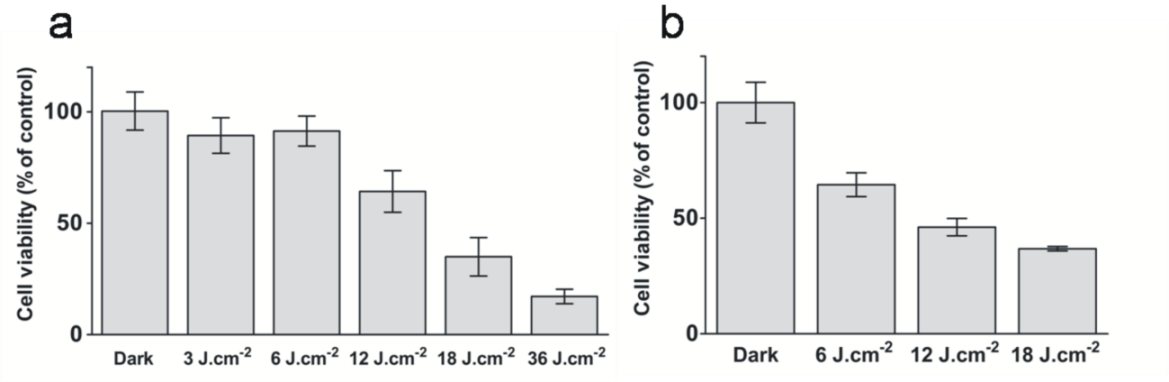

Figure S2.1. Viability curves as a function of UVA dose. Cell viability was measured 48 hours after irradiation and is expressed as percentage of MTT reduction by HaCaT **(a)** and NHK **(b)** cells. HaCaT and NHK cells reached survival of 50% at doses of 12 J.cm^{-2} and 6 J.cm^{-2}, respectively. Bars indicate mean ± standard deviation for three independent experiments.

LIPOFUSCIN

Figure S2.2

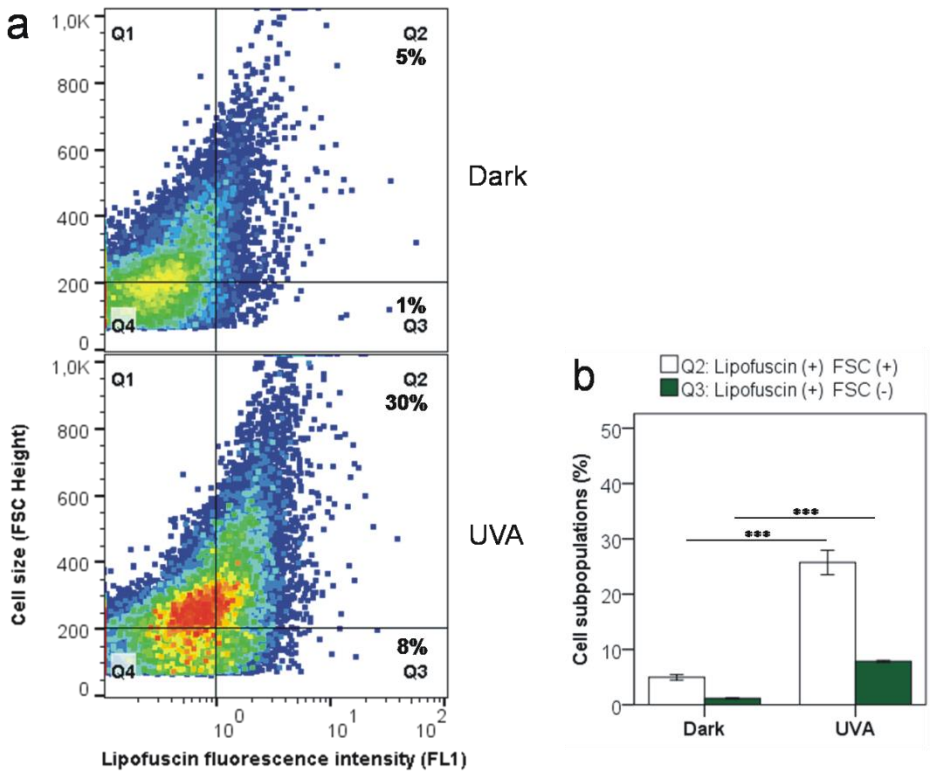

Figure S2.2. **UVA radiation induces lipofuscin accumulation in HaCaT cells. (a)** scatter-plot contour of lipofuscin autofluorescence (FL1) *versus* forward-scattered light (FSC height), obtained by flow cytometry for dark control (upper diagram) and UVA-irradiated cells (dose 18 J.cm^{-2}, lower diagram). **(b)** Mean values ± standard deviation of cell subpopulations for dark control and UVA-irradiated represented in the quadrant Q2, where lipofuscin was accumulated (Lipofuscin (+)) and increased cell size (FSC (+)), and quadrant Q3, where lipofuscin was accumulated without increasing in cell size (FSC (-)). Lipofuscin was excited at 488 nm and emission detected at 630 nm. Statistical analysis considered significant at $p<0.05$ (*** $p<0.001$).

Figure S2.3

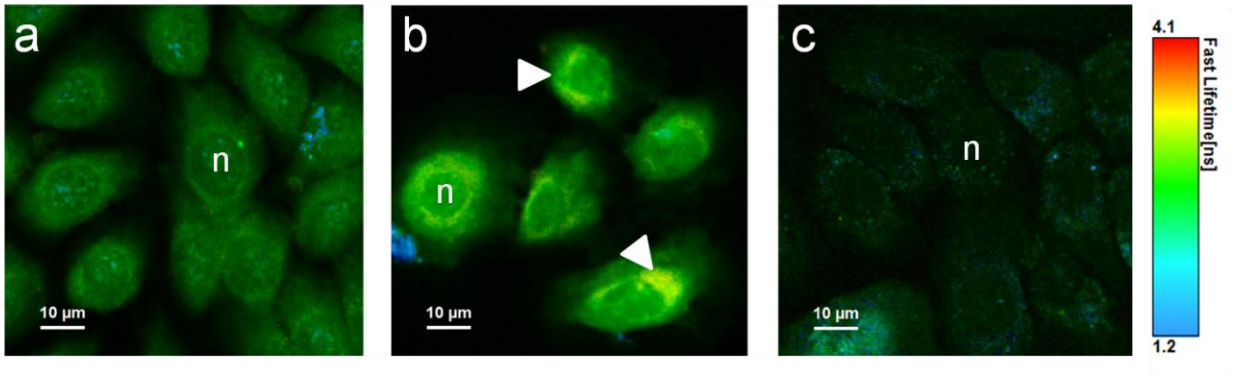

Figure S2.3. Lipofuscin accumulation and lifetime in NHK cells. (a) Dark control. **(b)** NHK UVA-irradiated cells (6 J.cm^{-2}). Emissive granules presented lifetime ~1.7 ns. White arrows indicate the perinuclear aggregates of lipofuscin. **(c)** visible light-irradiated cells (36 J.cm^{-2}). Images were obtained using a single molecule lifetime confocal microscope (Picoquant's Microtime 200). Samples were excited at 509 nm and emission was captured with long-pass filter at 519 nm. Fluorescence decay curves of lipofuscin fluorophores were recorded by TCSPC mode. n = nucleus.

Figure S2.4

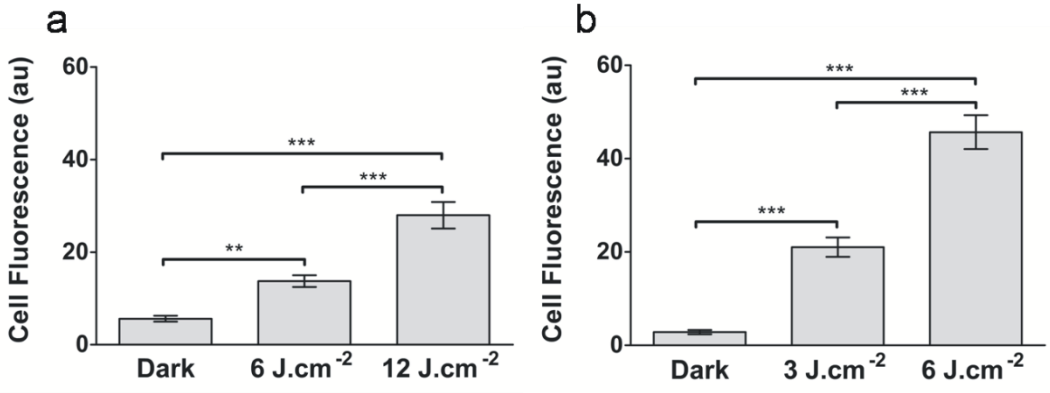

Figure S2.4. Lipofuscin fluorescence in HaCaT and NHK cells. Autofluorescence of HaCaT **(a)** and NHK **(b)** cells 48 hours after exposure to UVA. Cell fluorescence was measured from TIF images, converted to 16-bit, and delimiting fluorescent area with polygon selection, obtaining data about area, mean gray value, and integrated density from different images for each sample (HaCaT dark, 6 and 12 J.cm^{-2}; n=11, n=25, n=20, respectively; NHK dark, 3 and 6 J.cm^{-2}; n=5, n=8, n=8, respectively). Total cell fluorescence (TCF) was corrected using the following formula: TCF = integrated density – (area selected x mean fluorescence of background readings). Statistical analysis was performed using *SigmaStat* v.3.5. (Abacus Concepts, Berkeley, CA), running one-way ANOVA test, and statistical differences determined by Holm-Sidak post-test, considering statistically significant at $p<0.05$ (*), $p<0.01$ (**), and $p<0.001$(***).

Figure S2.5

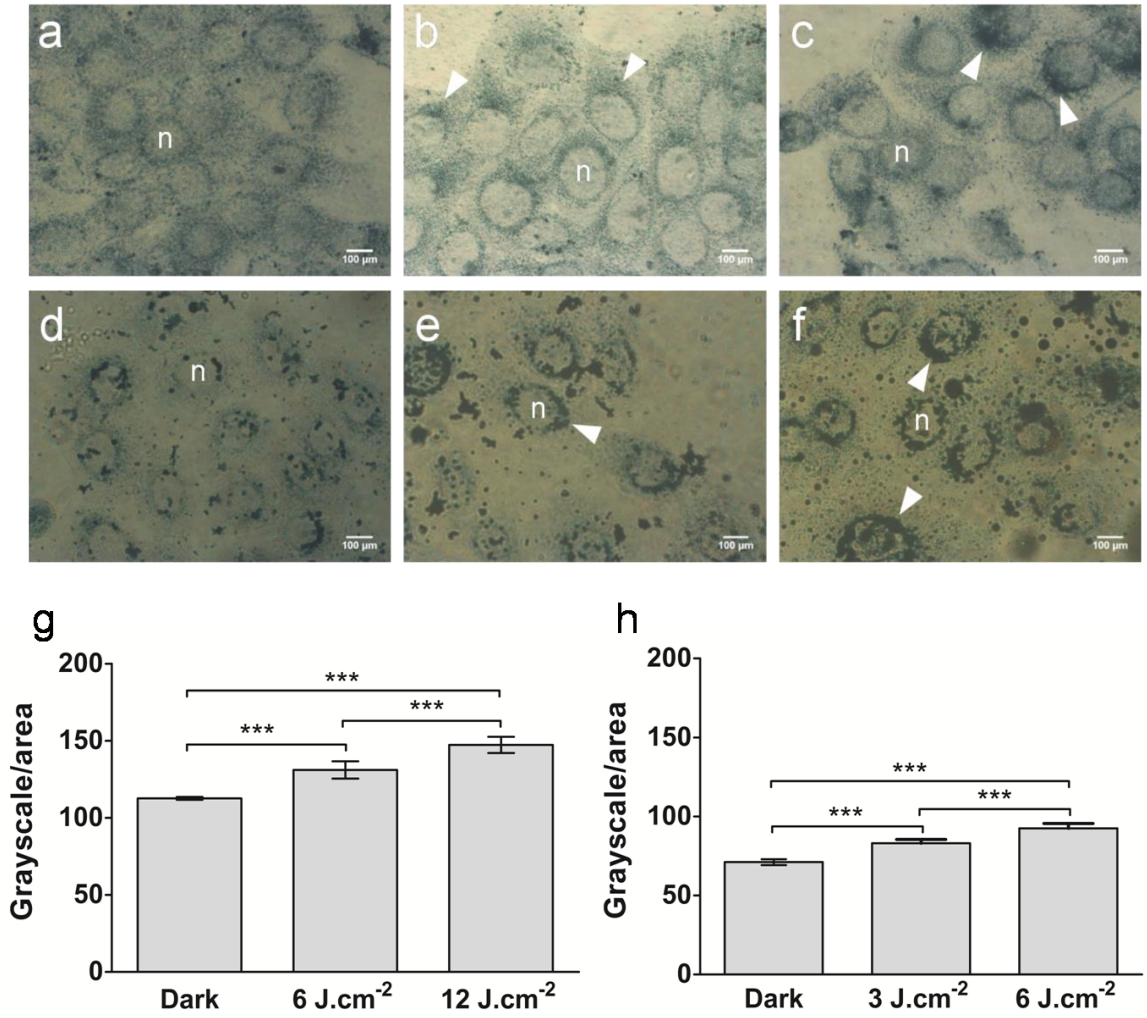

Figure S2.5. Lipofuscin identification by Sudan Black B staining in HaCaT and NHK cells. Both HaCaT and NHK cells were stained with Sudan Black B (SBB) 48 hours after UVA radiation. Images were obtained using bright-field transmitted light microscopy. White arrows indicate lipofuscin stained by SBB. n= nucleus. **(a)** HaCaT: Dark, **(b)** HaCat: UVA 6 J.cm^{-2}, **(c)** HaCaT: 12 J.cm^{-2}, **(d)** NHK: Dark, **(e)** NHK: 3 J.cm^{-2}, **(f)** NHK: 6 J.cm^{-2}. Quantification of SBB staining in HaCaT **(g)** and NHK **(h)** cells. Images were converted to8-bit grayscale. SBB-stained area was delimited by adjusting cutoff levels of gray value in order to obtain area and mean gray value. Integrated intensity was divided by area from different images for each sample (HaCaT dark, 6 and 12 J.cm^{-2}; n=3, n=10, n=10, respectively; NHK dark, 3 and 6 J.cm^{-2}; n=6, n=7, n=4, respectively). Statistical analysis was performed using *SigmaStat* v.3.5., running one-way ANOVA test, and statistical differences determined by Holm-Sidak post-test, considering statistically significant at $p<0.05$. All treatments showed statistical difference for $p<0.001$ (***).

Figure S2.6

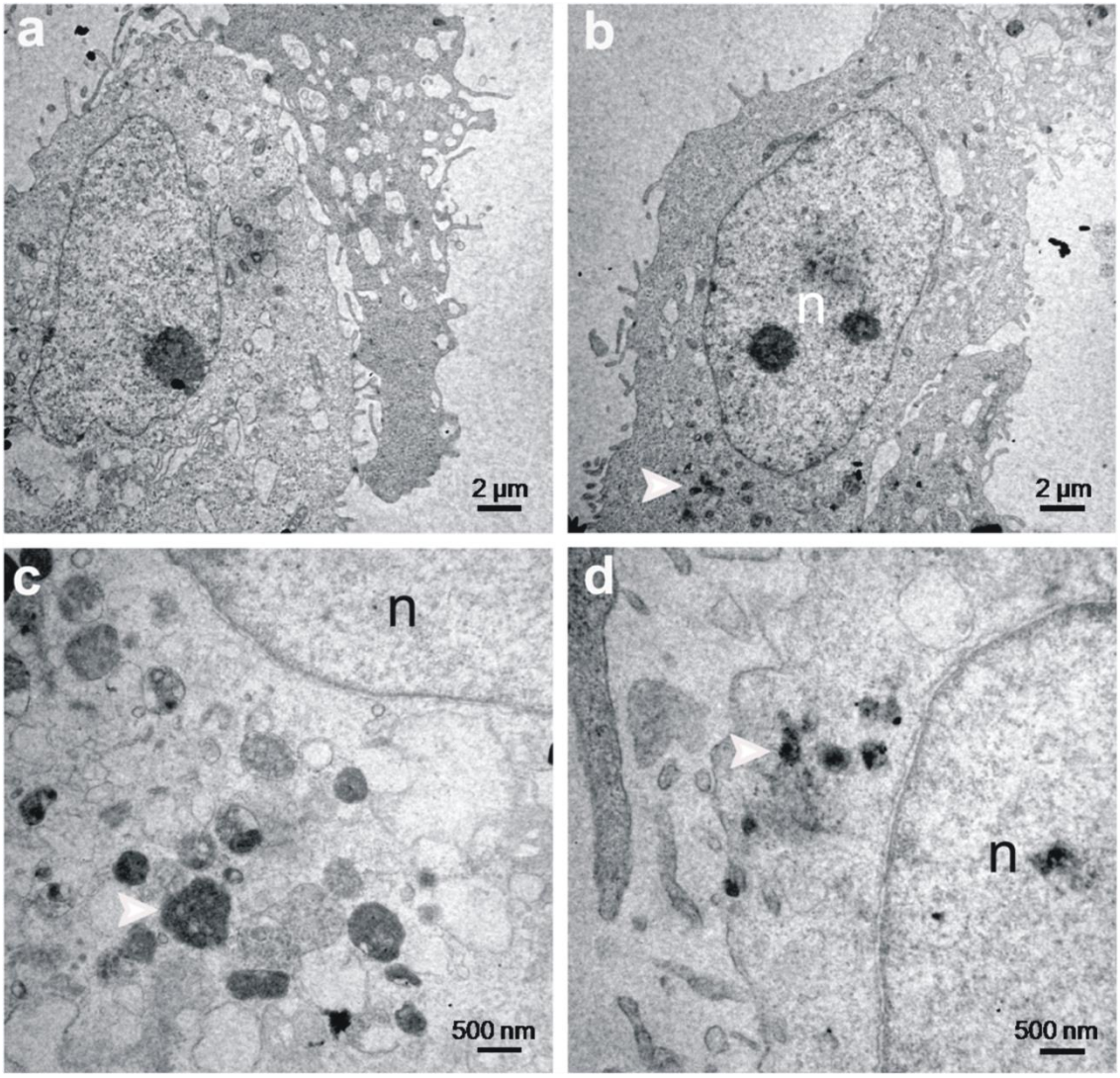

Figure S2.6. Lipofuscin accumulation in HaCaT cells after exposure to UVA by TEM. Lipofuscin was identified in the perinuclear region of HaCaT cells using transmission electronic microscopy 48 hours after exposition to UVA radiation. **(a)** Dark control. **(b)** UVA-irradiated cells (6 $J.cm^{-2}$) showing the typical accumulation of electrondenses granules of lipofuscin. **(c)** and **(d)** show lipofuscin in details. White arrows indicate lipofuscin granules. n = nucleus.

Figure S2.7

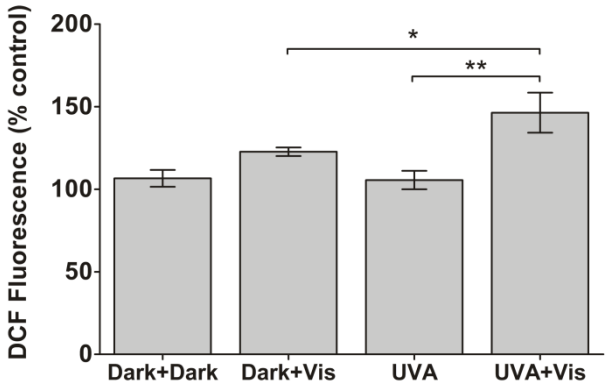

Figure S2.7.Dichlorofluorescein (DCF) assay for detection of oxidizing species in NHK cells measured immediately after exposure to visible light. The increasing percentage in fluorescence/well was calculated by $[(Ft_{30}-Ft_0)/Ft_0*100]$, where Ft_{30} is fluorescence at 30 minutes, Ft_0 is fluorescence at 0 minutes. After 48hours from first irradiation, cells were exposed to visible light (Dark+Vis and UVA+Vis). Bars indicate mean ± standard deviation obtained from three independent cell culture experiments (n=3). Statistical analysis was performed using *SigmaStat* v.3.5., running one-way ANOVA test, and statistical differences determined by Holm-Sidak post-test, considering statistically significant at $p<0.05$ (*) and $p<0.01$ (**).

Figure S2.8

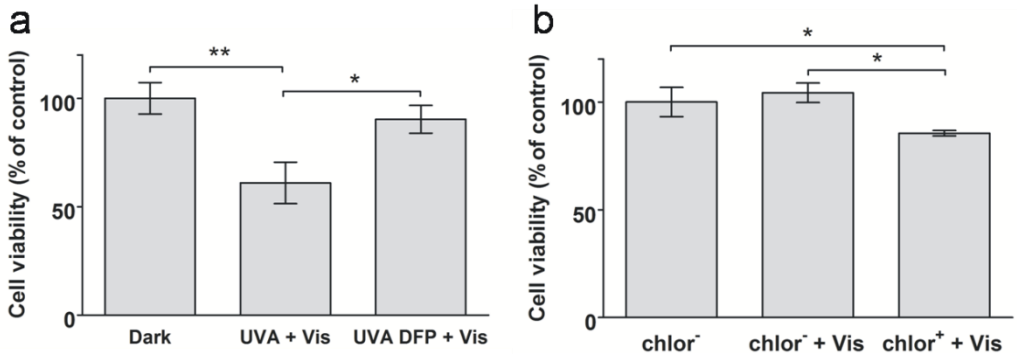

Figure S2.8. Cell viability based on reduction of MTT in HaCaT cells. UVA radiation or by treatment with 60 µM chloroquine **(a)** UVA-treated cells (12 $J.cm^{-2}$) were immediately incubated with 30 µM deferiprone (DFP), an iron-chelator, avoiding lipofuscinogenesis. Forty-eight hours after initial challenge cells were photosensitized with visible light (Vis) (36 $J.cm^{-2}$). **(b)** cells treated with chloroquine ($chlor^+$) or not ($chlor^-$). Forty-eight hours after cells were photosensitized with visible light (Vis).MTT assay was revealed after 48hours from last irradiation. Bars indicate mean ± standard deviation. Statistical analysis was performed using *SigmaStat* v.3.5., running one-way ANOVA test, and significance determined by Holm-Sidak post-test, considering statistically significant at $p<0.05$ (*) and $p<0.01$(**).

SOURCE LIGHT DESCRIPTION AND SPECTRAL CHARACTERIZATION

Figure S2.9

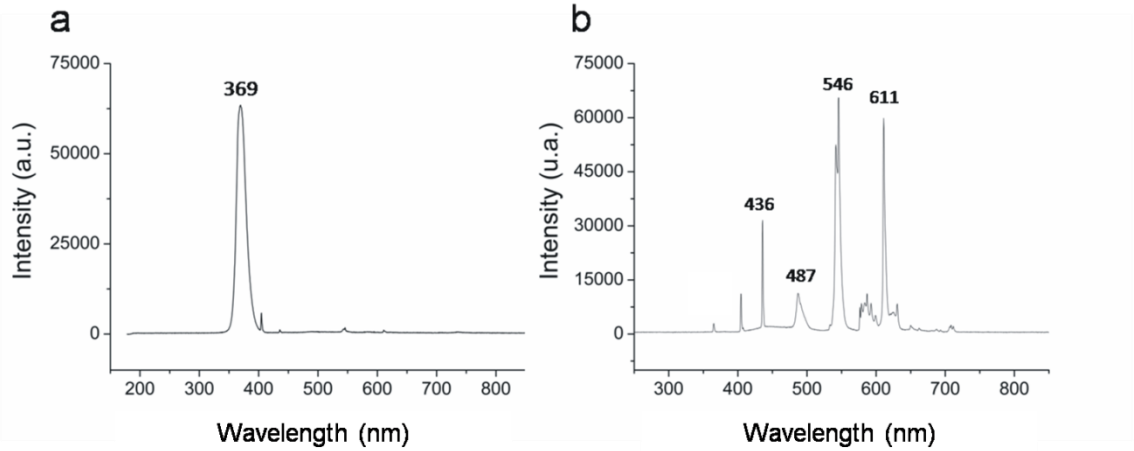

Figure S2.9. UVA and visible spectral emission of the light sources. (a) spectrum of UVA radiation system that was used in experiments indicate peak at 369 nm. **(b)** spectrum of visible light source showing peaks at 436 (blue), 546 (green), and 611 nm (red). Spectrum analyses were performed by employing a spectrophotometer USB2000+UV-VIS-ES and optical fiber QP50-2-UV-VIS (*Ocean Optics*, USA).

Chapter 3 – An Experimental Model for Studying Lipofuscin in Human Skin Keratinocytes

3.1. INTRODUCTION

Lipofuscin, which is an aging pigment that accumulates especially in postmitotic cells, has been extensively studied in the context of eye diseases, in order to elucidate the mechanism for age-related macular degeneration and other several retinal disorders (Gaillard *et al.*, 1995). Most studies have been performed with retinal pigment epithelium (RPE) cells (Sparrow and Boulton, 2005; Boulton, 2014). In these cells lipofuscin naturally accumulates with aging, furthermore allowing the establishment of a clear connection between lipofuscin accumulation and retinopathies.

Consequently, there are many research articles describing the photochemical properties of lipofuscin in retinal pigment epithelium (RPE) cells (Eldred *et al.*, 1982; Eldred and Katz, 1988; Boulton *et al.*, 1990; Reszka *et al.*, 1995; Rózanowska *et al.*, 1998). On the other hand, little is known about accumulation of lipofuscin in human skin cells and its role in possible phototoxicity mechanisms in skin.

The cellular composition of lipofuscin, including percentage level of lipids and protein, change among the different cell types, and consequently it is not trivial to extrapolate the knowledge about photochemical properties of lipofuscin from RPE with the lipofuscin generated in other cell types. Moreover, the composition of lipofuscin may also depend on the intracellular site of reactive oxygen species attack, as suggested in recent work (König *et al.*, 2017).

Therefore, in this thesis, we aim to develop an efficient way to investigate the photochemical properties of lipofuscin in human skin keratinocytes and its phototoxicity, inducing oxidative lesions and breaks in nuclear DNA.

In contrast to using RPE cells as a model to study the photochemical consequences of the lipofuscin accumulation, HaCaT cells are different in several ways and maybe even advantageous in this respect. RPE cells, which have active melanogenesis even during adult phase, accumulate melanin in melanosomes (Biesemeier et al. 2010; Schraermeyer & Heimann 1999), while HaCaT cells do not accumulate this pigment, which absorbs the visible light (Chiarelli-Neto et al. 2014). Thus, in a cell model without melanin detecting the specific effects of lipofuscin photosensitization by visible light may prove to be more sensitive due to less other fluorescent or absorbing species.

Yet, very little is known about lipofuscin in human skin cells. There are some studies of lipofuscin in dermal fibroblasts, which showed: the accumulation of this pigment after UVA exposure (Lamore et al. 2010); the adverse effects of this lipofuscin accumulation on protein turnover, oxidative stress, and senescence (Sitte et al. 2001); and increasing in sensivity to oxidative stress in lipofuscin-loaded fibroblasts (Terman et al. 1999). Additionally, there is a study in senescent epidermal keratinocytes on cellular and molecular characteristics, measuring changes in morphology, fluorometry, and biochemistry in monolayer cell culture and human skin (Soroka et al. 2008).

However, the first evidence that lipofuscin is formed in keratinocytes is from this work (*Chapter 2*, Tonolli et al. 2017). Besides that, we are presenting evidence that lipofuscin is one of the pigments responsible for the harmful effects of visible light. However, stimulating lipofuscin accumulation using UVA,

for example, is not a trivial task. There is a great level of cell death and the amount of lipofuscin formed is not enough to allow more detailed evaluation. Therefore, it became necessary to develop an experimental model that allows efficient lipofuscinogenesis, which is described in this chapter. Indeed, by damaging lysosomes and mitochondria there is an efficient blockade of the autophagic flux and lipofuscin accumulation. The specific damage in lysosomes and mitochondria was accomplished using a synthetic photosensitizer, the 1,9-dimethyl methylene blue (DMMB) (Figure 3.1), which is photosensitized by red light (λ = 633 nm or 650 nm, 11 J.cm^{-2}).

The DMMB is a cationic dye derived from methylene blue, containing two methylene groups at the 1- and 9-position of the phenothiazine ring. DMMB is highly lipophilic, effectively binding to membranes (Bacellar *et al.*, 2014), especially in lysosome and mitochondria. Besides, photosensitizers with positive charge, such as DMMB, are attracted to negative electrochemical environment, as found in mitochondria membrane. However, the endocytic internalization route is also important to define the intracellular site of localization (Tsubone *et al.*, 2017), which explains why DMMB is also found in the lysosomal membranes.

After photosensitization with red light, oxidative damage occurs in these organelles, compromising the autophagic flux (Martins et al. 2018; Master thesis from Nayra F. Santos, IQ-USP, 2014). Lipofuscinogenesis induction is explained by the “mitochondrial-lysosomal axis theory of aging” by Brunk & Terman (2002) (for more detail, see *Chapter 1*). This theory proposes that lysosomes are damaged, and recycling of damaged mitochondria can no longer be degraded by autophagy, promoting the formation of lipofuscin. We extended

this concept proposing that the parallel damage in these two organelles will maximize the production of lipofuscin (Martins et al. 2018).

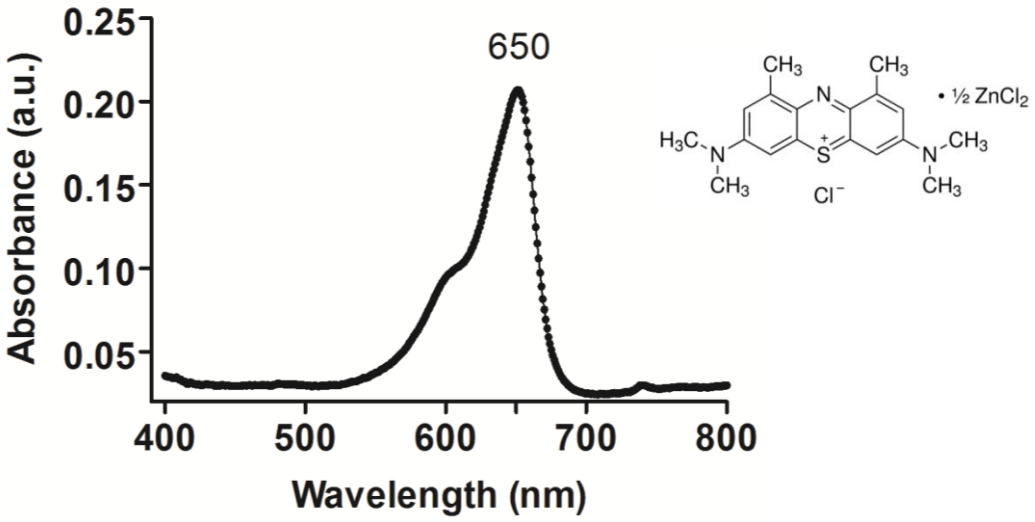

Figure 3.1. Molecular structure of 1,9-dimethyl methylene blue (DMMB) (taken from *Sigma-Aldrich*) with maximum absorption at 650 nm (in absolute ethanol).

3.2. MATERIALS AND METHODS

3.2.1. Cell Culture

Immortalized human skin keratinocyte cells (HaCat) were cultured in Dulbecco's Eagle medium (DMEM) in the presence of 10% fetal bovine serum (FBS) and 100 U/mL penicillin and 100 µg/mL of streptomycin, cultivated in a humidified incubator containing 5% CO_2, at 37°C. Cells were trypsinized, used for plating experiments, and reseeded in bottle of 75 cm^2 when confluence reached 80-90%. Cells were kept until 25^{th} passage for the accomplishment of the experiments.

3.2.2. Cell Plating

Cells were washed with PBS-EDTA, incubated for 10 minutes in the incubator with 5% CO_2, at 37°C, incubated with trypsin-EDTA for 5 minutes,

neutralizing the activity with DMEM 10%, and homogenizing the mixture to individualize the cells for plating. Cells were counted using a Neubauer chamber and Tripan blue with the aid of an optical microscope, and plated to obtain an approximate confluence of 80% for the day of the experiment.

3.2.3. Photosensitizer solution

Sterile stock solutions of 1,9-dimethyl methylene blue (DMMB) (*Sigma-Aldrich*) were prepared in Milli-Q water from solid samples, and their concentrations determined by Lambert-Beer law, by absorption in ethanol (for avoiding dimers) considering the molar absorptivity coefficient of 78.000 L. $mol^{-1}.cm^{-1}$.

3.2.4. The lipofuscin generation protocol

On the following day, after seeding the cells, DMEM 10% medium was removed and cells were washed once with PBS, and then incubated for 1 hour, at 5% CO_2 and 37°C with 10 nM DMMB in PBS. After incubation, the cells were washed twice with PBS and irradiated with red light LED (λ = 633 nm) for 40 minutes at dose of 11 $J.cm^{-2}$. Non-irradiated samples were kept in the dark in the presence of PBS, containing DMMB (DMMB +) or not (DMMB -). After photosensitization, PBS was replaced with DMEM 10%, 1% antibiotic (streptomycin/penicillin), incubating cells at 5% CO_2 and 37°C, for 48 hours for maximal accumulation of lipofuscin.

3.2.5. Cell viability assay by MTT reduction

The cell viability assay using MTT (3-[4,5-dimethylthiazol-2-yl]-2,5-diphenyl-2H-tetrazolium bromide) consists in the reduction of the yellow soluble compound MTT by the mitochondrial succinate dehydrogenase enzymes and cytochrome c oxidase, forming an insoluble purple product (formazan). This compound was solubilized using dimethyl sulfoxide (DMSO), and quantified spectrophotometrically using absorbance at 550 nm. This assay is indicative of cellular metabolic activity and is useful to evaluate cell proliferation and viability.

3.2.6. Analysis of lipofuscinogenesis and acidic vacuoles by FACS

To investigate the induction of lipofuscinogenesis, that is, the production of lipofuscin, associated with autophagic flow compromise, 48 hours after DMMB treatment, an experiment was performed using fluorescence activated cell sorting (FACS). HaCat cells were plated in 6-well plates at density of 6 x 10^4 cells.cm^{-2}. Treatment with DMMB + red light was performed according to the description above. Fourty-eight hours after treatment, cells were washed with 1mL PBS-EDTA, incubated for 5 minutes with 5% CO_2, at 37°C, trypsinized (400 µL trypsin/well), and neutralized with 1 mL of 10% DMEM medium. Cells were collected by centrifugation at 300g for 5 minutes, at RT, and resuspended in 1 mL of PBS-EDTA, assembling 200 µL of each tube of the non-irradiated control in one tube and 200 µL of each tube of the irradiated to constitute the blank control for the LysoTracker Red (LTR), a cationic fluorophore, which is specifically incorporated by the lysosome. Thereafter, LTR was added to a final concentration of 100 nM in each non-irradiated and irradiated tube, incubating for 15 minutes, at 37°C. After incorporation of the LTR, cells were collected by

centrifugation at 300g, for 5 minutes, at 4ºC. The supernatant was discarded and the pellet resuspended in 300 µL of PBS-EDTA, keeping the tubes protected from light. LTR fluorescence was measured with FL3 excitation filter and autofluorescence of lipofuscin with excitation at 488 nm and emission at 630 nm (FL1).

3.2.7. Transmission electronic microscopy

To perform the transmission electron microscopy, in order to visualize the accumulation of lipofuscin granules in HaCat cells, we established a collaboration with Prof. Dr. II-Sei Watanabe, Department of Anatomy, Institute of Biomedical Sciences (ICB-III), University of São Paulo.

We seeded 4 x 10^5 cells per well in 6 wells plate. Lipofuscinogenesis was induced according to description above. After 48h, the cells were incubated with PBS-EDTA, for 5 min, at 37°C, trypsinized (500 µL/ well), and resuspended in 1 mL PBS. Then the cells were collected by centrifugation at 600 g, 5 min, 25°C, and resuspended in modified Karnovsky fixative solution (2.5% glutaraldehyde, 2% formalin in 0.1 M sodium phosphate, pH 7.4) (Watanabe and Yamada, 1983). Cells were fixed for 8 h at 4°C and post-fixed in 1% osmium tetroxide solution for 2 h at 4°C. Dehydration was done in increasing series of ethanol (70-100%) and propylene oxide, and material was included in Spurr resin, according to the technique described in Watanabe & Yamada (1983). An Ultra-Cut Reichert ultramicrotome with a glass cutting blade was used to make thick cuts (0.5 mm thick). These sections were then stained with toluidine blue solution, and these samples were observed under an optical microscope to locate the groups of cells. The Ultra-Cut Reichert ultramicrotome was used with

a diamond cutting blade to make ultrathin cuts (90 nm thick). Ultrathin slices were mounted on 200 mesh Formvar films and coated with uranyl acetate and lead citrate (Watanabe and Yamada, 1983). These samples were examined using a *Jeol 1010* transmission electron microscope at 80 kV. The experiments were conducted at the Institute of Biomedical Sciences of the University of São Paulo, by Prof. Dr. II-Sei Watanabe.

3.2.8. Confocal Microscopy

The autofluorescence micrographs of lipofuscin were obtained from a *Zeiss Axiovert 200 LSM 510-Meta* laser scanning confocal microscope, equipped with a Plan-APOCHROMAT 63X/1.40 DIC M27 oil immersion objective (Zeiss). Nuclei were labeled with DAPI and lysosomes with *LysoTracker Green* (LTG) (Life Technologies). The autofluorescence of lipofuscin was detected after excitation with blue light and use of longpass filter for red (630 nm).

3.2.9. Fluorescence Lifetime Imaging Microscopy (FLIM)

For fluorescence lifetime images, a confocal microscope *MicroTime 200* (PicoQuant, Berlin, Germany) was used. The *MicroTime 200* consists of an inverted microscope (IX 73, Olympus) equipped with an Olympus UPlanSApo 60×/ NA 1.2 water immersion objective, a set of ps-pulse diode lasers (LDH-PC-405/509/650, PicoQuant, Berlin, Germany). We operated at 509 nm with a pulse of <64 ps as the source of excitation. The laser beam was directed at the microscope objective using a z485/640rpc dichroic mirror (AHF Analysentechnik, Germany). Fluorescence was directed through a 50 µm

pinhole and detected with a single-photon avalanche diode (SPAD, SPCM-AQR-13, Perkin Elmer, Waltham, USA). To capture the fluorescence and reject the excitation light, a 519LP longpass filter was used (AHF Analysentechnik, Germany). Time-resolved recordings were made in single-photon counting mode using the *TimeHarp 260 PICO* platform (PicoQuant, Berlin, Germany). For the experiments, the laser power was adjusted to reach a count $\leq 10^5$ photons / second, avoiding an overload in the TCSPC electronic system. The images were acquired by scanning the "xy" axes using the piezo positioned (PhysikInstrumente, Karlsruhe, Germany) of the MicroTime 200. The acquisition of the images and the analysis were done using the *SymPhoTime64* software version 2.1.3813, where all the photons collected in the image were used to constitute the global histogram of the fluorescence decay fitting.

3.2.10. Measurement of singlet oxygen

Measurements of singlet oxygen ($^1O_2$) were performed in an instrument designed to measure the near-infrared (NIR) luminescence emission, implemented by *Edinburgh Analytical Instruments*, with a Hamamatsu R55009 photomultiplier (Hamamatsu, Japan) cooled with a liquid nitrogen based cooling system (Bridgewater, NJ). Laser excitation was performed with an OPO (Quantel Laser Brilliant, 3W, Rainbow OPOTEC) at 422 nm, delivering 5 ns pulses at 10 Hz, 2 mJ/pulse. In addition to the spectral selection by monochromator, a 1270 nm bandpass filter was placed between sample and monochromator entrance slit. Phosphorescence decays were obtained with MSA_300 (Becker & Hickel, Berlin, Germany) and spectra were obtained with the *Edinburgh Instruments* acquisition platform with *F900* software. Lifetimes

were analyzed in *F900* software, with exponential fitting. The choice of the excitation wavelength was based on the excitation spectra observed in HaCat cells with accumulation of lipofuscin by fluorescence microscopy. For the experiment of quantification of generation of $^1O_2$ in HaCat cells loaded with lipofuscin, 48h after treatment with DMMB, 2 x 10^5 cells / well were plated in 6 wells plates. Treatment with DMMB and irradiation with red LED (λ = 633 nm) were done according to standard methods, as described above. The cells were trypsinized with 500 µL of trypsin-EDTA for 5 minutes after incubation with PBS-EDTA for 10 min at 37 ° C. Then, cells were resuspended with 1 mL of PBS-EDTA and cells were transferred to 1.5 mL microcentrifuge tubes and collected by centrifugation at 4,000 rpm for 5 min at 4°C. The supernatant was discarded, keeping the cells on ice until resuspended in 0.9% NaCl in deuterated H_2O (D_2O), prepared at the time of the experiment. The generation of $^1O_2$ was performed obtaining the phosphorescence decay spectrum (peak at 1270 nm), exciting cells at 422 nm, after performing a sweep in visible spectrum to find the lambda of higher generation of $^1O_2$.

3.2.11. Isolation of fraction enriched in lipofuscin

We performed a simplified protocol based on isolation of lipofuscin granules from RPE cells by Boulton & Marshall (1985). We seeded 2 x 10^6 cells in 100 mm culture dish plate (two plates for dark control and lipofuscin-loaded), performing, in the next day, the protocol of DMMB treatment + red light. Fourty-eight hours after treatment, cells were trypsinized, neutralized in DMEM 10% and collected by centrifugation at 300 g, 5 min, 4ºC. Cells were resuspended in PBS and collected again by centrifugation and lysed in cool PBS containing

inhibitor protease cocktail (1:100), rupturing the cells using Potter-Elvejem performing ten up-and-down strokes on ice. The lysate was centrifuged at 60 g, for 7 min, 4ºC, to remove cell debris, saving the supernatant which was centrifuged at 6,000 g, for 10 min, 4ºC, resulting in a pellet enriched in pigment granules.

3.2.12. Emission spectrum of lipofuscin fraction

Fluorescence emission spectra of fraction enriched in lipofuscin, generated from DMMB treatment + red light, and dark control without lipofuscin were measured in a range of 390 to 800 nm, exciting samples from 390 to 610 nm, in intervals of 20 nm, using a *Cary Eclipse* spectrofluorimeter (*Agilent Technologies*, USA). Pellets enriched in lipofuscin were resuspended in PBS and fluorescence measured in a quartz cuvette (500 µL), excitation light was selected via monochromator, and the emission was detected by a photomultiplier (PMT). Analyzing all the emission spectrum, we observed a higher difference in emission at 640 nm, thus, we subtracted the dark control spectrum from the lipofuscin spectrum to obtain the emission spectrum of fraction enriched in lipofuscin.

3.2.13. Comet assay

HaCat cells were plated 2 x 10^5 cells per well in 6-well plate. The next day, the cells were treated with DMMB and irradiated with red light, as described above. Fourty-eight hours after this treatment, the cells were irradiated with blue light (LED λ = 466 nm, 100 J.cm^{-2} dose) for lipofuscinogenesis. After irradiation, the cells were trypsinized with 300 µL of

trypsin, resuspended with 300 µL of PBS-EDTA. A volume of 30 µL of this cell suspension was mixed with 100 µL of 0.5% LMP agarose in PBS, distributed over 1.5% agarose precoated slides in PBS and covered by coverslips. For agarose solidification, the slides were incubated in the refrigerator (2-8°C) for 15 minutes, protecting them from light, to avoid further DNA damage. The coverslips were gently removed, and the slides were incubated in alkaline lysis solution (2.5 M NaCl, 0.1 M EDTA, 0.01 M Tris, 1% Triton X-100, pH 10) for at least 12 hours. After incubation in lysis buffer, the slides were treated with 0.2 U of the Fpg and Endo III enzymes (Sigma-Aldrich, USA) in buffer composed of 0.1 M KCl, 0.5 mM Na_2EDTA, 40 mM HEPES, 2 mg/mL BSA, pH 8 (20 µL for each coverslip region) for 30 minutes at 37°C. Subsequently, the slides were washed (three times for 20 minutes) in electrophoresis buffer (30 mM NaOH, 2 mM Na_2EDTA, pH 12.3) and incubated in that buffer at 4°C for 30 minutes, denaturing the DNA in the dark. Electrophoresis was performed with 25 V, 300 mA for 25 minutes in a cold chamber, with a buffer covering 1-2 mm above the agarose. After electrophoresis, the slides were washed and neutralized in distilled water for 5 minutes three times. Slides were allowed to dry in an inclined position and fixed in ethanol for 15 minutes, and stored for further analysis. For the analysis, slides were stained with 100 µL of ethidium bromide stock solution, and covered with a coverslip, allowed to incubate for 5 minutes, followed by analyzing the slides one by one and visualizing in a fluorescence microscope, exciting the sample in the range of 515-560 nm, and capturing the fluorescence using a 590 nm longpass filter. Using the *Komet* software (*Andor*, Belfast, NIR), we analyzed 50 cells in a 250x magnification.

3.3. RESULTS AND DISCUSSION

Several techniques have been widely used to detect lipofuscin in cells and tissues. Most of the methods are based on fluorescent properties of this pigment allowing detection by fluorescence microscopy, fluorescence spectroscopy, and fluorescence activated cell sorting (FACS) (Jung, Höhn and Grune, 2010). Lipofuscin granules can also be stained by Sudan Black B, a lipophilic histochemical dye, which is considered as a reference staining to indicate senescence, replacing the classical assay of β-galactosidase activity, which shows false positives (Georgakopoulou *et al.*, 2013). Here, we have used several fluorescence techniques to verify and quantify lipofuscin accumulation in keratinocytes 48 hours after photodamage.

In order to start the characterization of lipofuscinogenesis by the treatment with DMMB and red light, 48 hours after irradiating cells previously incubated with DMMB, we performed FACS analysis by gathering emission in the green fluorescence channel, which is capable to detect the red fluorescence emission of lipofuscin (excitation at 488 nm). DMMB is a dye that has small levels of fluorescence (Martins et al. 2018, *Autophagy*, accepted), but since it is used under very low concentration regimes (nM), we do not expect to have interference due to the fluorescence emission of the dye. Indeed, note in figure 3.2 that cells treated with DMMB + LIGHT have a substantial red fluorescence emission compared to control cells (DMMB): 58.6% (Q2+Q3) in DMMB + LIGHT and only 28.5% in DMMB control. Note also that almost 36% of the treated cells which are emitting in the red have larger cell size (Q2) (Figure 3.2). Also, by comparing HaCaT cells treated with DMMB, irradiated or not, and labeled with LTR, we were able to show a clear correlation between fluorescence emission

of lipofuscin and the amount of acidic vacuoles labeled with LTR in cells treated with DMMB + LIGHT (Figure 3.4). Note that 45.4% (compared with 28.1% in the control) of the treated cells showed an increase in lipofuscin autofluorescence in cells that also accumulate acidic vacuoles. These data are corroborated with acridine orange staining, detecting the accumulation of acidic vacuoles in HaCaT cells treated with DMMB + LIGHT, 24 hours after irradiation with red light (see Figure 4.2, in *Chapter 4*). This correlation is in agreement with the proposed mechanism of lipofuscin accumulation, which is the lack of digestion capability of lysosomes, causing the accumulation of acidic vacuoles because they are not anymore able to digest the oxidized products, providing conditions for lipofuscinogenesis. The photosensitization of DMMB causes the mitophagy and inhibition of the autophagic flux, due to damages in lysosome, accumulating oxidized molecules in these vacuoles, forming consequently the lipofuscin (Martins et al. 2018, *Autophagy*, accepted).

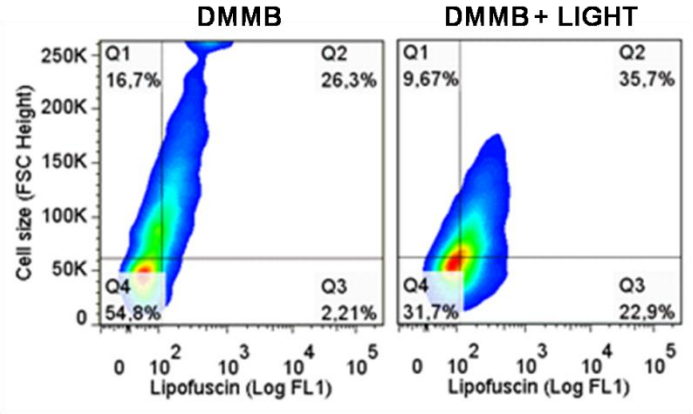

Figure 3.2. Autofluorescence of lipofuscin increasing related to increasing in FCS. FACS of HaCaT cells treated with DMMB 48 hours after irradiation with red light (λ = 633 nm). DMMB = dark control, treated with DMMB, but not irradiated; DMMB + LIGHT = cells treated with DMMB and irradiated with red light.

Cells that have blockage in the autophagic flux also have an increase in cellular size, besides the accumulation of acidic vacuoles. Figure 3.2 shows

the flow cytometry plots of cell size (FCS) as a function of level of acidic vacuoles, i.e., LTR-labeled acidic vacuoles were plotted versus the FSC parameter (forward scattering) in cells 48 hours after photosensitization (Figure 3.3) shows the number of events for autophagic vacuoles was higher in DMMB + LIGHT + LTR cells (HaCaT cells treated with DMMB + LIGHT and labeled with LTR) compared to the cells treated with DMMB + LTR (non-irradiated control): sum of Q6 + Q7 in the "DMMB + LTR" = 48.7%; sum of Q6 + Q7 in "DMMB + LIGHT + LTR" = 58.4%. Therefore, accumulation of acidic vacuoles occurs preponderantly in cells with increased size (FCS) (Figure 3.3).

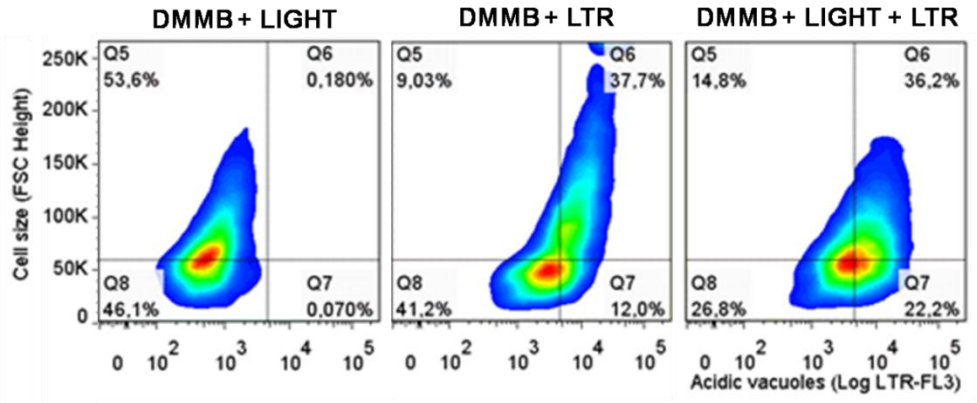

Figure 3.3. DMMB-treated HaCaT cells 48 hours after the exposure to red light (λ = 633 nm), accumulating acidic vacuoles, which are labeled with LysoTracker Red (LTR), and associated with increasing in cell size. DMMB + LTR = DMMB-treated, but not exposed to red light, and labeled with LTR; DMMB + LIGHT = DMMB-treated and irradiated with red light; and DMMB + LIGHT + LTR = DMMB-treated, irradiated with red light and labeled with LTR.

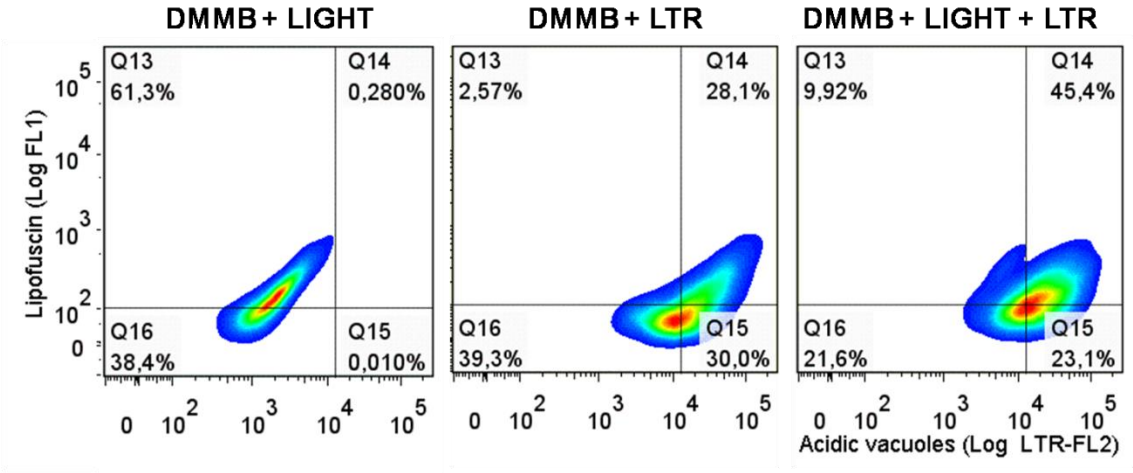

Figure 3.4. HaCaT cells treated with DMMB + red light (λ = 633 nm) show, 48 hours after the irradiation, a positive relation between lipofuscin autofluorescence and acidic vacuoles accumulation. DMMB + LTR = dark control, treated with DMMB and labeled with LTR; DMMB + LIGHT = treated with DMMB and red light, but without LTR labeling; DMMB + LIGHT + LTR = cells treated with DMMB, irradiated with red light, and incubated with the LTR.

Lipofuscin accumulates as cytoplasmic granules (Brunk and Terman, 2002a; Höhn *et al.*, 2010) and our next goal was to visualize the existence and the sub-localization of lipofuscin granules in HaCat cells treated with DMMB and irradiated with red light. For this purpose, we performed several microscopic analysis: (i) Transmission electron microscopy (Figure 3.5): direct observation of characteristic lipofuscin granules with typical perinuclear cellular sub-localization (lysosomes, mitochondria, cytoplasm); (ii) Fluorescence confocal microscopy (Figure 3.6): co-localization of lysosomal labeling and autofluorescence of lipofuscin; (iii) Fluorescence lifetime microscopy (FLIM) (Figure 3.7, 3.8): characterization of the presence of the granules by the lipofuscin fluorescence lifetime.

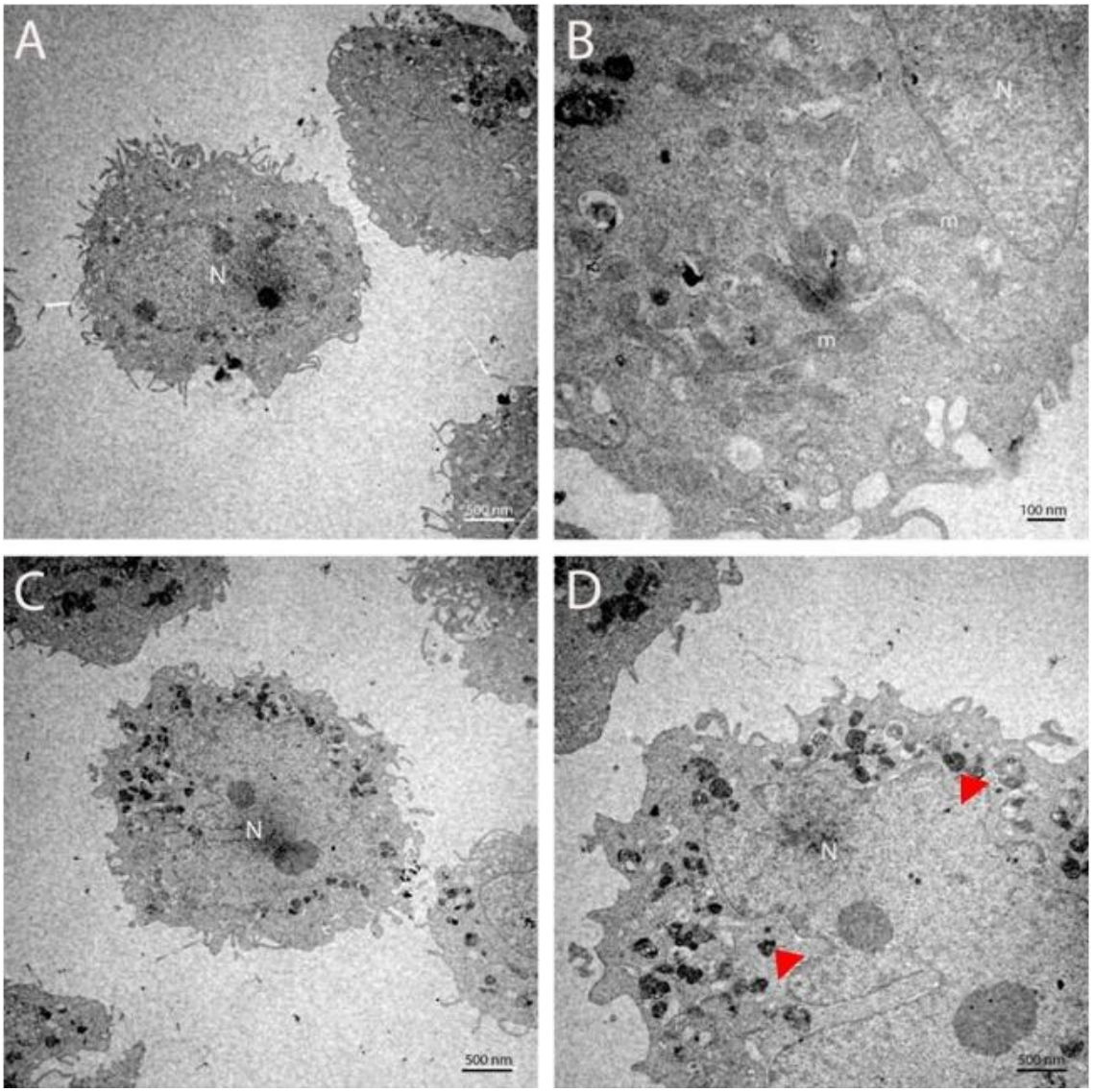

Figure 3.5. Electron micrograph of transmission of HaCat cells post-48h of induction of lipofuscinogenesis by irradiation of DMMB-treated cells with red light at the dose of 11 $J.cm^{-2}$. **(a)** Dark control treated with DMMB. **(b)** mitochondrial network (m = mitochondria) of dark control cells treated with DMMB. **(c)** Irradiated cells treated with DMMB. **(d)** Lipofuscin granules, indicated by red arrows, located in perinuclear region (N = nucleus).

When we compared the lipofuscin yield generated by DMMB + LIGHT protocol with the UVA-treatment (Figure 2.1, *Chapter 2*), using TEM micrographs, a mean value of lipofuscin granules was two-fold higher in DMMB + LIGHT protocol than UVA-treatment (Figure 3.6). This is probably a result of the specific damage in lysosomes and mitochondria differently than generic

lesions promoted by UVA exposure, and less specific as the pathway of synthesis reactions of lipofuscin.

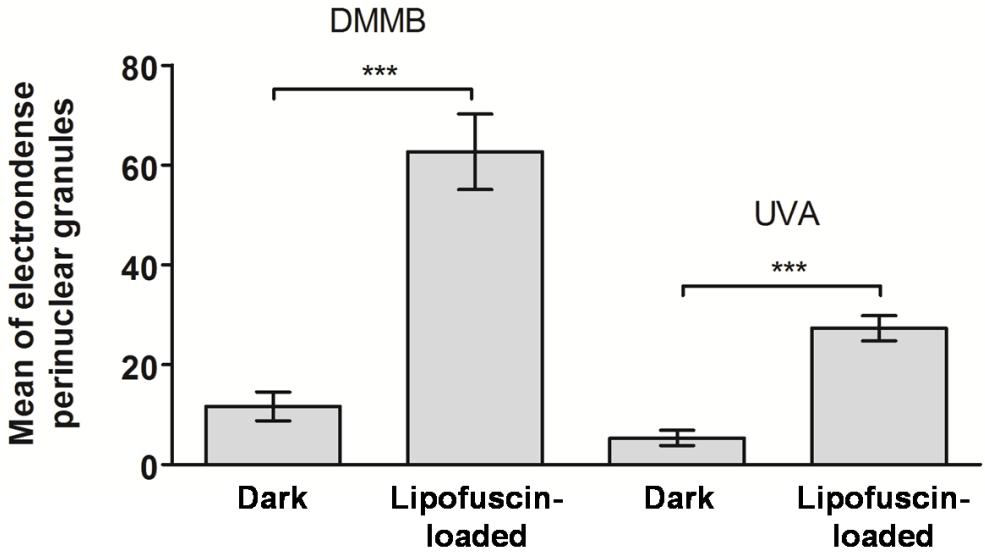

Figure 3.6. Number of electrondense granules in perinuclear region in HaCaT cells using the DMMB-treatment + red light protocol is much higher than UVA-treatment protocol (showed in *Chapter 2*). Mean number of electrondense granules in perinuclear region visually counted (n=3, from different TEM micrographs) ± standard deviation. Statistical analysis was performed using t-test, $p<0.001$ (***).

In order to identify the subcellular localization of lipofuscin granules, we performed a co-localization protocol using the lysosomal specific labeling fluorophore *LysoTracker Green* (LTG). Indeed we observed the perinuclear autofluorescence colocalization between lipofuscin (red) and the green fluorescence in lysosomes labeled with LTG (Figure 3.7 b,c). Dark control cells, as expected, did not show red autofluorescence for lipofuscin (Figure 3.7 a). An interesting result was that with the addition of the Fe^{2+} chelator, deferiprone, lipofuscinogenesis was repressed (Figure 3.7 d), indicated by the absence of lipofuscin autofluorescence - similar to that of dark control cells (Figure 3.7 a).

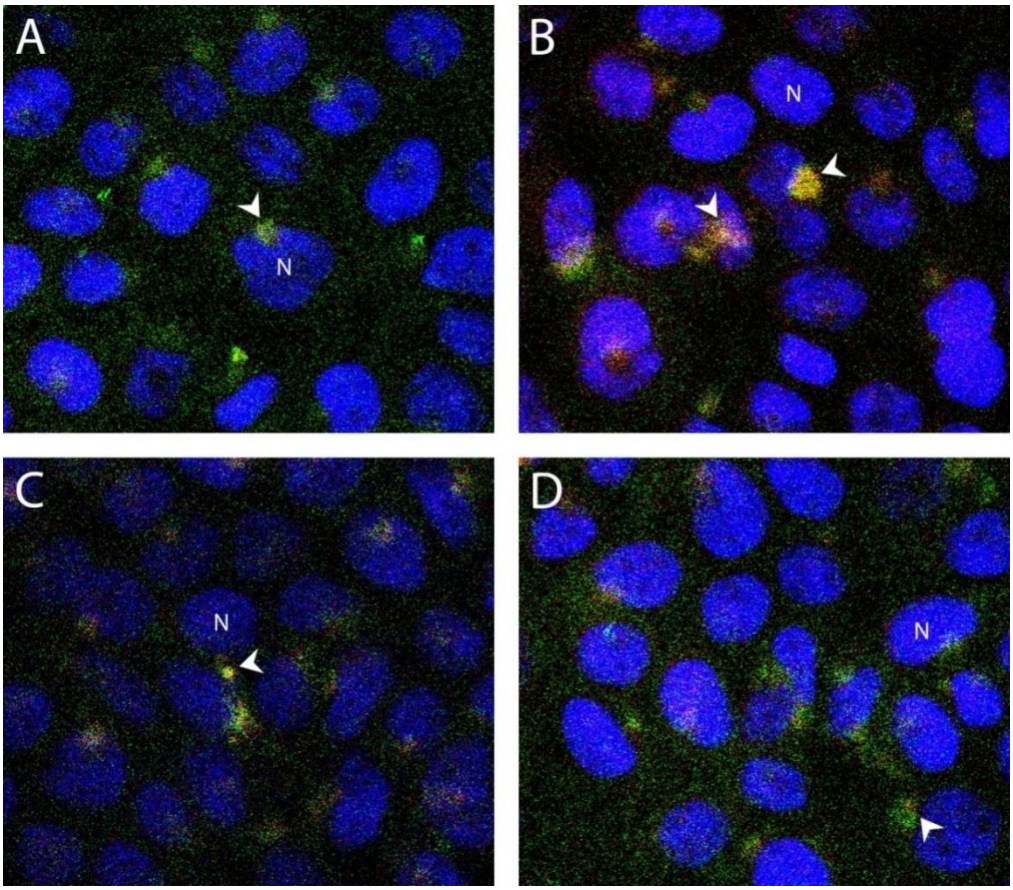

Figure 3.7. Confocal fluorescence microscopy of lipofuscin-loaded HaCaT cells 48h after the DMMB-treatment + red light. Lysosomes were labeled with *Lysotracker Green* and lipofuscin autofluorescence was recorded using a red-emission filter. Nuclei (N) were stained with DAPI. **(a)** Dark control. White arrow indicates labeled lysosomes in the perinuclear region. **(b)** Cells irradiated with red light. White arrows indicate colocalization of lysosomes (green) and lipofuscin (red), resulting in the yellow regions of the micrograph. **(c)** Cells irradiated with red light, located in distinct coverslip from figure "b". **(d)** Cells irradiated with red light and incubated in medium containing deferiprone. White arrows indicate lysosomes. Magnifying 63x.

The fluorescence lifetime of a fluorophore is defined as the time it takes for a 1/e fraction of a population of molecules in the excited state to return to the ground state (presuming a mono-exponential decay process). This characteristic time depends on the nature of each molecule and its microenvironment (Trautmann et al, 2013). Thus, using FLIM (Figure 3.8), we observed a homogeneous lifetime of fluorescence decay for lipofuscin granules in DMMB-treated and chloroquine-treated cells (Figure 3.8 b-d). In these

micrographs, on the upper right, there is a grey scale of fluorescence intensity and on the lower right there is a colored scale of fluorescence lifetime. The estimated fluorescence lifetime for lipofuscin in keratinocytes was 2 ns, which is near the value found in the literature for lipofuscin granules in RPE cells (1.7 ns) (Yakovleva *et al.*, 2017).

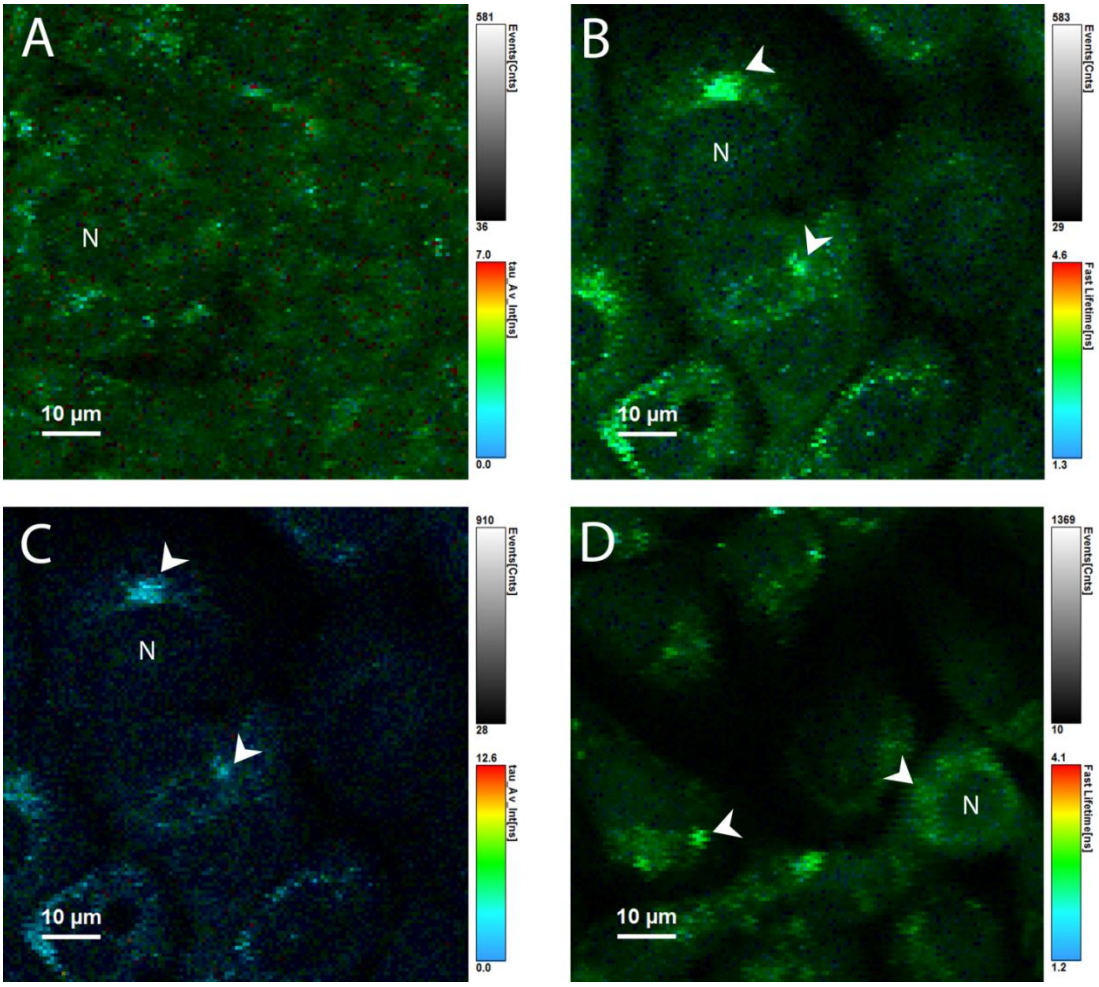

Figure 3.8. Fluorescence lifetime imaging microscopy of lipofuscin-loaded HaCaT cells, 48 hours after the DMMB-treatment + red light (λ = 633 nm, 11 J. cm^{-2}). **(a)** Fast FLIM analysis of dark control cells. Note the nucleus (N) and the absence of accumulation of lipofuscin perinuclear granules. **(b)** Fast FLIM analysis of irradiated cells. **(c)**Fit FLIM analysis of irradiated cells (same position of "b"). **(d)** Fast FLIM analysis of lipofuscin-positive control cells after 48 hours of treatment with 60 µM chloroquine. White arrows indicate perinuclear accumulation of lipofuscin granules. Excitation at 509 nm using a longpass filter with cut at 630 nm.

We have shown that lipofuscin-loaded cells exhibit an increased phototoxicity when exposed to visible light, due to lipofuscin acting as a

photosensitizer in the visible light spectrum, generating singlet oxygen and other reactive species (*Chapter 2*, JID article). However, the experiments performed with UVA stimulation do not provide enough lipofuscin in order to study other properties such as its excitation spectra, action spectra of singlet oxygen generation ‘within the cells, i.e., which wavelength range in the visible light range is more efficient in generating intracellular damage.

Lipofuscin extracted from RPE cells is relatively well characterized. It has absorption peaks in ultraviolet range (280-330 nm) with emission in 570-605 nm range (Eldred and Katz, 1988; Eldred et al., 1982) and also absorbs blue light (λ= 420 nm), which also leads to the generation of singlet oxygen (Rózanowska et al., 1998). Similarly, lipofuscin from human skin keratinocytes, obtained in an enriched fraction of DMMB plus red light cells, showed clear maxima of excitation efficiency (by quantifying emission in the red, above 640 nm), the blue region between 430 to 490 nm (Figure 3.9).

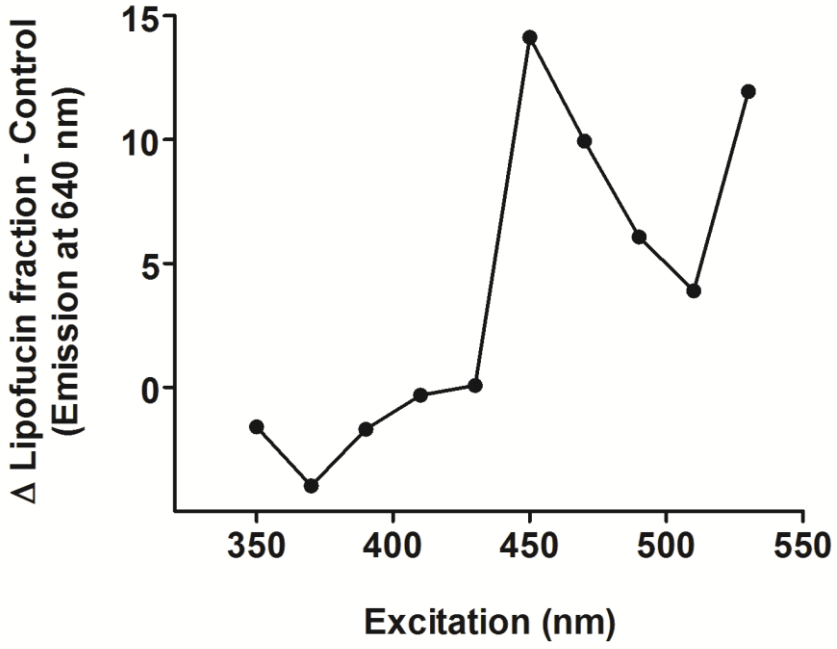

Figure 3.9. Excitation spectrum of fraction enriched of lipofuscin emitting at 640 nm, which was obtained subtracting the excitation spectrum of control cells (without lipofuscin) from fraction enriched in lipofuscin.

After investigating the effect of lipofuscin photosensitization on cell viability, we investigated the generation of singlet oxygen as soon as cells were exposed to blue light. For this purpose, we performed an excitation wavelength scanning with the lipofuscin-loaded cells, in order to obtain the highest intensity of singlet oxygen phosphorescence decay. Thereby, we found that excitation at 420 nm produced the best signal of phosphorescence intensity in lipofuscin-loaded keratinocytes (Figure 3.10).

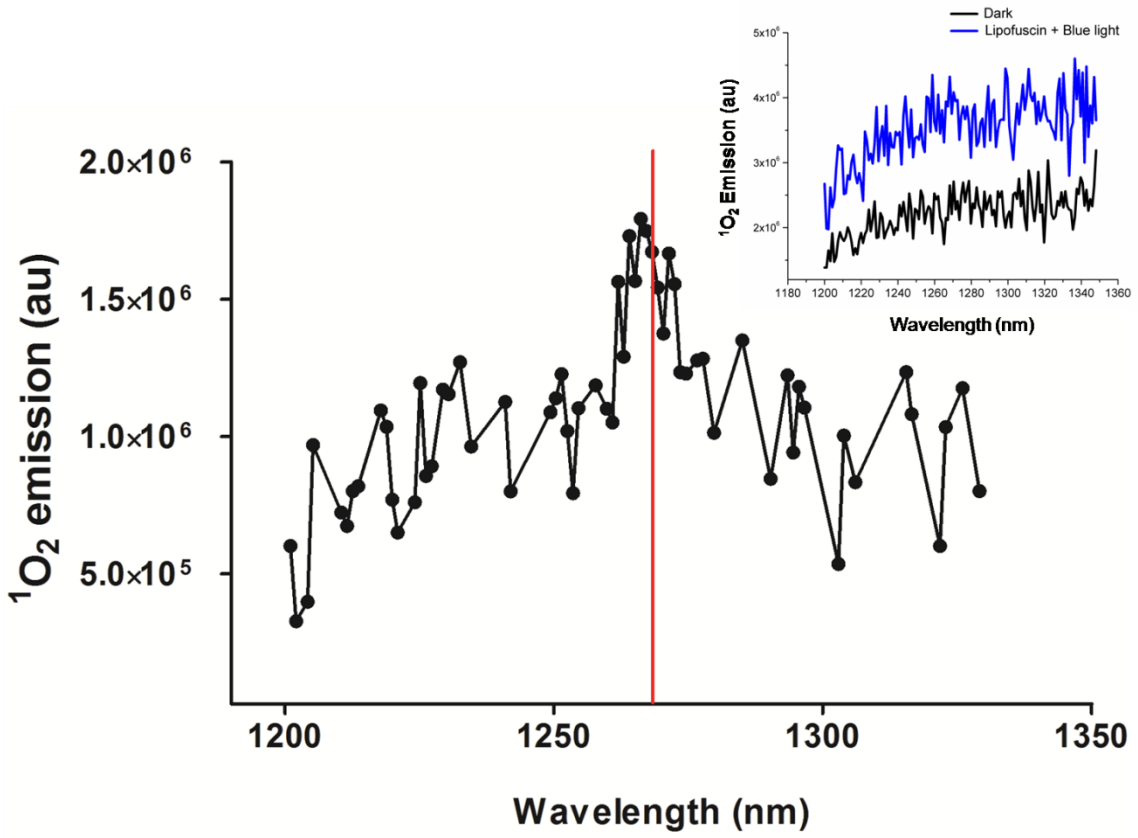

Figure 3.10. Phosphorescence intensity of singlet oxygen at 1270 nm (red line) in lipofuscin-loaded cells is higher than dark control cells when photosensitized with blue light (λ= 420 nm). The main graph corresponds to subtraction between lipofuscin-loaded cells and dark control, respectively. The upper graph, in insert, represents the lipofuscin-loaded cells (blue color) and dark control (black color) photosensitized with blue light.

In order to investigate which fraction of the visible light spectrum photosensitize lipofuscin from human skin keratinocytes, we initially generated lipofuscin in cells by exposing them with DMMB plus red light, wait 48 hours and then treated those cells with increasing doses of blue (λ= 466 nm, Figure 3.11) and green light (λ= 522 nm, Figure 3.12).

Lipofuscin-loaded cells exposed to blue light showed almost no response to the smaller doses of blue light but showed a substantial decrease in cell viability 24 hours after a dose of 100 J.cm^{-2} (Figure 3.11). Note that DMMB plus red light causes a substantial decrease in cellular viability by itself (column referred as “Red”), but blue light affects further cellular viability, especially at higher doses (subsequent columns) (Figure 3.11). As shown above (Figures 3.6-3.9), this treatment also led to the generation of lipofuscin. Lipofuscin accumulating in these cells absorbs blue light and facilitates the generation of singlet oxygen. Indeed, with the dose of blue light of 100 J.cm^{-2}, there is a decreasing around 50% in cell viability 24 hours after red light irradiation. As we will show in *Chapter 4* (Figure 4.1), HaCaT cells without lipofuscin exposed to the doses of blue light used in this experiment did not exhibit reduction in cellular viability 24 hours after irradiation.

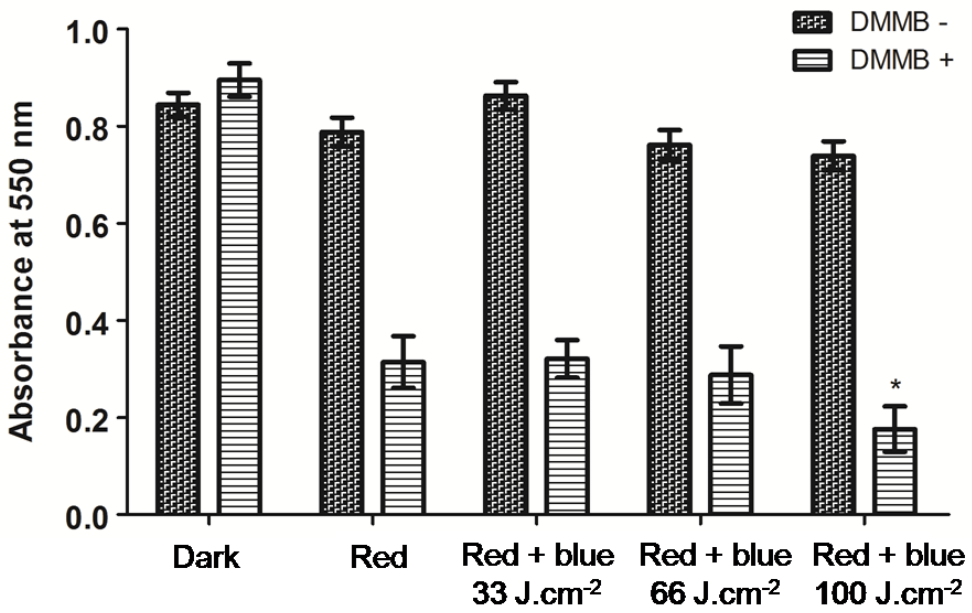

Figure 3.11. Cellular viability assay based on reduction of MTT was performed in HaCaT cells treated with DMMB, irradiated with red light, accumulating lipofuscin after 48 hours. Lipofuscin-loaded cells were photosensitized with increasing blue light doses, performing the MTT assay 24 hours after the blue light irradiation. Statistical analysis was performed using one-way ANOVA and post-test Holm-Sidak, $p<0.05$ (*).

The lipofuscin-loaded HaCaT cells were also exposed to increasing doses of 522 nm, in order to verify if lipofuscin is photosensitive to green light. Note that no significant alteration occurred in cellular viability when the lipofuscin-loaded cells were exposed to 522 nm (Figure 3.12). Therefore, irradiation of lipofuscin with green light does not seem to generate significant amounts of ROS – not leading to cell death. In fact, these data were corroborated by other techniques: (i) fluorescence microscopy, where lipofuscin is just detected using blue laser (450-490 nm) (*Chapter 2*); (ii) the excitation spectrum obtained in enriched fraction of lipofuscin, where there is a significant absorption only between 420 to 490 nm (Figure 3.9); (iii) the characteristic of phosphorescence emission of singlet oxygen is only detected after excitation of lipofuscin-loaded cells at 420 nm (Figure 3.10).

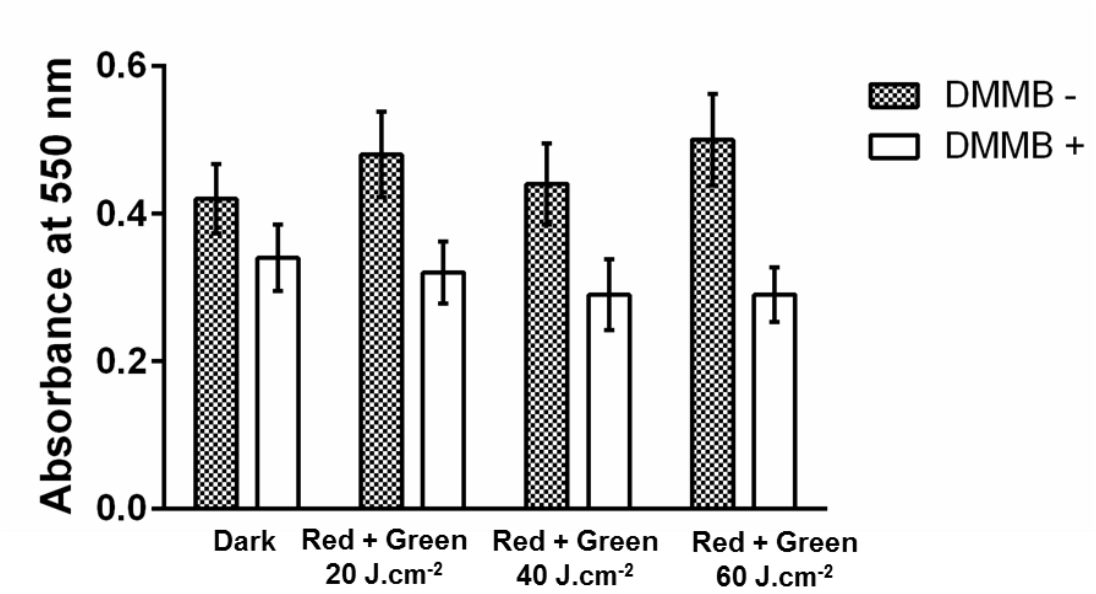

Figure 3.12. Cellular viability based on reduction of MTT in lipofuscin-loaded cells (DMMB +) 24 hours after the irradiation with increasing doses of green light (λ= 522 nm). Photosensitization of lipofuscin with green light did not reduce the cell viability. Mean (n=3) ± standard deviation.

In order to investigate whether blue light can lead to the increase in oxidative lesions of nuclear DNA, an isolated cell gel electrophoresis test (comet assay) was carried out in alkaline condition. We also used DNA glycosylase Fpg and endonuclease III in order to identify lesions originated directly from photoinduced oxidative reactions. The lipofuscin-loaded cells that were irradiated with blue light showed a significant increase in OTM in comet assay in the presence of Fpg (Figure 3.13). Fpg-DNA glycosylase recognizes mainly the 8-oxo-7,8-dihydro-guanine (8-oxo-dG), which is a DNA lesion generated by singlet oxygen. The 8-oxo-dG is a premutagenic DNA lesion, if not repaired, responsible for the transversion mutations (GC → TA) (Kino and Sugiyama, 2001) (Figure 1.9, *Chapter 1*).

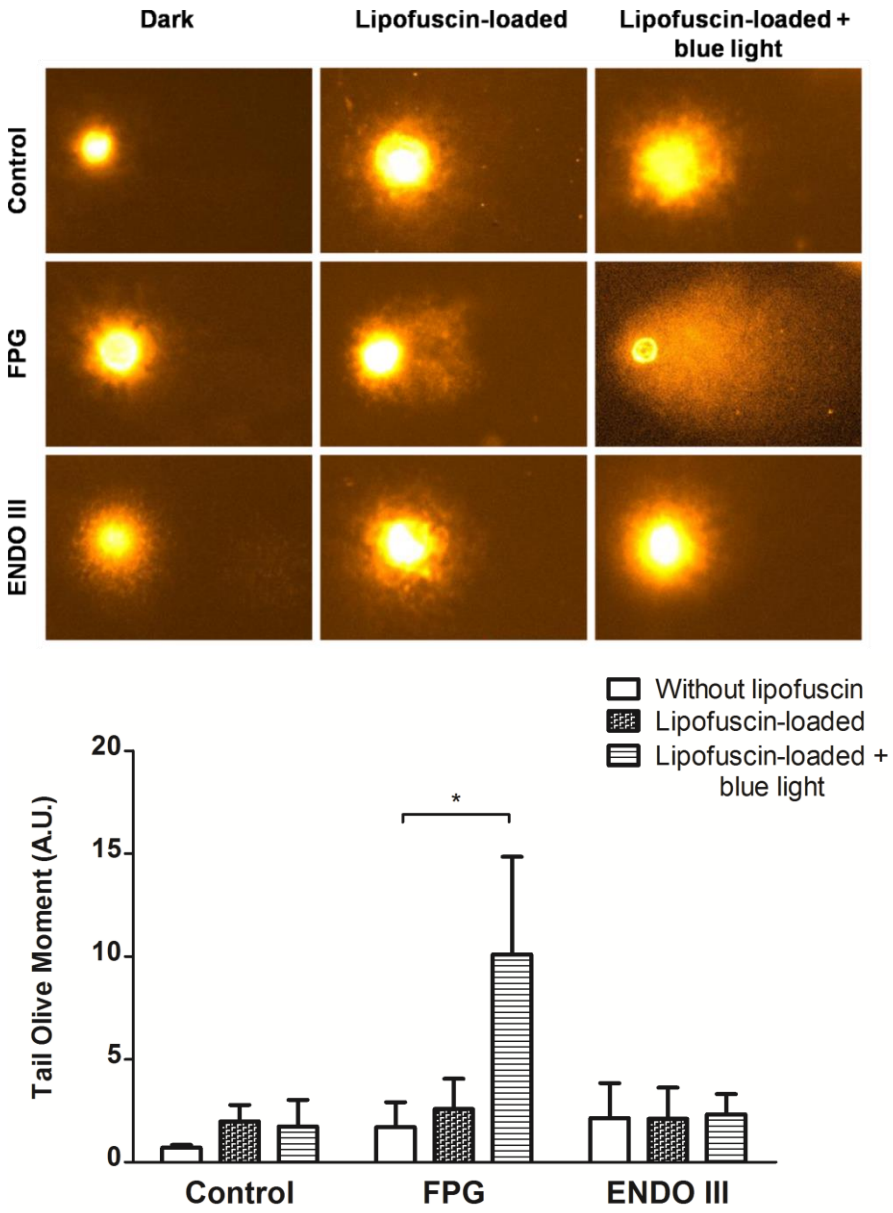

Figure 3.13. Photosensitization of lipofuscin by blue light generates increased oxidative modifications sensitive to Fpg. HaCaT cells 48 hours after the DMMB treatment were irradiated with blue light (λ = 466 nm, dose 100 J.cm^{-2}). Sites sensitive to Endo III did not present a significant increase in relation to control and Fpg. Statistical analysis was performed using one-way ANOVA and post-test Holm-Sidak, $p<0.05$ (*).

Another high mutagenic lesion that can be induced by photosensitization is the DNA double-strand breakage (Pfeiffer 1998). One of the defense mechanisms against this DNA lesion is the phosphorylation of H2AX histone, which is a component of the octamer in the nucleosomes in eukaryotic cells (Figure 3.14 a,b). Phosphorylation of histone H2AX is effected by ATM kinase

(ataxia telangiectasia mutated) and ATR (ATM-Rad3-related), being an early mechanism for recruiting DNA repair proteins (Hanasoge and Ljungman, 2007) (Figure 3.14 b). Thus, the detection of phosphorylation in histone H2AX is an evidence of double-strand breaks in nuclear DNA (Kuo and Yang, 2008). Lipofuscin-loaded HaCaT photosensitized with blue light (466 nm) at the dose of 100 J.cm^{-2} showed higher level of phosphorylation of histone H2AX at Ser139, 2 hours after irradiation. Interestingly, this result is correlated to immortalized human fibroblasts exposed to UV radiation, showing also a peak of H2AX phosphorylation 2 hours after irradiation (Hanasoge and Ljungman, 2007). The increase of H2AX phosphorylation in lipofuscin-loaded cells exposed to blue light was significant compared to dark control and non-irradiated lipofuscin-loaded cells (Figure 3.14 c).

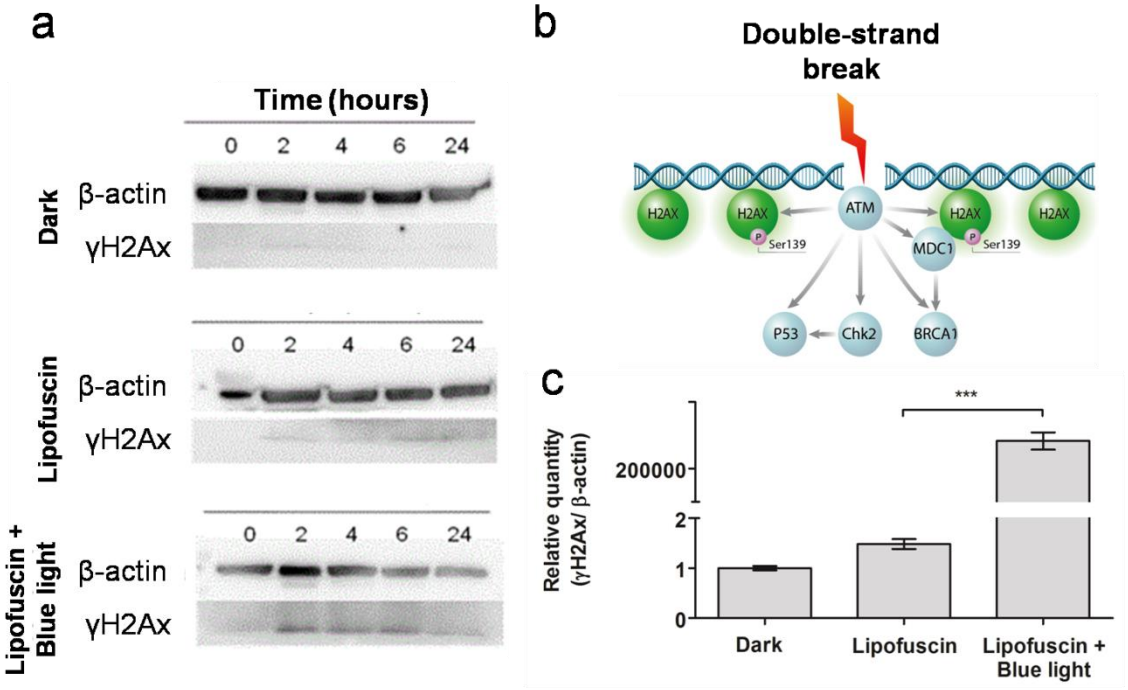

Figure 3.14. Lipofuscin-loaded cells, 2 hours after the exposure to blue light, increased the phosphorylation of H2Ax (γH2Ax), an indicative the occurrence of double-strand breaks in nuclear DNA due to oxidative stress induced by irradiation, compared to the dark control and lipofuscin-loaded cells. (a) Western blot to detect γH2Ax level, using the β-actin as loading control (20 µg total protein/well). (b) gamma-H2AX signaling in DNA double strand-break. Image taken from *Cisbio* homepage. (c) Graph corresponds to densitometry analysis at 2h point, using ImageJ. Statistical analysis was performed using one-way ANOVA, and post-test Holm-Sidak, p<0.001 (***).

3.4. CONCLUSIONS

By treating HaCaT cells with DMMB and irradiating in the red we were able to generate a large population of cells showing an accumulation of lipofuscin. Therefore, induction of lipofuscinogenesis using DMMB-treatment + red light is an effective protocol to study lipofuscin in a skin cell line, a basis for investigating its properties in tissue. We could then study with greater detail the properties of this aggregate. Below, we showed the main conclusions:

(a) Lipofuscinogenesis induced through DMMB-treatment plus red light is more effective in the generation of lipofuscin compared to the generic and nonspecific lesions generated by UVA due to specific damage in lysosomes and mitochondria;

(b) Lipofuscinogenesis is clearly induced in keratinocytes, which are the major component of the skin;

(c) The lipofuscin generated in keratinocytes absorbs blue light, emits in the red and can generate singlet oxygen.

(d) As a consequence keratinocytes accumulating lipofuscin become a lot more responsive to blue light in terms of having reduced viability and also DNA damage, but not to the green light.

Chapter 4 – Visible light (408 - 650 nm) and damage on lysosomes and mitochondria

4.1. INTRODUCTION

Constantly our skin cells suffer oxidative damage inducing a variety of processes, including those photochemically induced. Damaged organelles and molecules are continuously repaired and removed by an efficient mechanism of survival and turnover, which is named autophagy. Usually, during cell aging that occur as a consequence of the number of replication or oxidative stress, there is accumulation of the autofluorescent pigment, named lipofuscin (Figure 1.11, 1.12). We have demonstrated that UVA radiation generates lipofuscin in human skin keratinocytes (*Chapter 2*).

The mechanism of accumulation and damage amplification has been recently proposed by Brunk & Terman (2002), which have shown the roles played by both mitochondria and lysosome in the accumulation of lipofuscin. The authors have called this process the mitochondrial-lysosomal axis in aging of cells and accumulation of lipofuscin. Here, we ask if different wavelengths of visible light (i.e., high-energy blue (408 nm), blue (466 nm), green (522 nm), and red (650 nm) light) can damage lysosomes and mitochondria and trigger the formation of lipofuscin.

Mitochondria play a key role in the internal pathway of apoptosis in mammalian cells, releasing caspase activators, such as cytochrome c, changing the electron transport, dropping ATP production and loss of transmembrane potential (Green and Reed, 1998). Additionally, Terman et al.

(2006) introduced lysosomes as new player in the context of aging and apoptosis, proposing the existence of mitochondrial-lysosomal axis where cells accumulate lipofuscin, a subproduct of oxidized proteins, lipids and organelles (mainly damaged mitochondria). Lysosomal enzymes attempt to degrade lipofuscin, an indigestible material, decreasing the autophagy effectiveness, which leads to the accumulation of damaged mitochondria and increase in ROS production. The integrity of the lysosomal membrane is affected during oxidative stress conditions, releasing hydrolytic enzymes in the cytosol, promoting apoptotic or necrotic death, depending on the magnitude of insult (Serrano-Puebla and Boya, 2015). Lysosomal rupture can start apoptosis by releasing cytochrome c by mitochondria, which activate caspases (Terman et al. 2006).

In a recent paper, our group has shown that lipofuscin accumulation and cell aging can be catalyzed by the parallel damage in the membranes of these two organelles, i.e. lysosomes and mitochondria (Martins *et al.*, 2017). Lamore & Wondrak (2012) reported the inactivation of cathepsin B activity in human dermal fibroblasts, after chronic exposure to noncytotoxic doses of UVA (9.9 $J.cm^{-2}$, twice a week, three weeks), being a novel molecular mechanism involved in skin photodamage induced by UVA. They have shown that UVA damages lysosomes leading to lipofuscin accumulation two days after photodamage.

During a long time, lipofuscin has been reported to absorb visible light in retinal pigment epithelial cells, especially blue light, generating ROS, damaging these cells, leading to macular degeneration, cell death and loss of vision.

We have recently shown (*Chapter 2*) that UVA-induced accumulation of lipofuscin makes keratinocytes photosensitive to visible light. The mechanism of

lipofuscin accumulation is correlated with damages induced by UVA, which are mainly due to the photosensitization effect of flavins and flavin proteins (Baier *et al.*, 2006). Blue light was shown to play a role in light-induced oxidative stress in skin cells (Nakashima, Ohta and Wolf, 2017). However, it is not evident that blue light will lead to lipofuscin accumulation in keratinocytes, similarly as we have shown for UVA (*Chapter 3*). Also, it is not clear which component of visible light will lead to damages in mitochondria and lysosomes, ultimately leading to the accumulation of lipofuscin.

In this way, we have investigated the effects of photosensitization with different wavelengths of visible light in HaCaT cells, focusing mitochondria and lysosome integrity, as well as induction of lipofuscinogenesis, a hallmark of cell aging. Thus, we aim to investigate if visible light is involved in photodamage and aging of human skin keratinocytes.

4.2. MATERIALS AND METHODS

4.2.1. Cell culture

Human skin immortalized keratinocytes cells (HaCaT) (Boukamp et al., 1988) were cultivated in Dulbecco Modified Eagle Medium (DMEM), supplemented with 10% fetal bovine serum (FBS), 4 mM L-glutamine, 100 U/mL penicillin and 100 µg/mL of streptomycin, in 5% CO_2 at 37ºC.

4.2.2. Irradiation of cells

HaCaT cells were exposed to different wavelengths of visible range, using LED sources with peaks at 408, 466, 522, and 650 nm (Figure 4.1).

Doses were determined based on clonogenic assays, using those where survival fraction was approximately 50%. Measurements of the power were made using a Laser Power Meter (*Coherent Inc.*, Santa Clara, CA, US), using a silicon power sensor for visible range (LM-2 Vis, 1061323), putting a piece of polypropylene lid of culture plate to take into account the effect of this material (in the form of the culture plate material) on light dose.

High-energy blue light LED array, a set of 24 blue LEDs arranged in a 6x4 grid, with peak at 408 nm and irradiance equal to 4.77 $mW.cm^{-2}$ in center of LED array, was made by Optics and Photonics Research Center, Institute of Physics, University of São Paulo, São Carlos, Brazil. Cells were irradiated from bottom, during 2h50min (dose of 50 $J.cm^{-2}$) in culture plates, controlling the temperature around of 30ºC through a cooler installed on LED array.

Blue light LED array, containing a set of 12 LEDs in a 3x4 grid, with peak at 466 nm, and irradiance of 20.40 $mW.cm^{-2}$ at center of LED array, was constructed in a homemade way in our laboratory. Cells were irradiated on sulfite paper, during 1h30min (dose of 100 $J.cm^{-2}$), and the temperature was kept around 25ºC during irradiation.

The green and red light LEDs array were made by *Ethik Technology* (Sao Paulo, Brazil), arranged inside of an irradiation chamber system with control for temperature, time, and light intensity. For these experiments we used the maximum light intensity, maintaining the temperature at around 25ºC.

The green light LED array has a peak at 522 nm, 72 green LEDs arranged in a 18x4 grid. To diminish the time of irradiation (2h30min) we elevated the irradiation surface by 5 cm, reaching an irradiance of 8.67 $mW. cm^{-2}$ in the center of LED array.

The red light LED array with a peak at 650 nm, arranged in 12x4 grid, was elevated by 1.25 cm from the normal irradiation surface, reaching an irradiance of 23.47 $mW.cm^{-2}$ in the center of the LEDs array, irradiating cells during 1h18min.

The maximum dose of 100 $J.cm^{-2}$ is the higher used in our experiments due to limitation in irradiation time and absence of optimal conditions for the culture.

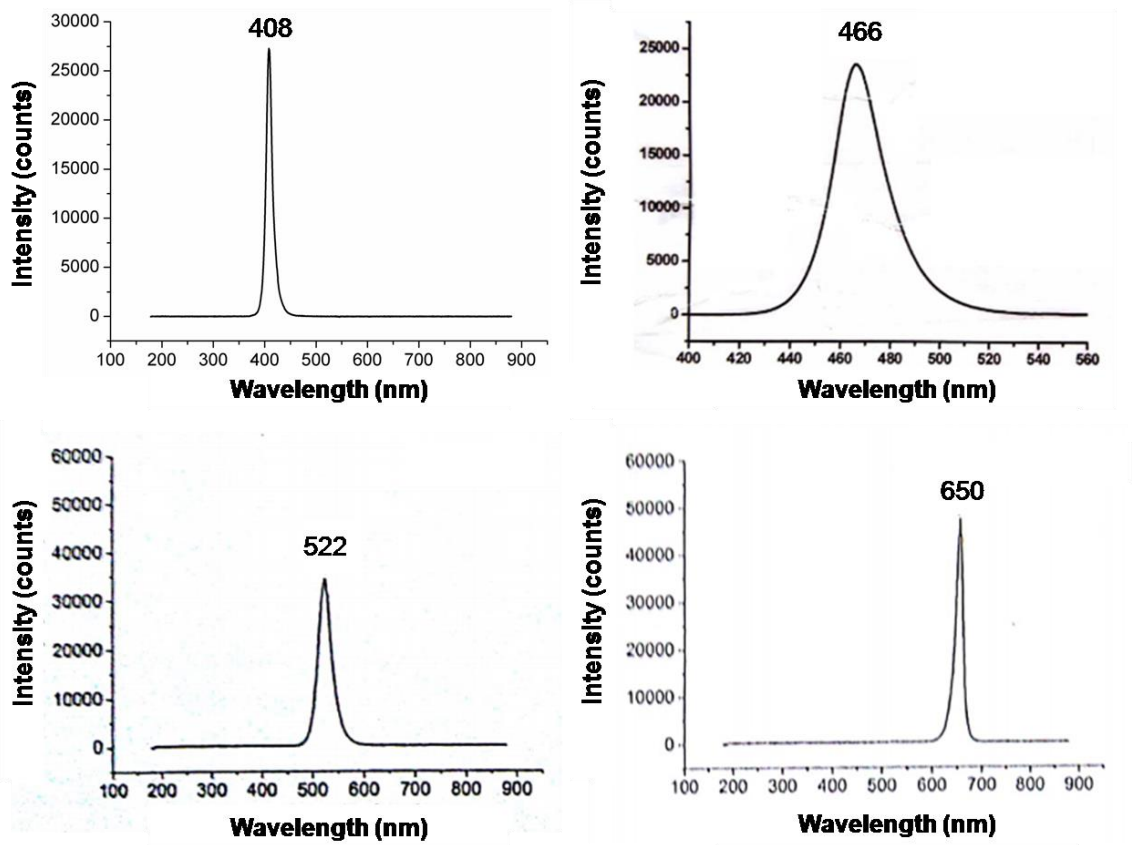

Figure 4.1. Emission spectrum of LEDs (408, 466, 522 and 650 nm) used in the experiments of irradiation in HaCaT cells.

4.2.3. Acridine orange staining

To detect the acidic vacuoles accumulation in HaCaT cells 24 hours after exposure to different visible wavelengths, cells were incubated with 1ug/mL of Acridine Orange in PBS, for 10 min, 37ºC, 5% CO_2, washing twice with PBS.

Slides were prepared with PBS and analyzed in fluorescence microscope, using filter 09 Zeiss.

4.2.4. Sudan Black B (SBB) staining

We stained HaCaT cells with SBB, as described previously (*Chapter 2*), fourty-eight hours after exposure to different visible wavelengths to verify lipofuscin accumulation. To analyze the number of particles, we performed the command “analyze particles” on *ImageJ*, considering circularity between 0.5 to 1, measuring particles in the entire image, which was previously converted to 8-bit for data processing. The threshold was adjusted to “red”, getting the mean values from five images. Data were plotted in relation to dark control and statistical analysis performed using *SigmaStat*.

4.2.5. Long Extension-Polymerase Chain Reaction (LX-PCR)

This technique was performed according to Kovalenko & Santos (2009) with minor modifications. The DNA was isolated using *DNeasy Blood and Tissue kit* (*Qiagen,* Germany), according to manufacturer’s recommendations. For the reaction, we used the *AccuPrime Taq DNA Polymerase* kit (*ThermoFisher Scientific*, 12339016), with a final reaction volume of 50 µl, consisting of: 5 µl 10x Buffer II, 10 pmol of each primer (Table 1), 30 ng for mtDNA and 120 ng for nuclear DNA, 0.2 µl Taq DNA polymerase. The reaction was initiated by hot start of the reaction at 94°C, for 30 seconds. For the amplification of the long mtDNA fragment (16.3 kbp), 26 cycles of denaturation at 94°C for 30 s, annealing at 60°C, for 30 seconds, and amplification at 68° C, for 18 min.

4.2.6. Polymerase chain reaction of short fragments

For PCR, the *Platinum PCR Supermix kit* (*ThermoFisher Scientific*, 12532016) was used in an assay consisting of 45 ul *Platinum PCR Supermix*, 200 nM of the primers (ND1 forward, ND1 reverse) (Table 1), 3 ng of DNA. Twenty-five cycles (94°C, 30"/56°C, 30"/72°C, 1") were performed with initial activation of Taq polymerase through a hot start (94°C, 2').

Table1. Primer sequences used in PCR to detect lesions on mitochondrial DNA, shortly after exposure of HaCaT cells to different visible wavelengths

Primer	Sequence (5'→3')
LongmtDNAForward	TGAGGCCAAATATCATTCTGAGGGGC
LongmtDNA Reverse	TTTCATCATGCGGAGATGTTGGATGG
ND1 Forward	ACTACGCAAAGGCCCAACG
ND1 Reverse	GAGCTAAGGTCGGGGCGGTG

4.2.7. Comet assay

HaCat cells were plated at $2x10^5$ cells per well in a 6-well plate. The next day, the cells were irradiated with different visible wavelengths. Soon after irradiation, the cells were trypsinized with 300 µl of trypsin, resuspended with 300 µl of PBS-EDTA. A volume of 30 µl of this cell suspension was mixed with 100 µl of 0.5% LMP agarose in PBS, distributed over 1.5% agarose precoated slides in PBS and covered by coverslips. For agarose solidification, the slides were incubated in the refrigerator (2-8°C) for 15 minutes, protecting them from light, to avoid further DNA damage. The coverslips were then gently removed, and the slides were incubated in alkaline lysis solution (2.5 M NaCl, 0.1 M EDTA, 10 mM Tris-HCl, 1% Triton X-100, pH 10) for at least 12 hours.

A modified comet assay protocol to detect Fpg-sensitive sites in nuclear DNA was performed as described by Collins et al. (1993). After incubation in lysis buffer, the slides were treated with 0.2 U of the Fpg enzyme (*Sigma-Aldrich*, USA) in buffer composed of 0.1 M KCl, 0.5 mM Na_2EDTA, 40 mM HEPES, 2 mg/ml BSA, pH 8 (20 µl for each coverslip region) for 30 minutes at 37°C. In the conventional comet assay, this step is skipped.

Subsequently, the slides were washed (three times for 20 minutes) in electrophoresis buffer (30 mM NaOH, 2 mM Na_2EDTA, pH 12.3) and incubated in that buffer at 4°C for 30 minutes, denaturing the DNA in the dark. Electrophoresis was performed with 25 V, 300 mA for 25 minutes in a cold chamber, with a buffer covering 1-2 mm above the agarose. After electrophoresis, the slides were washed and neutralized in distilled water for 5 minutes three times. Slides were allowed to dry in an inclined position and fixed in ethanol for 15 minutes, and stored for further analysis. For the analysis, slides were stained with 100 µl of ethidium bromide stock solution, and covered with coverslip, allowed to incubate for 5 minutes, analyzing the slides one by one and visualized in a fluorescence microscope, exciting the sample of 515-560 nm, and capturing fluorescence using a 590 nm longpass filter. Using the *Komet 7* software (*Andor Technology*, Belfast, NIR), we analyzed 100 cells in a 250x magnification.

4.2.8. Clonogenic assay

A colony formation assay was performed seeding 500 cells/well in six-well plates. After 12 hours, cells were exposed to different wavelengths (408, 466, 522, and 650 nm) and doses in PBS buffer, incubating cells for seven days

in DMEM, supplemented with 10% fetal bovine serum (FBS), 4 mM L-glutamine, 100 U/mL penicillin and 100 µg/mL of streptomycin, in 5% CO_2 at 37ºC. Colonies (>50 cells) were fixed with 4% paraformaldehyde (500 µL/well), for 15 min, at room temperature. Cells were washed with PBS and stained with 0.5% crystal violet solution (w/v in H_2O), for 15 min. Wells were rinsed with distilled water and dried at room temperature. Colonies were manually counted. Survival factor (SF) was calculated as follow: SF= number of colonies formed after treatment/number of cells seeded x PE, where PE is the plating efficiency ([number of colonies formed/number of colonies seeded] x 100%).

4.2.9. Western Blotting

Cells were lysed in RIPA buffer (50 mM Tris-HCl pH 8, 150 mM NaCl, 5 mM EDTA, 1% NP-40, 0.5% Na-deoxycholate, 0.1% SDS) with protease inhibitor cocktail (1:100) (*Sigma*, P8340), and through freeze/thaw cycles (three times) and up-down in syringe (twenty times), on ice. Lysate was centrifuged at 17000g, for 30 min, 4ºC, removing the supernatant and performing the Bradford method for total protein quantification. SDS-PAGE was made in 12% polyacrylamide gel, using 10-20 µg total protein/well. Western blot was performed at 100V, for 2 hours, in cooled Novex Tris-glycine transfer buffer, with 20% methanol (*Life Technologies*). PVDF membrane was blocked with 5% skim milk in TBS-T 0.05%, for 1 hour, and incubated overnight with polyclonal rabbit primary anti-LC3 (Sigma, L8918)(1:1000) and loading control monoclonal mouse primary anti-β-actin (*Abcam*, ab6276) (1:1000) in 1% skim milk in TBS-T. The membrane was incubated with secondary antibody-HRP conjugated: anti-mouse 1:1000 (*Millipore*, AP160P) and anti-rabbit (*Millipore*, AP188P) (1:1000)

in 1% skim milk in TBS-T, for 2 hours. Chemiluminescent detection was performed using the *SuperSignal West Femto Maximum Sensivity Substrate* (*ThermoFisher Scientific*, 34096). Images were acquired using a photodocumentator (*Uvitec* Limited, *Cambridge*, UK).

4.2.10. FACS *MitoTracker Deep Red* and *LysoTracker Green*

We performed the flow cytometry using *MitoTracker Deep Red* (MTDR) (*ThermoFisher Scientific*, M22426) and *LysoTracker Green DND-26* (LTG) (*ThermoFisher Scientific*, L7526) to be incorporated in mitochondria and lysosomes, respectively, in a way dependent on membrane integrity (lysosomes) and electrochemical membrane potential (mitochondria). When the lysosomal lumen pH and mitochondrial electrochemical potential are affected, the fluorescence intensities of MTDR and LTG are decreased.

We seeded 2.5 x 10^5 cells in 12-well plates. For positive control, we used HaCaT cells treated with DMMB (1,9-dimethyl methylene blue), as described in *Chapter 2*, trypsinizing cells for FACS analysis 1 hour after treatment. The next day, cells were washed twice with PBS, and exposed to different visible wavelengths (408, 466, 522, and 650 nm), at a dose of 50 J.cm^{-2} (408 nm) and 100 J.cm^{-2} (466, 522 and 650 nm). Cells were trypsinized (200 µl/well), for 10 min, 37ºC, 5% CO_2, neutralizing with 1.3 mL of DMEM 10%. Cells were pelleted by centrifugation (300 g, 5 min, at RT). Pellets were washed in PBS, collecting cells by centrifugation (300 g, 5 min, at RT).

Pellets were resuspended in 600 µl of PBS, preparing a pool with 200 µl from each sample (dark, 408, 466, 522, 650, and positive control). Cells were labeled with 4 µM MTDR and 4 µM LTG DND-26, for 15 min, at 37ºC, in the

dark. Cells were washed with 1 mL PBS, collected by centrifugation (300 g, 5 min, at RT), resuspended in 300 µl of PBS and analyzed by flow cytometry in *BD-FACS Verse* (*Becton Dickinson*, San Jose, CA), 50.000 events, using FL1 and FL3.

4.3. RESULTS

By analyzing only the data from the MTT assay (Figure 4.2), it seems that cells do not suffer the oxidative stress induced by exposure to different wavelengths of visible light 24 hours after irradiation, since there is no significant reduction in cell viability, even at high doses, such as 100 J.cm^{-2} (Figure 4.2).

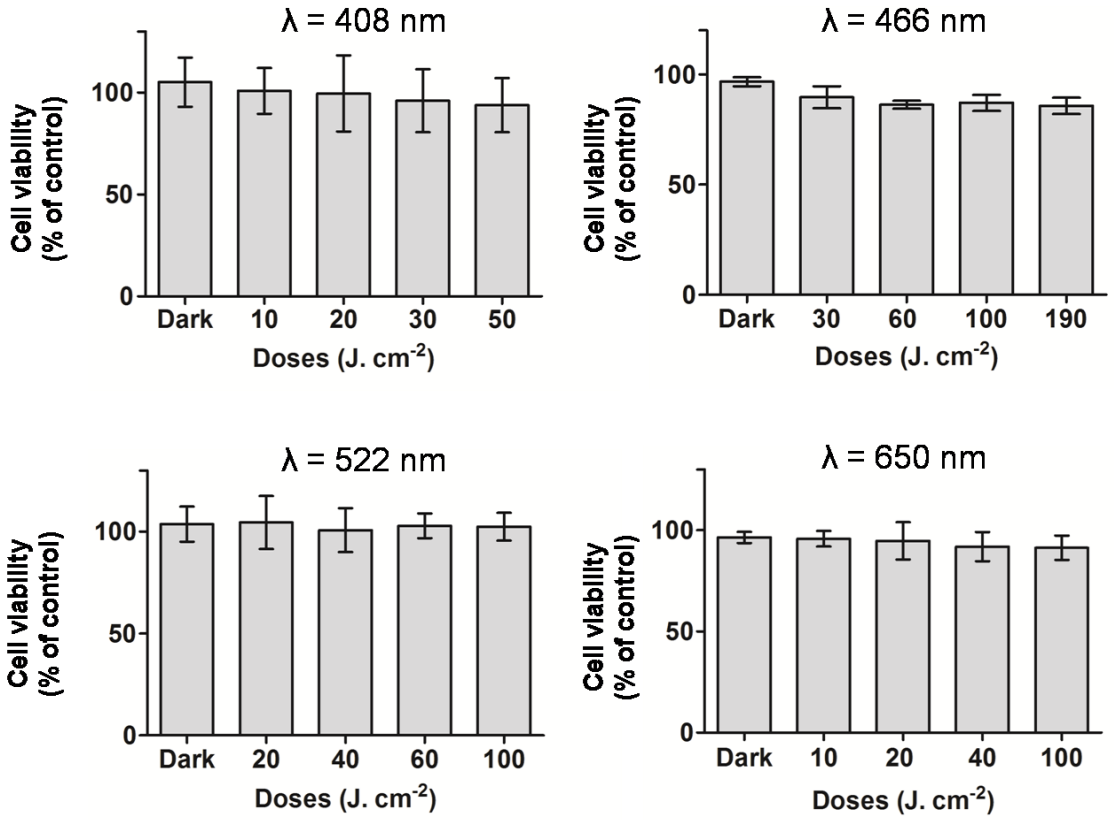

Figure 4.2. Cell viability assays based on MTT of HaCaT exposed to different wavelengths and doses of visible light. MTT was performed 24 hours after the treatment. Bars represent mean (n=3) ± standard deviation. Statistical analysis was performed using *SigmaStat* v.3.5, running one-way ANOVA test, and statistical differences determined by Holm-Sidak post-test, considering statistically significant at $p<0.05$(*), $p<0.01$(**).

However, the response obtained from clonogenic assays showed a significant decrease in cell survival seven days after photodamage (Figure 4.3), especially in HaCaT cells exposed to 408 nm and 466 nm light. We suppose that this result is a long-term consequence of oxidative stress, possibly involving blockade of autophagy, and lipofuscin accumulation (Figure 4.3).

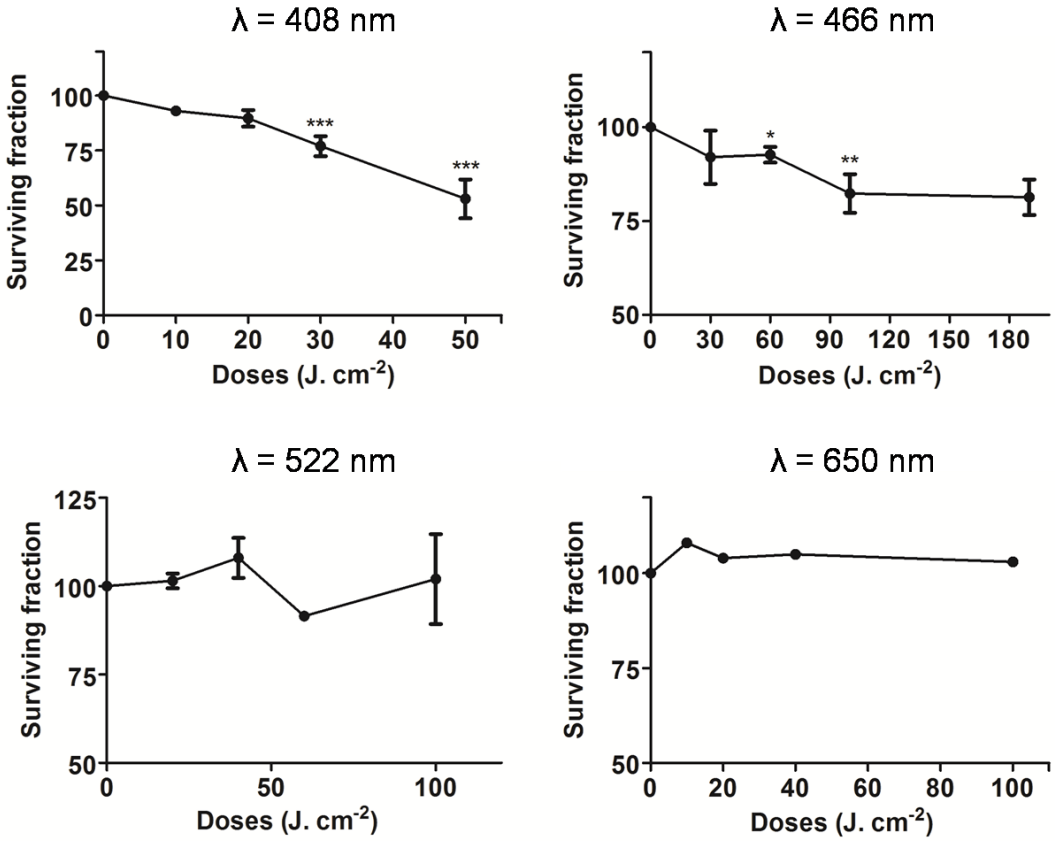

Figure 4.3. Clonogenic assays of HaCaT seven days after exposure to different wavelengths and doses of visible light. Bars represent mean (n=3) ± standard deviation. Statistical analysis, in relation to dark control was performed using *SigmaStat* v.3.5, running one-way ANOVA test, and statistical differences determined by Holm-Sidak post-test, considering statistically significant at $p<0.05$(*), $p<0.01$(**), $p<0.001$(***).

In the context of cell survival, cells present important mechanisms to guarantee homeostasis and viability. One of these mechanisms is autophagy, which can remove and recycle damaged biomolecules and organelles. However, due to photodamage, autophagic flux can be disturbed (Martins et al.

2015). Nevertheless, there is no information in the literature regarding the wavelengths of visible light causing intracellular damage and the autophagic blockade. In order to monitor the mitochondrial membrane integrity after exposure of HaCaT cells to different visible light wavelengths (Figure 4.4 a), we used *MitoTracker Deep Red* (MTDR), a cationic and mitochondrial potential-dependent dye with a far-red fluorescence (exc. 644 nm/ em. 665 nm), which has been used to monitor changes in mitochondrial membrane potential (MMP), where decreasing MMP inhibits accumulation of MTDR in mitochondria (Zhou et al. 2011; Xiao et al. 2016; Tsubone et al. 2017). Besides, for checking lysosomal membrane integrity we used *LysoTracker Green* (LTG), which has been used in literature to indicate the lysosomal membrane damage. Damaged lysosomes cannot retain these dyes due to changing in intralysosomal pH (Li et al. 2016, Repnik et al. 2016, Tsubone et al. 2017).

The HaCaT cells analyzed one hour after exposure to blue (408 and 466 nm) and green (522 nm) light showed significative alterations in mitochondrial membrane integrity, which was measured adding the percentage of events (i.e., cells) in non-labeled MTDR quadrants (i.e., $MTDR^-/LTG^+$ plus $MTDR^-/LTG^-$ quadrant) (Figure 4.4 a,b). Considering the blue light, 408 nm was more damaging to the mitochondrial integrity than the 466 nm light, which showed a level of decrease in MTDR-labeling near to the dark control (1.06% and 1.12%, respectively). On the other hand, the green light evoked an expressive level of mitochondrial damage compared to the blue light: five- and fifteen-fold higher than 408 nm and 466 nm, respectively (Figure 4.4 b).

The damage in lysosomal membrane integrity was obtained adding the percentage of events in non-labeled LTG quadrants (i.e., $MTDR^+/LTG^-$ plus

MTDR^{-}/LTG^{-} quadrant) (Figure 4.4 c). In this analysis, only the 408 nm and 466 nm light induced a significative level of decrease in LTG-labeling compared to the dark control: 5.58% in 408 nm and 4.37% in 466 nm compared to 3.0% in dark control (Figure 4.4 c). This decrease in LTG-labeling observed in both to 408 nm and 466 nm light-treated cells was even higher than those observed in cells exposed to the green (2.34%) and red light (2.30%) (Figure 4.4 c).

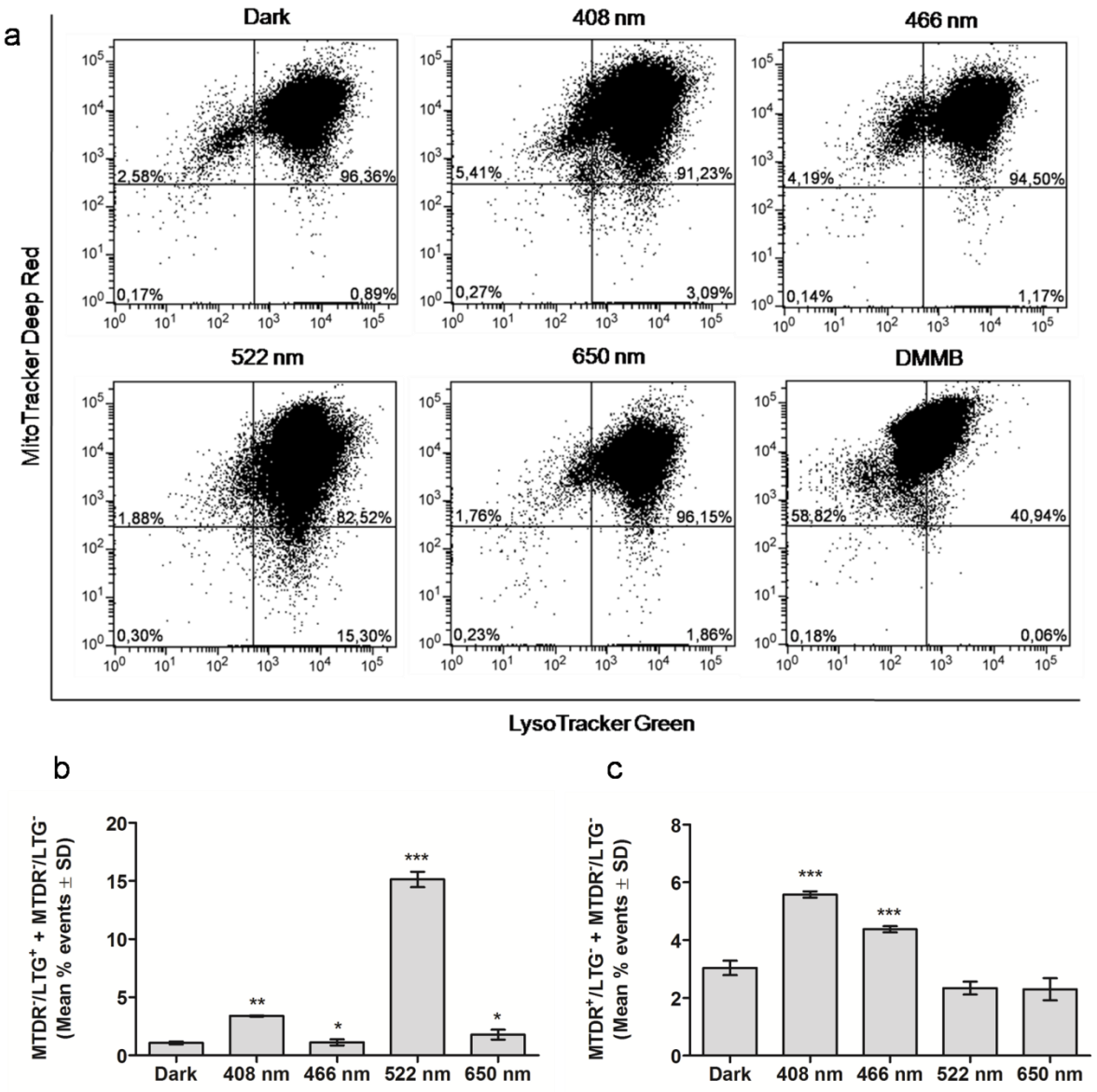

Figure 4.4. Mitochondrial and lysosomal damage measured by FACS using *MitoTracKer Deep Red* (MTDR) and *LysoTracker Green* (LTG), performed 1 hour after exposure to 408 (50 J.cm^{-2}), 466 (100 J.cm^{-2}), 522 (100 J.cm^{-2}) and 650 nm (100 J.cm^{-2}) light. (**a**) Scatter plots of cells exposed to different wavelengths of visible light and positive control for damage in lysosomes and mitochondria. (**b**) Histogram of the mitochondrial damage. (**c**) Histogram of the lysosomal damage. Bars represent mean (n = 3) of sum from non-labeled quadrants (MTDR$^-$ or LTG$^-$) ± standard deviation (SD). Statistical analysis was made running one-way ANOVA test, and statistical differences determined by Holm-Sidak post-test, considering statistically significant at $p<0.05$ (*), $p<0.01$ (**), and $p<0.001$(***) in relation to dark control.

Another technique that can evaluate with great precision and sensivity the damage in mitochondria is the long-extension PCR (XL-PCR) (Figure 4.5). This technique is based on the ability of DNA polymerase to extend strands

from DNA templates. In this case, the entire intact mitochondrial DNA sequence (mtDNA). If mtDNA is oxidatively damaged, forming the single-strand breaks, abasic sites, bulky adducts that block DNA polymerase progression, the effectiveness of amplification is reduced (Furda *et al.*, 2012). By this way, the intensity of the oxidative damage in the mtDNA is an indicative of the oxidative stress condition in cells and the mitochondrial damage.

The cells exposed to 408 nm light showed a decrease about 40% in relative amplification (mtDNA:ND1) compared to dark control, inducing the highest level of mtDNA lesion among all the wavelengths used in this chapter (Figure 4.5). The cells exposed to 466 nm and 522 nm light presented a similar level of mtDNA lesions, showing a decrease of 24% and 26%, respectively, in relative amplification compared to control (Figure 4.5). On the other hand, exposure to red light (650 nm) showed to be innocuous to mitochondria of HaCaT cells.

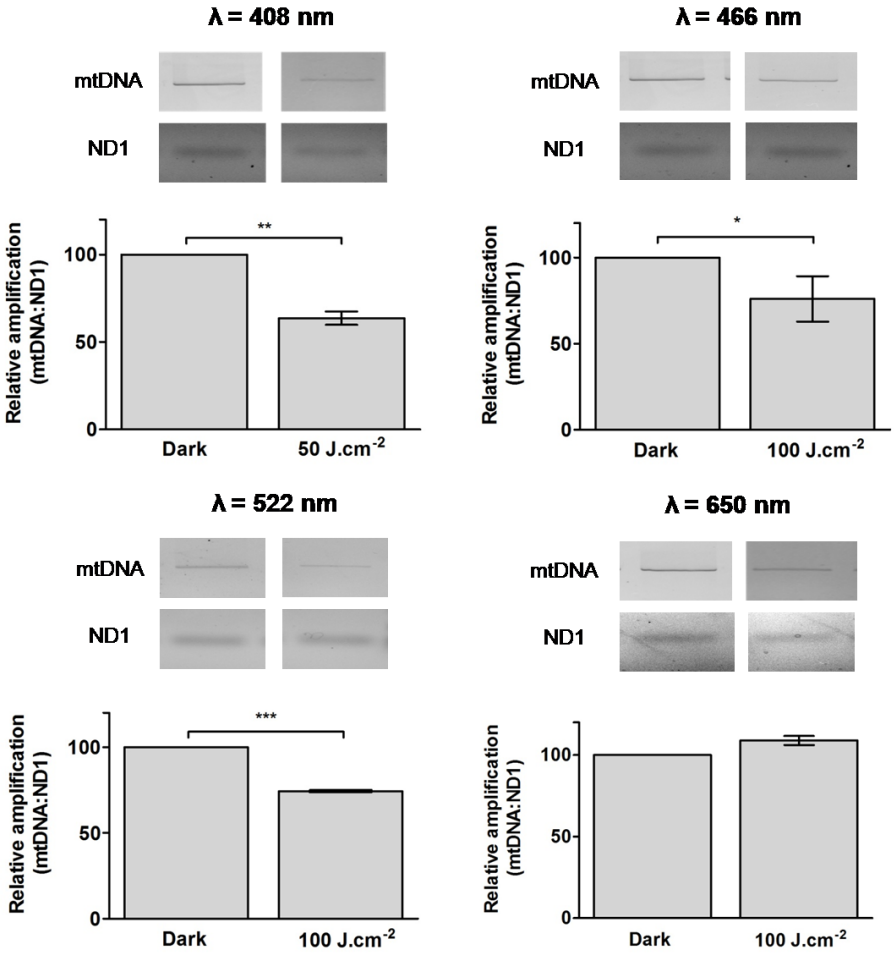

Figure 4.5. Mitochondrial DNA damage measured by long extension PCR at mtDNA in HaCaT cells exposed to maximum doses of different wavelengths of visible light. Bars represent mean ± standard deviation of three independent experiments. Statistical analysis was performed using *SigmaStat* v.3.5., running t-Student test, considering statistically significant at $p<0.05$ (*), $p<0.01$ (**), $p<0.001$(***).

These results were coherent with those obtained by FACS analysis (Figure 4.4). Blue light is known to photosensitize flavins and porphyrins in mitochondria, generating excited species and radicals that generate the mtDNA strand breaks and oxidation in bases. Interesting, this technique allowed detecting mitochondrial damage induced by 522 nm at high dose (100 $J.cm^{-2}$), suggesting that even green light seems dangerous to keratinocytes.

The damage in organelles and biomolecules leads to an increase of autophagic vacuoles inside the cells, which in the oxidative stress context can block the autophagic flux. Twenty-four hours after irradiation of HaCaT cells with different wavelengths of visible light, we aimed to determine which wavelengths cause a significant accumulation of acidic vacuoles in cells, as detected by acridine orange staining (Figure 4.6 a-f). As expected, based on other results shown above, blue light (both 408 nm and 466 nm) presented a higher accumulation of acidic vacuoles compared to dark control, green (522 nm) and red light (650 nm) (Figure 4.6 g). While green light promoted a slight increase in the level of acidic vacuoles in relation to dark control and red light (Figure 4.6 g).

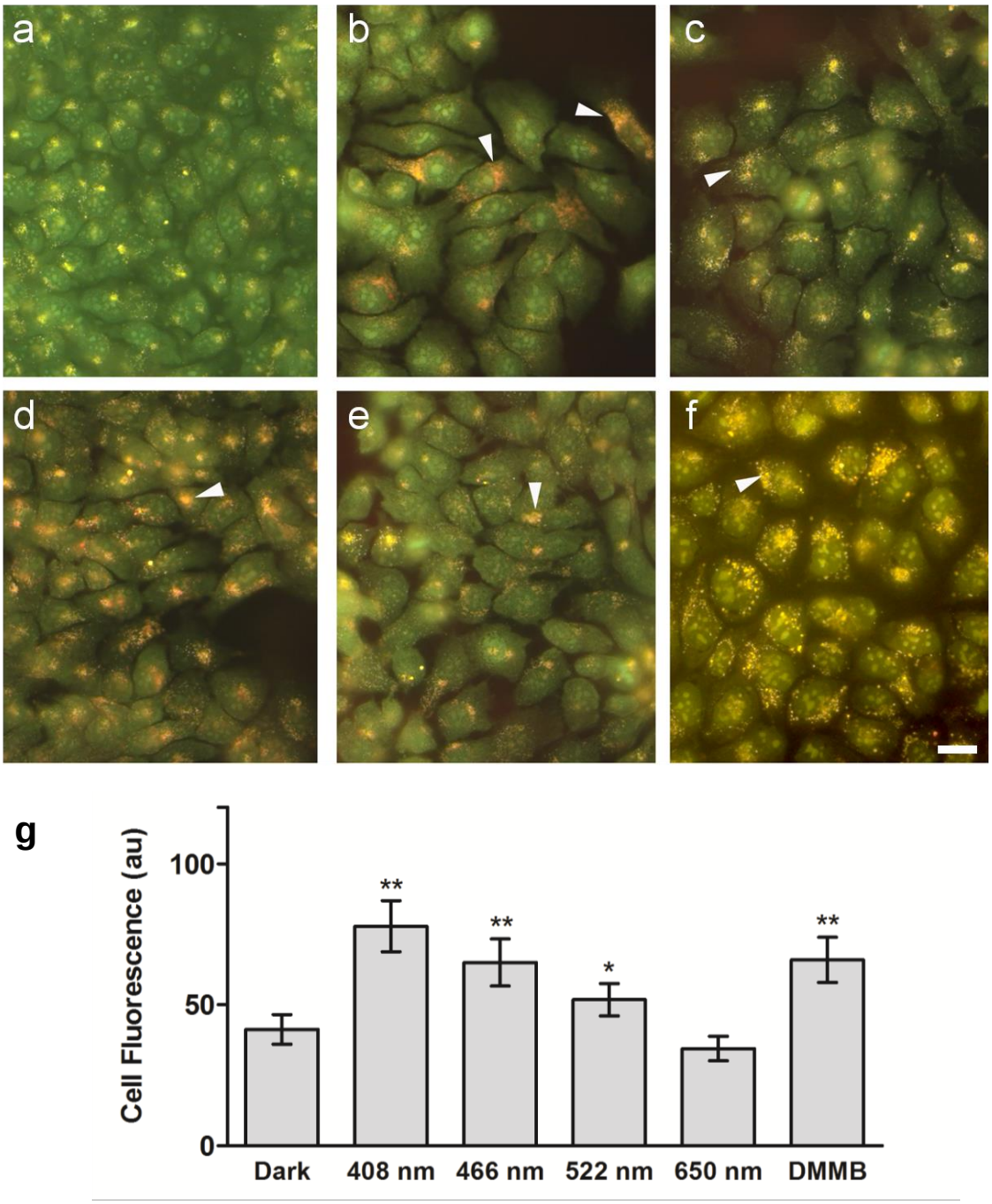

Figure 4.6. Accumulation of acidic vacuoles in HaCaT cells detected by acridine orange staining, 24 hours after the exposure to different wavelengths of visible light. **a.** Dark control. **b.** 408 nm (50 J.cm^{-2}). **c.** 466 nm (100 J.cm^{-2}). **d**. 522 nm (100 J.cm^{-2}). **e**. 650 nm (100 J.cm^{-2}). **f.** positive control using DMMB to induce the parallel damage in mitochondria and lysosomes. Bar scale = 20 µm. **g**. Cell fluorescence measured from images converted to 16-bit, using n = 20 cells for each sample. Total cell fluorescence (TCF) was calculated using the following formula: TCF = integrated density – (area selected x mean fluorescence of background readings). Statistical analysis was made running one-way ANOVA, and statistical differences determined by Holm-Sidak post-test in relation to the dark control, considering statistically significant at $p<0.05$ (*), $p<0.01$ (**).

Increased level of acidic vacuoles in the cytosol can occur either through the stimulation of the autophagy or by blockade of the autophagic flux. In order to evaluate if acridine orange is correlated with accumulation of autophagosomes, we quantified a particular molecular process resulted from LC3-II level, which is the phosphatidylethanolamine-conjugated form of LC3-I, present in autophagosomes. Here, we noted the increase in LC3-II level compared to the housekeeping protein β-actin (Figure 4.7), showing the blockade in autophagic flux in HaCaT exposed to 408 nm and 466 nm. As we saw in Figure 4.6, 522 nm and 650 nm showed similar accumulation of acidic vacuoles, which is demonstrated by an even level of LC3-II/ β-actin (Figure 4.7).

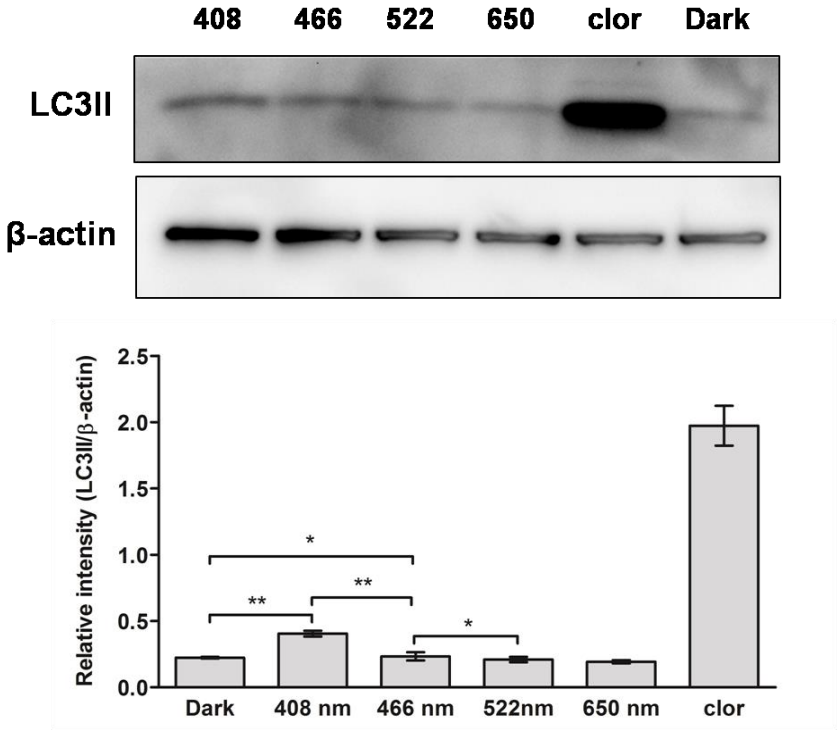

Figure 4.7. LC3II accumulation through the blockade in autophagic flux 24 hours after exposure to different wavelengths of visible light. Cells treated with chloroquine (clor) were used as a positive control. Graph represent densitometry analysis of bands detected by Western blot, normalizing data with β-actin (loading control). Bars are means ± standard deviation from the three independent experiments. Statistical analysis was performed using *SigmaStat* v.3.5., running one-way ANOVA test, and statistical differences determined by Holm-Sidak post-test, considering statistically significant at $p<0.05$(*), $p<0.01$(**).

As seen in *Chapters 2* and *3*, the blockade of autophagic flux can lead to lipofuscinogenesis, which, indeed was observed in HaCaT cell 48 hours after exposure to 408 nm, 466 nm and 522 nm using Sudan Black B staining (Figure 4.8).

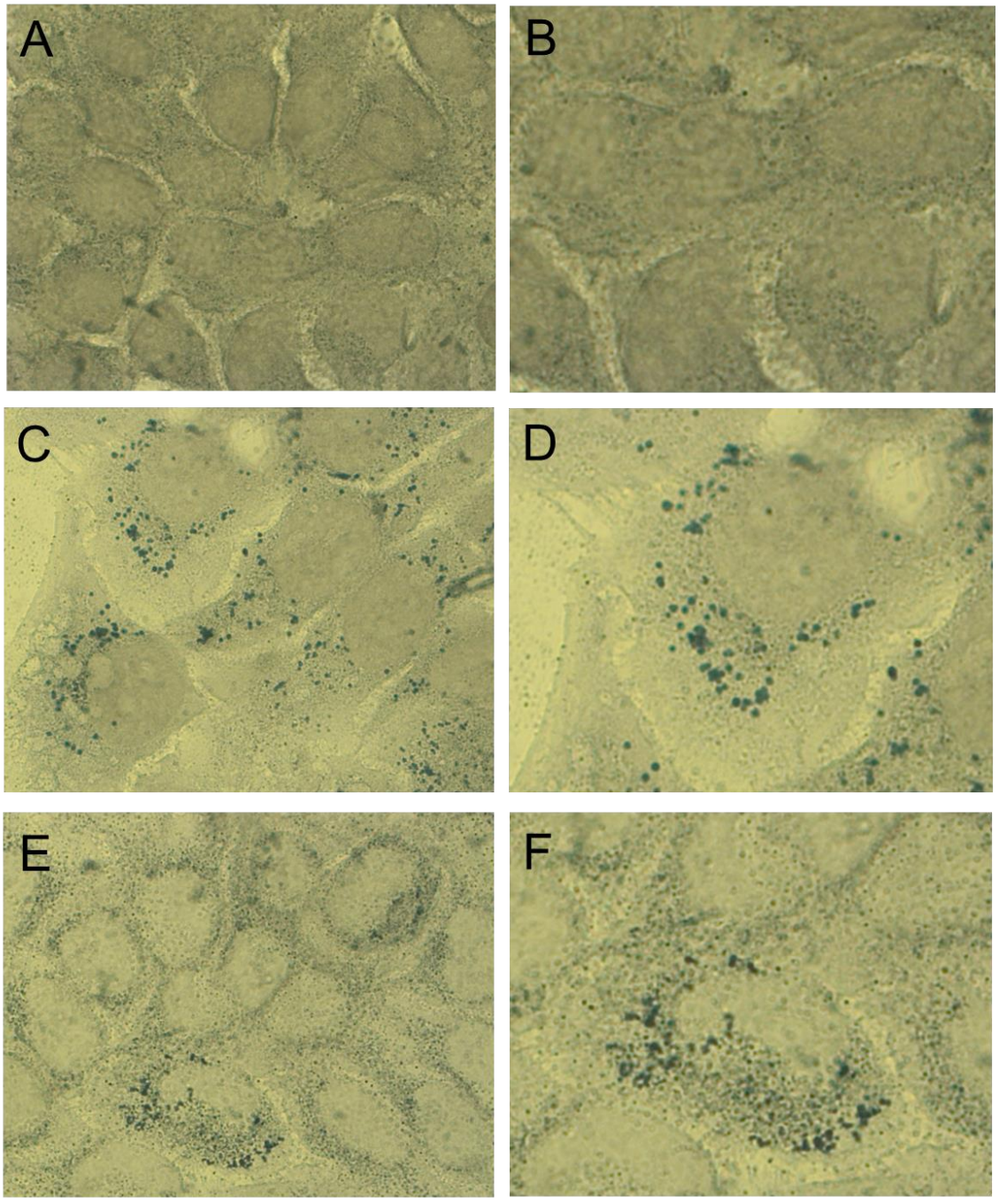

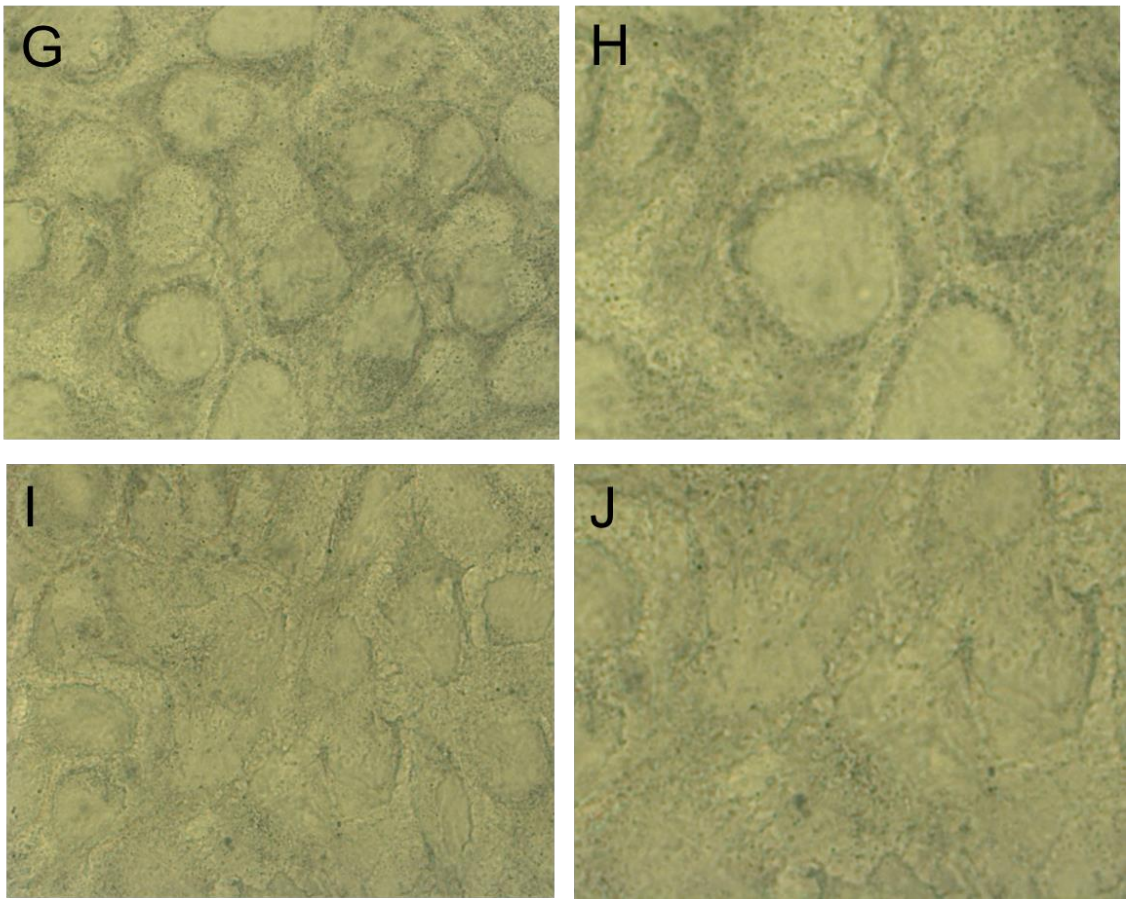

Figure 4.8. Lipofuscin accumulation detected by Sudan Black B staining, 48 hours after the irradiation of HaCaT cells with different wavelengths of visible light. (A) Dark control, (C) 408 nm, (E) 466 nm, (G) 522 nm, (I) 650 nm. (B), (D), (F), (H) and (J) are the respective magnifying images.

HaCaT cells exposed to 408 nm showed a higher accumulation of lipofuscin compared to 466 nm, 522 nm and 650 nm (Figure 4.9). Both blue and green light cause an effective induction of lipofuscinogenesis, but especially 408 and 466 nm, which increase Sudan Black B staining by almost 20%.

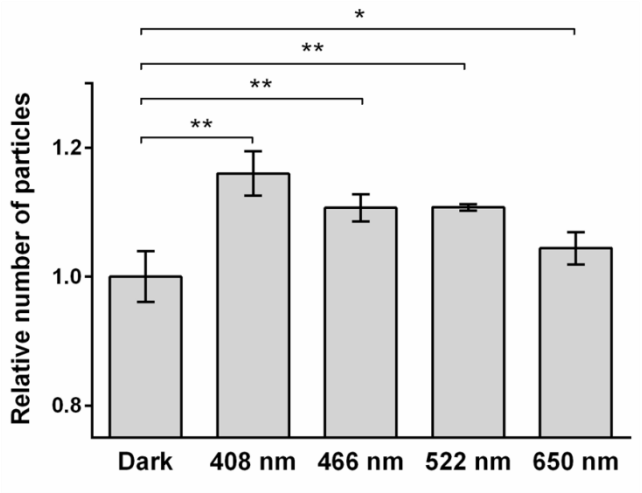

Figure 4.9. Quantification of Sudan Black B-stained particles in HaCaT cells, 48 hours after the irradiation with different wavelengths of visible light. Bars are means ± standard deviation from ten images analyzed using *ImageJ*. Statistical analysis was performed using *SigmaStat* v.3.5., running one-way ANOVA test, and statistical differences determined by Holm-Sidak post-test, considering statistically significant at $p<0.05$(*), $p<0.01$(**), $p<0.001$ (***).

The most remarkable consequence of lipofuscin accumulation in human skin keratinocytes, as it has been already reported by us, is the rise in sensitivity of these cells to visible light (400-750 nm) (*Chapter 2, JID*). The lipofuscin is a powerful photosensitizer in the visible and can further impair cell function when they are irradiated with visible light. Indeed, 48 hours after exposure to 408 nm and 466 nm, HaCaT cells were exposed to broad-spectrum of visible light (400-750 nm), showing a significant reduction in cell viability (around of 25% for 408 nm, and 30% for 466 nm) (Figure 4.10).

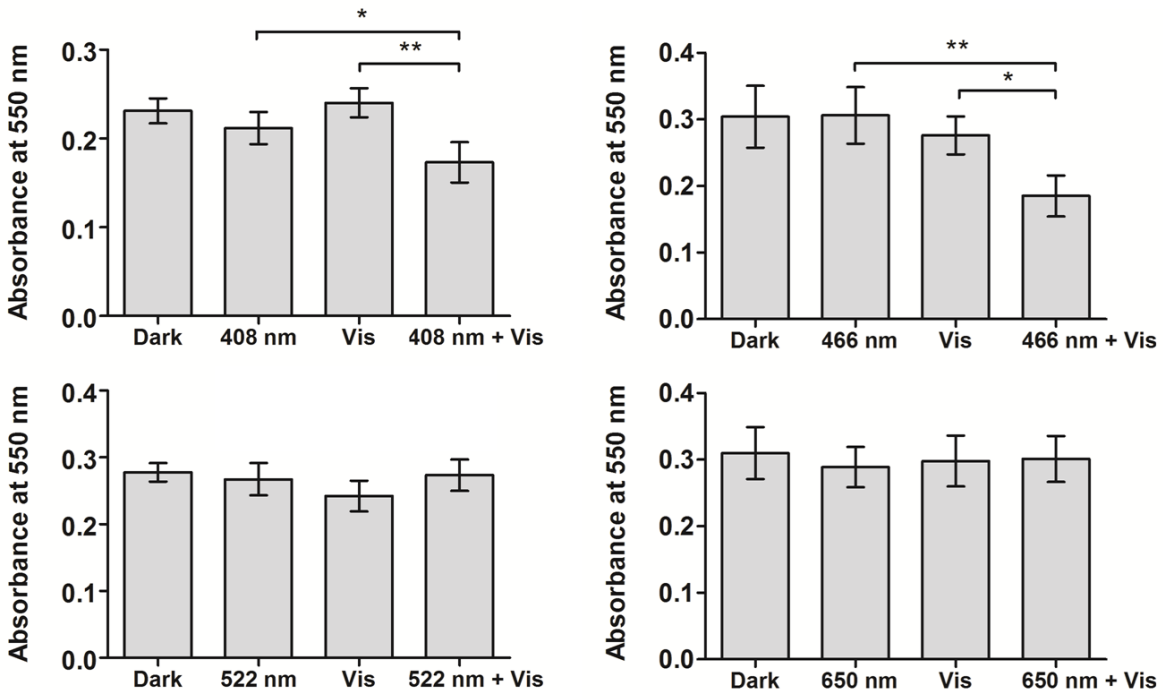

Figure 4.10. Cell viability was reduced 24 hours after photosensitization of lipofuscin-loaded HaCaT cells with visible light (Vis) (400-750 nm). Mean (n=3) ± standard deviation. Statistical analysis was performed using *SigmaStat*, one-way ANOVA, and post-test Holm-Sidak, considering significant at p≤0.05 (*), p≤0.01 (**).

In contrast, the HaCaT cells exposed to 522 nm showed same level of lipofuscin accumulation, however, photosensitization of these cells with visible light did not reduce the cell viability, suggesting that the decrease in cell viability depends on the amount of lipofuscin accumulation. Indeed, lipofuscin granules are found on a low level in HaCaT cells exposed to 522 nm, compared to 408 nm and 466 nm. Consequently, the intensity of ROS generation is lower and we hypothesize that the antioxidant mechanisms in HaCaT cells are able to counteract the oxidative stress.

Finally, using a Comet assay, we investigated the oxidative damage and strand breaks in nuclear DNA induced by direct photosensitization of HaCaT cells with different wavelengths of visible light. The 408 nm blue light was by far the most dangerous wavelength to nuclear DNA, leading to a 5-10 fold increase

level of strand breaks (Figure 4.11) and oxidized purines detected by Fpg-DNA glycosylase (Figure 4.12). Both 466 nm and 522 nm showed increased (2-5 fold) levels of strand breaks and oxidized purines, compared with dark control and the 650 nm irradiation. Red light (650 nm), at a dose of 100 $J.cm^{-2}$, caused no measurable increase in DNA strand breaks and oxidative lesions in nuclear DNA compared to dark control (Figure 4.11, 4.12).

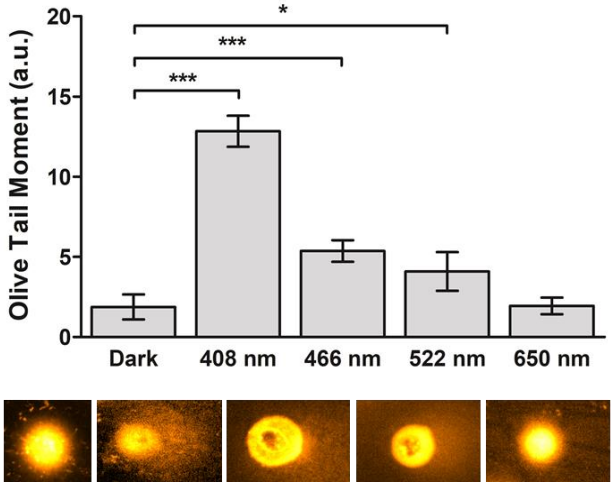

Figure 4.11. Alkaline comet assay to check nuclear DNA strand breaks shortly after exposure of HaCaT cells to different wavelengths of visible light. Statistical analysis was performed using *SigmaStat* v.3.5., running one-way ANOVA, and statistical differences determined by Holm-Sidak post-test, considering statistically significant at $p<0.05$ (*), $p<0.001$(***).

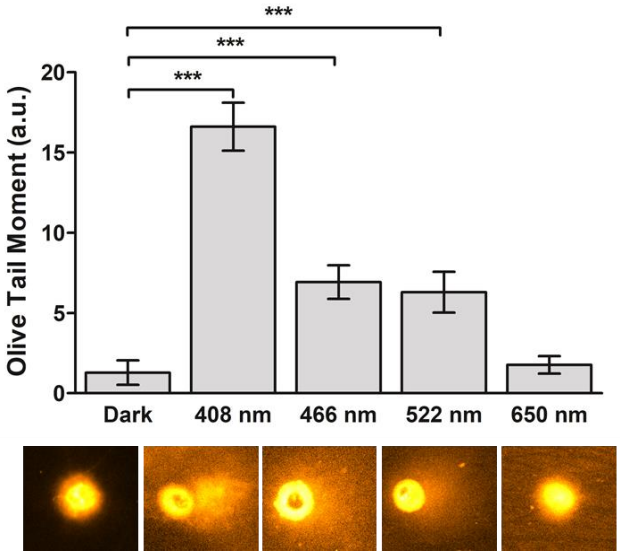

Figure 4.12. Modified comet assay detecting oxidized bases using Fpg DNA glycosylase, after exposure of HaCaT cells to different wavelengths of visible light. Statistical analysis was performed using *SigmaStat* v.3.5., running one-way ANOVA, and statistical differences determined by Holm-Sidak post-test, considering statistically significant at $p<0.05$ (*), $p<0.001$(***).

4.4. DISCUSSION

The knowledge that visible light affects cells is not a novelty. However, the quantification of this effect has been poorly investigated. We aimed to understand the direct damage in nuclear DNA and key organelles, as well as the consequences to cell homeostasis some days after the initial damage. Although, we know that visible light can induce oxidative stress and cell death, the light doses used in this study did not generate enough ROS drastically to kill cells by necrosis or through apoptosis 24 hours after light irradiation. However, in the long-term (several days after photodamage), damaged biomolecules and organelles accumulated inside the cells, amplifying the cell damage and decreasing the cell survival. In this case, the main actor seems to be lipofuscin, which is accumulated as a consequence of parallel damage in mitochondria and lysosomes. According to Terman et al. (2006), cells overloaded with defective

mitochondria have an increased ROS generation and an ineffective autophagy due to disturbances of the lysosomal activity by lipofuscin accumulation, leading cells to accumulate more lipofuscin and die, since they cannot maintain their vital functions. In fact, it is well-known that lipofuscin accumulation increases the ROS generation and disturbing the lysosomal and inhibiting the proteasomal activity, which are involved in the mechanisms of cell survival (Shamsi and Boulton, 2001; Höhn *et al.*, 2011). When we look at the data of lipofuscin accumulation (Figure 4.8, 4.9) and compare them to cell survival (Figure 4.2), we observe a direct correlation between the reduction in cell survival and level of lipofuscin accumulation: HaCaT cells which accumulate more lipofuscin (408, 466, and 522 nm) have a decreasing in cell survival after seven days.

The most investigated fraction of visible light is the high-energy blue light (400 - 450 nm), which is known to photosensitize the mitochondrial flavins, riboflavins and cytochrome oxidases, which are molecules highly prevalent in the membranes of key organelles, such as mitochondria, generating ROS, oxidative stress and cell death (King et al. 2004; Godley et al. 2005; del Olmo-Aguado et al. 2016; Osborne et al. 2014).

In fact, our results have corroborated that, both blue light (408 nm and 466 nm) and green light (522 nm) in a lesser extent, promote damage in mitochondrial and lysosomal membrane integrity, blocking the autophagic flux, and forming lipofuscin. Accumulation of lipofuscin is a typical condition of senescent cells, which have undergone aging and die.

We showed in *Chapter 2* that human skin keratinocytes exposed to UVA accumulate lipofuscin, becoming photosensitive to visible light. Here, we go further, demonstrating that blue and green light, in relevant doses, also induces

the formation of lipofuscin, inducing photoaging and increasing the formation of premutagenic and strand break lesions in nuclear DNA. Therefore, from this we have established a new paradigm for sun protection, where we appoint the relevance to protect ourselves against the prolonged exposure to visible light and urge the implementation of visible light-protection factors in sunscreens formulations.

Besides, we observed that blue and green light promote lesions in mitochondrial DNA, which can generate a plethora of diseases, if not repaired, such as cancer (Lee and Wei, 2009) and diabetes (Wang *et al.*, 2013), as well as cell aging. Also, the blue light causes an expressive direct damage in nuclear DNA.

Mitochondrial DNA has 37 genes, which encodes 13 proteins, 22 tRNAs, and 2 rRNAs (Anderson *et al.*, 1981). All proteins encoded by mtDNA produce subunits of enzyme complexes of the oxidative phosphorylation system. Thus, if oxidative stress is acute and the mechanisms of mtDNA repair cannot remove the lesions, mutations can accumulate in mtDNA, deregulating the aerobic respiration and, consequently, generating more ROS, oxidative lesions and mutations (Chial, 2008). In this sense, blue light-treated cells showed a high level of mtDNA damage, and, thus, it is the most dangerous fraction of visible light, leading cells to aging and death in long-term. The green light also showed similar effects on HaCaT cells, but in lower level than blue light. Red light proved to be harmless, not inducing oxidative damage in mitochondrial, lysosome, mtDNA and nuclear DNA.

Interestingly, the results from other labs have shown that red light seems to have the opposite effect of blue and green light: λ = 670 nm is known to

increase the mitochondrial membrane potential and to be absorbed by cytochrome c oxidase (COX), enhancing the efficiency of oxidative phosphorylation, increasing the ATP production and decreasing the ROS generation in retinal pigment epithelium cells (Begum *et al.*, 2013). Thus, a slight change in the electrochemical potential of the inner mitochondrial membrane promoted by the red light (650 nm) probably reduces the MTDR labeling in HaCaT cells, in a way independent on ROS damage, differently from the blue and green light. In HeLa cells a cytotoxicity of 650 nm was detected only at a dose of 380 $J.cm^{-2}$, inducing apoptosis (Zhang *et al.*, 2009), which corroborates with our data that 100 $J.cm^{-2}$ is innocuous to HaCaT cells and cannot reduce the cell viability.

The higher level of DNA strand breaks and oxidative lesions in nuclear DNA of HaCaT cells exposed to blue (408 nm) and green light (522 nm) showed the genotoxic and mutagenic potential of these wavelengths in skin cells. DNA strand breaks are the most dangerous lesion in DNA, disrupting the DNA template for replication and transcription, resulting in chromosome rearrangements, mutations, and carcinogenesis (Pfeiffer 1998; Tubbs & Nussenzweig 2017). Besides, the higher level of Fpg-sensitive sites detected in nuclear DNA from cells exposed to 408 nm, followed in magnitude by 466 nm and 522 nm, indicates the formation of 8-oxo-dG, which can lead to transversion mutations GC → TA, if the lesion was not removed (Suzuki and Kamiya, 2017).

As we have investigated in *Chapter 5*, the blue light 408 nm is the most dangerous in induction of genomic modifications and its ability in starting a profile of malignant transformation in human skin keratinocytes. In turn, the 466

nm and 522 nm induce a lower level of DNA lesions compared to 408 nm, showing a smaller potential to induce the malignant transformation in skin keratinocytes. At last, the red light, as expected, was unable to damage the nuclear DNA and, probably, being highly ineffective to generate neoplasia in skin keratinocytes.

4.5. CONCLUSIONS

This work reported the harmful effects of blue and green light on the key targets, nuclear DNA, mitochondria and lysosomes, and the consequences to cell homeostasis, focusing in the blockade of the autophagic flux and leading to the accumulation of lipofuscin, a visible-photosensitizer which can potentialize the photodamage promoted by visible light in skin keratinocytes. Besides, we have demonstrated the genotoxic and mutagenic potential of blue light, especially 408 nm, and in a lower extent of 466 nm and green light (522 nm). Red light was ineffective in damaging lysosomes and mitochondria, as well as mitochondrial and nuclear DNA, in contrast to what was observed using the blue and green light. Similar results had been shown before in melanocytes and in this chapter we extend the concept to the keratinocytes. Therefore, these data contribute with another warning sign of the necessity to protect ourselves against the prolonged exposure to visible light, especially blue and green light, which showed to induce aging and DNA lesions in human skin keratinocytes.

Chapter 5 – HaCaT cells chronic irradiated with Blue light show some signs of malignant transformation

During any exposition to sun, light penetrates our skin, allowing several photochemical processes that can bring benefits, but also detrimental consequences. Obviously, excessive exposition favors damage and may cause life-long problems such as skin aging and cancer. Although sun screens claim to avoid these consequences, the reality is different. Visible light is also known to be absorbed by the skin, and consequently to somehow affect skin cells. Furthermore, visible light is able to reach the deepest layers of the epidermis. Within the visible range (400-750 nm), the blue light (400-490 nm) is only to be absorbed by the same endogenous photosensitizers absorbing in the UVA (340-400nm), e.g., flavins, melanin, and lipofuscin, consequently inducing photosensitization reactions with similar efficiency. These reactions can generate damage and oxidative lesions in DNA, showing a potential to cause mutagenesis and carcinogenesis. However, no study has yet demonstrated the mutagenic potential of visible light.

5.1. INTRODUCTION

The harmful effects of the ultraviolet range (290-400 nm) of the sunlight have been well studied, and it is clear its contribution to skin photoaging, mutagenesis and carcinogenesis (Setlow *et al.*, 1993; Pfeifer and Besaratinia, 2012). On the other hand, few studies have given importance to the other ranges of the solar spectrum. This is especially critical in case of visible light, because it excites to a large degree the same chromophores as UVA radiation (340-400 nm). The literature already brings conclusive evidence that visible light (400-700 nm) promotes photoxidative lesions in nucleic acids, lipids and proteins, as well as photoprotective skin pigmentation (Liebel *et al.*, 2012; Randhawa *et al.*, 2015).

The effects of blue light on epithelial cells have been reasonably well studied, such as its role in keratinocyte differentiation (Liebmann, Born and Kolb-Bachofen, 2010); ROS generation leading to nuclear and mitochondrial DNA damage (Nakashima et al. 2017; Godley et al. 2005); decreasing in the cell antioxidant defense (Vandersee *et al.*, 2015). Besides, blue light has been widely used in medicine, such as for treatment of acne (Wheeland and Dhawan, 2011), psoriasis (Weinstabl *et al.*, 2011), dermatitis (Becker *et al.*, 2011), and wound healing (Adamskaya *et al.*, 2011).

Liebmann et al. (2010) irradiated primary human keratinocytes every 24 hours, on three successive days, with different LED arrays of blue light range (412, 419, 426, 453 nm), in a very similar protocol used by us in this chapter (three successive days irradiation). That work observed reduction in cell viability, which was dependent of dose and wavelength: at 412 nm, the dose at 33 $J.cm^{-2}$ (during three days) reduced 34% the cell viability, while treatment with

426 nm did not show significant reduction. At high doses (100 J.cm^{-2}), irradiation with 412 nm led to total loss of viability, in its turn, both 419 nm and 426 nm decreased to 20% the number of viable cells. At 453 nm the irradiation 100 J.cm^{-2} (three successive days) reduced to 57% the cell viability; however, decreasing in the cell viability was not related to cell death, but due to differentiation process in keratinocytes, which is associated with reduction in cell proliferation and possibly associated with releasing of NO (nitric oxide) from nitrosated proteins by a nonenzymatic process induced by blue light (Liebmann, Born and Kolb-Bachofen, 2010; Opländer *et al.*, 2013).

A study using a LED array of λ= 405 nm was performed by Lawrence *et al.* (2018), which investigated the effects of short wavelength range of visible light on HaCaT and *in vivo* keratinocytes. This work observed the reduction of cell viability, increase in ROS generation, and overexpression of genes involved in inflammation (IL1A, IL6, among others) and photoaging (metalloproteinase, such as MMP1).

The *in vivo* irradiation of human skin with blue-violet light (380-495 nm, with peak at 440 nm, at dose 50-100 J.cm^{-2}) was reported by Vandersee et al. (2015) to decrease the epidermal antioxidant defense, especially due to carotenoids degradation.

Our group has reported the adverse effects of visible light on human skin cells after photosensitization by endogenous pigments, increasing the oxidative stress, cytotoxicity, and DNA damage (Chiarelli-Neto et al. 2011, Chiarelli-Neto et al. 2014). We already showed in *Chapter 2* that UVA and visible light amplify the effects of each other by generation and photosensitization of lipofuscin (Tonolli et al. 2017). Also, as shown in *Chapter 4*, we have detected 8-oxo-dG

and DNA strand breaks in HaCaT cells shortly after exposure to blue (408 and 466 nm) and green light (522 nm). Nakashima et al. (2017) also observed ROS generation in human skin keratinocytes after exposure to blue light (400 to 480 nm, at 11 $mW.cm^{-2}$, for 10 minutes), mainly due to photosensitization of flavin, suggesting that blue light contributes to skin aging. Since, the human skin is chronically exposed to sunlight, a powerful pro-oxidant agent, skin cells constantly live under oxidative stress condition.

The maintenance of genomic stability is critical to protect cells against mutagenesis and cancer (Tubbs and Nussenzweig, 2017). Under the circumstance of continued oxidative stress, the antioxidant and DNA repair activities can be supplanted, accumulating DNA lesions and damage, generating genomic instability, mutations and as a consequence malignant transformation (Visconti and Grieco, 2009; Reuter *et al.*, 2010). Indeed, He et al. (2006) reported the neoplastic transformation in HaCaT cells chronically exposed to UVA radiation, acquiring apoptotic resistance, elevation in phosphorylation by protein kinase B (PKB)/AKT and reduced expression of PTEN. If visible light causes similar photooxidative processes to UVA, especially leading to premutagenic oxidative lesions in DNA, we decided to answer in this chapter an important question in sun care: can visible light promote the malignant transformation in human skin cells? In this chapter, we described, for the first time in literature, the results of HaCaT cells chronically exposed to high-energy blue light (λ= 408 nm), at relevant dose, verifying its mutagenic and carcinogenic potential. Indeed, our results showed that these cells acquired several typical characteristics of the malignant cells after some cycles of chronic exposure.

5.2. MATERIALS AND METHODS

5.2.1. Cell culture

Human skin immortalized keratinocytes cells (HaCaT) (Boukamp et al., 1988) were cultivated in Dulbecco modified Eagle medium (DMEM), supplemented with 10% fetal bovine serum (FBS), 4 mM L-glutamine, 100 U/mL penicillin and 100 µg/mL of streptomycin, in 5% CO_2 at 37ºC.

5.2.2. Irradiation of cells

Blue light irradiation

HaCaT cells ($5x10^5$ cells/100 mm plate) were exposed to high-energy blue light LED source (λ=408 nm) made by Optics and Photonics Research Center, Institute of Physics, University of São Paulo, São Carlos, Brazil. The spectral properties of the LED sources are shown in Figures S1, in comparison with the spectral irradiance of sun light. Cells were irradiated in phosphate saline buffer up a dose of 50 $J.cm^{-2}$, three times a week (until forty-second irradiation, i.e., during fourteen weeks). After that, irradiated cells were left recovering until the next irradiation. When the cell culture reached 90% of confluence, cells were trypsinized, seeding 5×10^4 cells to maintain the culture. One day after seeding, the next irradiation was performed, checking the growth curves to verify shifting in proliferation.

Physiologic relevance of blue light dose used in experiments

We estimated the relevance of blue light dose used in this work based on comparing the emission intensity profile with the standardized solar spectrum *Air Mass 1.5 spectrum (AM 1.5)*, a reference spectrum of sun irradiance at sea level for typical latitudes of most major cities with the sun at about 48º from

zenith (sometimes referred to noon sun), e.g. most places in US taking into account direct radiation, sky and ground reflection (Hulstrom & Riordan 1990). The dose of 50 J.cm^{-2} at 408 nm in the LED (irradiance = 0.28 mW.cm^{-2}, for 2h57min), corresponds to six hours of exposure to the reference sun (irradiance = 0.13 mW.cm^{-2}), since irradiance in blue LED is two-fold higher than solar radiation (Figure 5.1). So, the dose used in this study is physiologically relevant, being easily reached in a vacation day on the beach.

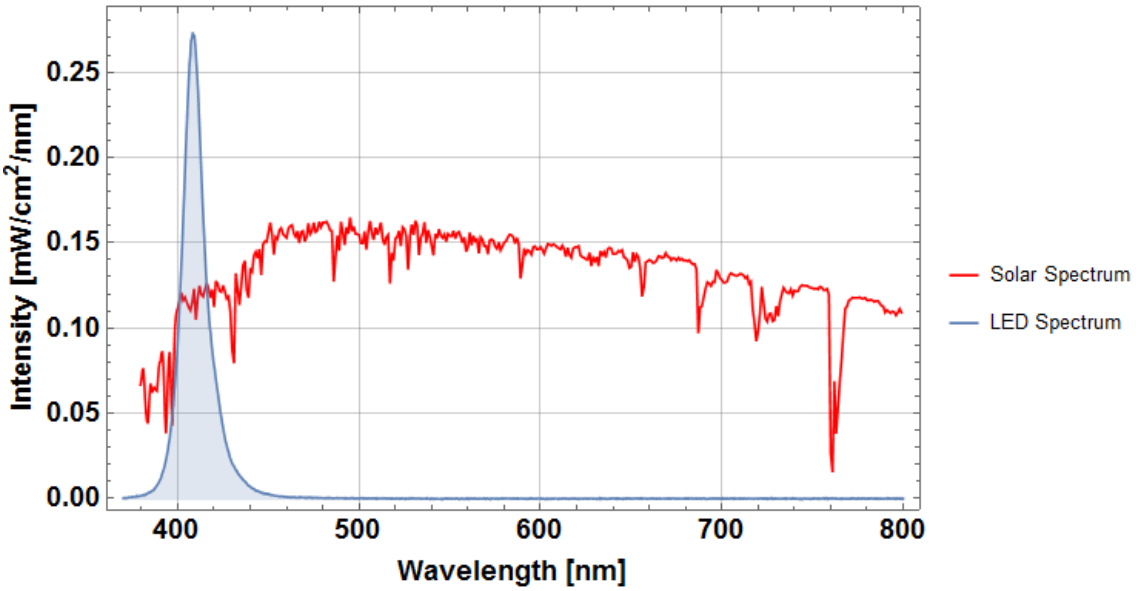

Figure 5.1. Blue light (LED λ= 408 nm) spectrum compared to solar radiation spectrum in range of 400-800 nm, considering the irradiance used to reach 50 J.cm^{-2} in 2h57 min. Solar radiation spectrum is a reference solar spectrum at sea level measured by *American Society for Testing and Material* (ASTM) at Air Mass 1.5, document ASTM G173-03.

UVA irradiation

For checking the resistance to UVA radiation (Figure 5.2), 1.5 x 10^3 cells/well were plated in 48 wells plate, and after 12 hours, irradiated with different doses of UVA (6 and 12 J.cm^{-2}) using a LED source (λ= 365 nm, *BioLambda*, São Paulo, Brazil), at 30ºC.

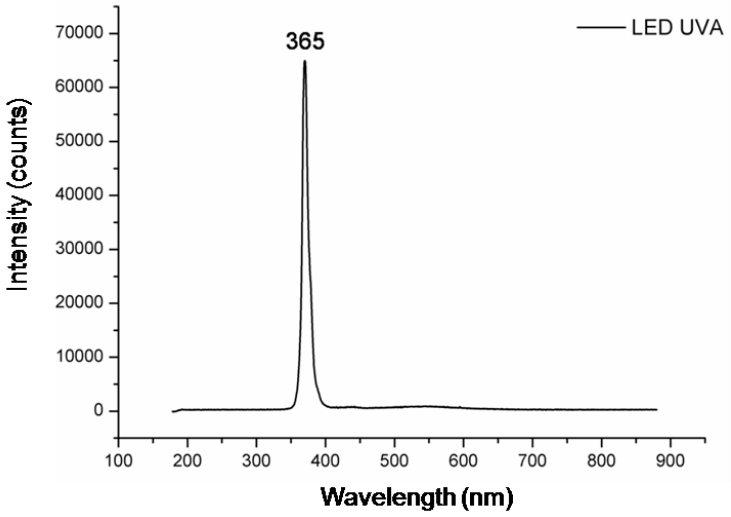

Figure 5.2. Emission sprectrum of LED UVA, with maximum at 365 nm.

5.2.3. Clonogenic assay

A colony formation assay was performed seeding 500 cells/well in six-well plates. After 12 hours, cells were exposed to blue light in different doses (10, 20, 30 and 50 $J.cm^{-2}$) in PBS buffer, incubating cells for seven days in DMEM, supplemented with 10% fetal bovine serum (FBS), 4 mM L-glutamine, 100 U/mL penicillin and 100 µg/mL of streptomycin, in 5% CO_2 at 37ºC. Colonies (>50 cells) were fixed with 4% paraformaldehyde (500 µL/well), for 15 min, at room temperature. Cells were washed with PBS and stained with 0.5% crystal violet solution (w/v in H_2O), for 15 min. Wells were rinsed with distilled water and dried at room temperature. Colonies were manually counted. Survival factor (SF) was calculated as follow: SF= number of colonies formed after treatment/number of cells seeded x PE, where PE is the plating efficiency ([number of colonies formed/number of colonies seeded] x 100%).

5.2.4. Cell viability assays

HaCaT cells were plated $2x10^5$ cells/well in 48-well cell culture plates (*Corning Costar*, cod. 3548). After 24h, cells were washed in PBS and irradiated with UVA radiation. Twenty-four hours after irradiation was performed colorimetric assays of cellular viability based on reduction of MTT.

5.2.5. Detection of ROS generation by oxidation of DCFA

Twenty-four hours after being seeded $1x10^4$ cells/well in 96-well plates (black clear flat bottom, *Greiner-BioOne*, Austria), HaCaT cells were irradiated with blue light at 50 $J.cm^{-2}$. After irradiation, 200 µL of 10 µg/mL DCFDA solution (prepared in PBS from a 5 mg/mL stock in ethanol) were immediately added to each well, and fluorescence was monitored during the following 30 min in a microplate reader *Spectramax i3* (*Molecular Devices*, USA), using excitation at 485 nm and detecting the emission at 535 nm. The slope of the curve was used to calculate the oxidation rate of DCFDA to DCF, with increasing percentage in fluorescence/well calculated by $[(Ft_{30}-Ft_0)/Ft_0*100]$, where Ft_{30} is fluorescence at 30 minutes, Ft_0 is fluorescence at 0 minutes (Wang & Joseph 1999).

5.2.6. Confocal microscopy

Around $2x10^5$ cells were seeded on coverslips in 60 mm culture dishes (*Corning Costar*). After 24 hours, cells were rinsed with PBS and fixed in 4% paraformaldehyde (w/v) for 10 minutes, washed three times/5 minutes with PBS, incubating fixed cells in 0.1% Triton X-100 solution, for 10 minutes, at 37ºC. Cells were washed with PBS and incubated in 1:500 solution of *Alexa*

Fluor-488 phalloidin (*ThermoFisher Scientific*) in PBS, for 1h in the dark, at 37ºC. Cells were washed three times with PBS and slides were mounted in *Prolong-Gold Antifade with DAPI* (4',6-diamidino-2-phenylindone) (P36935, *ThermoFisher Scientific*). Slides were analyzed in *Zeiss LSM 510 Meta* confocal microscope, exciting at 488 nm (*Alexa Fluor-488 phalloidin*) and 351 nm (DAPI).

5.2.7. Cell proliferation assays

Around 5 x10^3 cells/well of dark control and blue-light treated cells were seeded in 24-well plates, in triplicate for four different days: usually, day 1, day 2, day 3 and day 5 starting from plating day. Each day, cells were washed with PBS and fixed in 10% trichloroacetic acid solution (TCA) (w/v in dH_2O), for 5 min, at room temperature. TCA was removed, leaving the wells to dry. After all points were fixed, cells were hydrolyzed in 2M NaOH (200 µL/well), for 15 minutes, at room temperature, diluting the lysate in Milli-Q water (1:4), reading absorbance at 260 nm, in a spectrophotometer, for total DNA content quantification. Data were plotted in *Origin v. 8* (*OriginLab Corp.*), performing the exponential fitting, optimizing data for best linear regression coefficient (near to R^2=1). Data were converted to semilogarithmic plot, getting an angular coefficient (α) from which we got the ratio *α blue-light irradiated/α dark control*, a relative factor of cell proliferation.

5.2.8. BrDU cell proliferation assay

Cells were plated in 96-well plate (5-10x10^3 cells for each treatment). After 12 hours, cells were incubated with BrDU solution in DMEM 10%, during four hours, in 5% CO_2 at 37ºC. Detection of BrDU was performed by ELISA

assay (reading absorbance at 490 nm), using *BrDU Cell Proliferation Assay Kit* (*Cell Signaling Technology*), following the manufacturer recommendations.

5.2.9. Western blot

Dark control and *Blue*-treated cells were pelleted by centrifugation (3000 g, for 5 min, 4ºC), rinsed with PBS, and pellets were frozen at -80ºC until protein extraction. Cells were lysed in RIPA buffer (50 mM Tris-HCl pH8, 150 mM NaCl, 5 mM EDTA, 1% NP-40, 0.5% Na-deoxycholate, 0.1% SDS) with protease inhibitor cocktail (1:100) (Sigma, P8340), and lysed through freeze/thaw cycles (three times) and up-down in syringe (twenty times), on ice. Lysate was centrifuged at 17000g, for 30 min, at 4ºC, removing the supernatant and performing the Bradford method for total protein quantification. SDS-PAGE was made in 12% polyacrylamide gel, using 10-20 µg total protein/well. Western blot was performed at 100V, for 2 hours, in cooled Novex Tris-glycine transfer buffer, with 20% methanol (*Life Technologies*). PVDF membrane was blocked with 5% skim milk in 0.05% TBS-T, for 1 hour, and incubated overnight with primary antibodies (anti-CDKN2A/p16INK4a, ab108349, *Abcam* 1:1000; anti-cytochrome c, ab1375, *Abcam*, 1:1000) in 1% skim milk in TBS-T. Membrane was incubated with secondary antibody-HRP conjugate (anti-mouse 1:1000, *Millipore*; anti-rabbit 1:1000, *Cell Signaling*) in 1% skim milk in TBS-T, for 2 hours. Chemiluminescent detection was performed using the *SuperSignal West Femto Maximum Sensivity Substrate* (*ThermoFisher Scientific*, 34096), acquiring images using *UVITEC photodocumentation* system (*Uvitec* Limited, *Cambridge*, UK).

5.2.10. Determination of apoptosis

To determine apoptosis cells were treated with Annexin-V/propidium iodide (*ThermoFischer Scientific*), 18 hours after UVA irradiation (λ= 365 nm, 12 $J.cm^{-2}$), and analyzed by flow cytometry, according to the manufacturer's recommendations.

5.2.11. CPD detection by immunofluorescence

About $2.5x10^5$ HaCaT cells, under chronic irradiation with blue light (*Blue*) and dark control (*Dark*), were seeded in 60 mm cell culture plate on coverslips. On the next day, cells were washed 2x with PBS, fixed in 4% paraformaldehyde (w/v), for 10 min, at room temperature, washing 2x with PBS. Cells were permeabilized with 0.5% Triton X-100 in PBS, for 5 min, on ice, and washed 2x with PBS. DNA was denatured incubating cells with 2M HCl, for 30 min, at room temperature, washing 5x with PBS. Non-specific antibody binding sites were prevented by blocking cells with 20% FBS in PBS. Cells were washed 5x with PBS and incubated overnight at 4ºC with anti-CPD (1:1000 in 5% FBS in PBS). The next day, cells were washed 5x with PBS and incubated with 4 µg/mL of AlexaFluor-633 goat anti-mouse IgG (H+L) in 5% FBS in PBS, for 30 min, at 37ºC. Cells were washed 5x with PBS, mounting slides with *Prolong Gold Antifade* with DAPI. Slides were analyzed in *Zeiss LSM 510 Meta* confocal microscope. To analyze the colocalization between anti-CPD and DAPI, we performed the Manders coefficient method (Manders, Verbeek and Aten, 1993), using the *Fiji ImageJ* software, getting the Manders coefficients (M1 and M2) and scatterplots from four micrographs of different regions of slides for every sample.

5.2.12. Detection of CPD by ELISA assay

Cells were irradiated with blue light at 50 $J.cm^{-2}$ and the DNA was isolated shortly after irradiation using *DNeasy Blood and Tissue kit* (*Qiagen*), preparing 1 µg/mL DNA solutions, denaturing DNA in PCR machine (single cycle, 100ºC, 10 min, chill immediately in ice for 15 min), adding 50 ng DNA/well (triplicate wells for each sample) in 0.05% protamine sulfate precoated wells, allowing to dry overnight at 37ºC. DNA-coated wells were washed 5x with 150 µl/well PBS-T (0.05% Tween-20 in PBS) and blocked in 2% FBS, at 37ºC, for 30 min. CPDs were detected by mouse monoclonal anti-cyclobutane pyrimidine dimers (clone TDM-2, *Cosmo Bio*, Tokyo, Japan), 1:1000 in 2% FBS, for 30 min, at 37ºC. Plates were washed 5x with PBS-T and incubated with Biotin-F(ab')2 fragment anti-mouse IgG (H+L), 1:2000 in 2% FBS, for 30 min, at 37ºC, washing again 5x with PBS-T. Wells are incubated with streptavidin-HRP (1:10000), for 30 min, at 37ºC, washed with PBS-T (five times) and once with citrate-phosphate buffer (24.3 mM citric acid monohydrated and 51.4 mM sodium phosphate dibasic, pH 5). Detection of HRP activity was visualized by substrate *o*-phenylene diamine in 0.05 M citrate-phosphate buffer (pH 5), adding 30% of H_2O_2, during 30 min, at 37ºC. Colorimetric reaction was stopped with 2 M sulfuric acid, and absorbance at 490 nm was determined using a microplate reader.

5.2.13. Quantification of nuclei area

Micrographs were converted to 8-bit images, adjusting threshold and delimiting nucleus area by polygonal selection. Nucleus area measurement was

performed in 100 nuclei from fluorescence micrographs with nuclei labeled with DAPI.

5.2.14. Soft agar

Anchorage-independent growth assay was performed with HaCaT cells under chronic irradiation with blue light. $1x10^4$ HaCaT and $2x10^4$ HeLa cells (positive control) were suspended in 1.5 mL of DMEM 10%, 100 U/mL penicillin and 100 µg/mL of streptomycin, containing 0.3% agarose. Cell suspensions were plated on previously solidified 0.5% agar (1.5 mL) in 6-well plates. Cells were grown at 37ºC, 5% CO_2, and incubating cells for 14 days after seeding. Subsequently, colonies (> eight cells) were stained with 50 µg/mL of MTT in DMEM 10%, overnight. Well images were acquired using the *UVITEC photodocumentation system (Uvitec* Limited, *Cambridge*, UK).

5.3. RESULTS AND DISCUSSION

In order to define the conditions of chronic exposition to blue light, immortalized human keratinocytes cells (HaCaT) were exposed to increasing doses of blue light (λ= 408 nm). Light doses from 10 to 50 $J.cm^{-2}$ induced an increasing reduction of cell survival by clonogenic assay, and a 50% reduction in colony formation was observed at the light dose of 50 $J.cm^{-2}$ (Figure 5.3 a). This dose was also able to induce a substantial increase in DCF fluorescence, which is indicative of the oxidative stress shortly after irradiation (Figure 5.3 b) (Wang & Joseph 1999). As showed in *Chapter 4*, the blue-light treatment induces oxidative damage in key intracellular organelles (lysosome and

mitochondria), and also allows accumulation of Fpg-sensitive sites, and strand breaks in nuclear and mitochondrial DNA (Figure 4.11, 4.12).

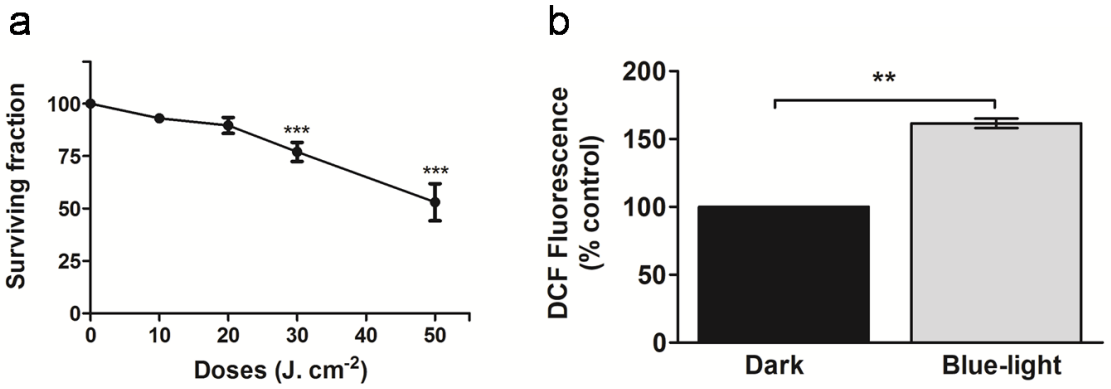

Figure 5.3. High-energy blue light treatment in HaCaT cells reduces the cell survival (a), and increase the ROS generation, which was detected by DCF fluorescence. (b) Bars indicate mean ± standard deviation obtained from three independent cell culture experiments (n=3). Statistical analysis was performed using in (a) one-way ANOVA and statistical differences determined by Holm-Sidak post-test; and in (b) t-test, considering statistically significant considering statistically significant at $p<0.01$ (**), $p<0.001$(***).

This scenario of oxidative stress induced by photosensitization reactions, forming premutagenic lesions, e.g., 8-oxo-dG, and DNA strand breaks in blue-treated HaCaT cells can lead to mutations and genomic instability. Godley et al. (2005) reported the induction of nuclear and mitochondrial DNA damage, as well as premutagenic DNA lesions in retinal epithelial cells after exposure to 390-550 nm light source, which was defined as blue light. We supposed that is a questionable result, since there is a spectral contamination of green light, which, according to our results (*Chapter 4*), also promotes mitochondrial damage.

We wonder if visible light is also able to induce an accumulation of lesions typically correlated with UV exposition, which were originally shown to be generated by direct DNA excitation, such as cyclobutane pyrimidine dimers (CPD) and 6,4-photoproducts. Traditionally, the occurrence of pyrimidine dimers

in DNA was based on the property of thymines or cytosines directly absorb UVB photons, which was suggested not to happen in UVA and visible light range (Freeman *et al.*, 1989). However, the UVA-induced CPDs have been reported in literature both in melanocytes and keratinocytes (Delinasios et al. 2018; Premi et al. 2015; Mouret et al. 2010; Young et al. 1998). Mouret et al. (2010) concluded that formation of CPDs can be promoted by direct photochemical process, that is, CPDs are generated from direct absorption of UVA by DNA. On the other hand, Premi et al. (2015) proposed a radiation-independent mechanism to explain the formation of UVA-induced CPDs. In the proposed mechanism, triplet states can be generated from intracellular pigments (in this case the fragments of melanin) are able to donate enough energy to create CPDs. On the other hand, some studies showed generation of CPD after exposure to UVA in a way independent of type I reaction (Jiang et al. 2009; Schuch et al. 2009).

We decided to test whether HaCaT cells irradiated with 50 $J.cm^{-2}$ would also form DNA lesions that are recognized by anti-CPD antibodies. Indeed, we observed the accumulation of CPDs by ELISA assay in nuclear DNA of HaCaT cells right after exposure to blue light (Figure 5.4). To our knowledge this is the first report of visible light inducing CPDs in DNA, as they are well known only to be formed through exposure to UVB and UVA radiation (Delinasios et al. 2018; Premi et al. 2015; Rochette et al. 2003). The CPDs are the primary DNA photoproducts responsible to cause mutations in melanocytes, the cells of the deeper layers of skin, leading to melanoma.

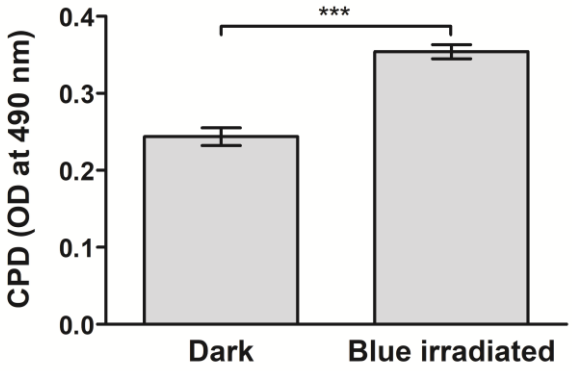

Figure 5.4. Cyclobutane pyrimidine dimers (CPDs) are generated soon after exposure of HaCaT cells to high-energy blue light (λ= 408 nm, 50 J.cm^{-2}). CPDs were detected by DNA ELISA. Bars indicate mean ± standard deviation obtained from two independent cell culture experiments (n=3) Statistical analysis was performed using t-test, considering statistically significant at $p<0.05$ (*** $p<0.001$).

Although, we are not focusing on an elucidation of the mechanism of CPD formation by visible light, we think the mechanism involves photosensitization of endogenous molecules by blue light and triplet energy transfer mechanism, rather than a direct excitation process, like shown to occur after exposure to UVA (Nakashima et al. 2017; Lhiaubet et al. 2001). Also, as we have described in *Chapter 4*, blue light generates lipofuscin, which has been speculated to be involved in UVA-induced CPD generation in HaCaT cells (Delinasios *et al.*, 2018). Lipofuscin from human skin keratinocytes is photosensitive to blue light (*Chapter 2*), generating excited states that could form CPDs. However, we need to measure if excited states of lipofuscin can donate enough energy for CPD formation. Nevertheless, the observation of CPD accumulation after blue light exposure is a further evidence to support our hypothesis that blue light is able to cause malignant transformation in skin keratinocytes.

To test our hypothesis that skin keratinocytes chronically exposed to high-energy blue light can undergo a malignant transformation, we submitted the HaCaT cells, a well-established cell lineage to study skin human epidermal

biology and physiology (McNeilly et al. 2012; Colombo et al. 2017), to chronic exposure to blue light, using a LED of 408 nm, and a dose of 50 $J.cm^{-2}$, exposing the cells to three successive irradiations in a week. This regime of irradiation, performing three successive irradiations a week at dose of 50 $J.cm^{-2}$, has been shown as a good threshold for genotoxic insulting induced by blue light, damaging DNA (*Chapter 4*) and holding 50% of cell viability along the chronic irradiation cycle.

Although HaCaT has been developed based on the spontaneous immortalization (Boukamp *et al.*, 1988), showing genetic alterations in p53 gene and loss of senescence due to expression of telomerase, it is a non-tumorigenic cell lineage, that is, cells cannot grow tumors when transplanted onto nude mice nor form colonies in soft agar assay (Fusenig and Boukamp, 1998). So, HaCaT shows immortalization (the loss of replicative senescence), one of many modifications in a tumorigenic cell. However, the HaCaT cells are not tumorigenic, but can be converted to this phenotype through the additional genetic alterations, such as *ras* genes (Fusenig and Boukamp, 1998). These genetic alterations can be induced by chronic exposure to carcinogenic agents, such as UVA radiation (He et al. 2006).

The first question that we ask is whether the CPD lesions identified after the acute high-energy blue light exposure, were also present in the HaCaT cells exposed chronically to high-energy blue light (*Blue*-treated or *Blue* cells) after 30^{th} irradiation. Performing the confocal fluorescence microscopy, labeling nucleus with DAPI and detecting CPD lesions in nuclear DNA using monoclonal antibody against CPDs labeled with *AlexaFluor 633*, we detected accumulation of CPDs in *Blue* cells (Figure 5.4).

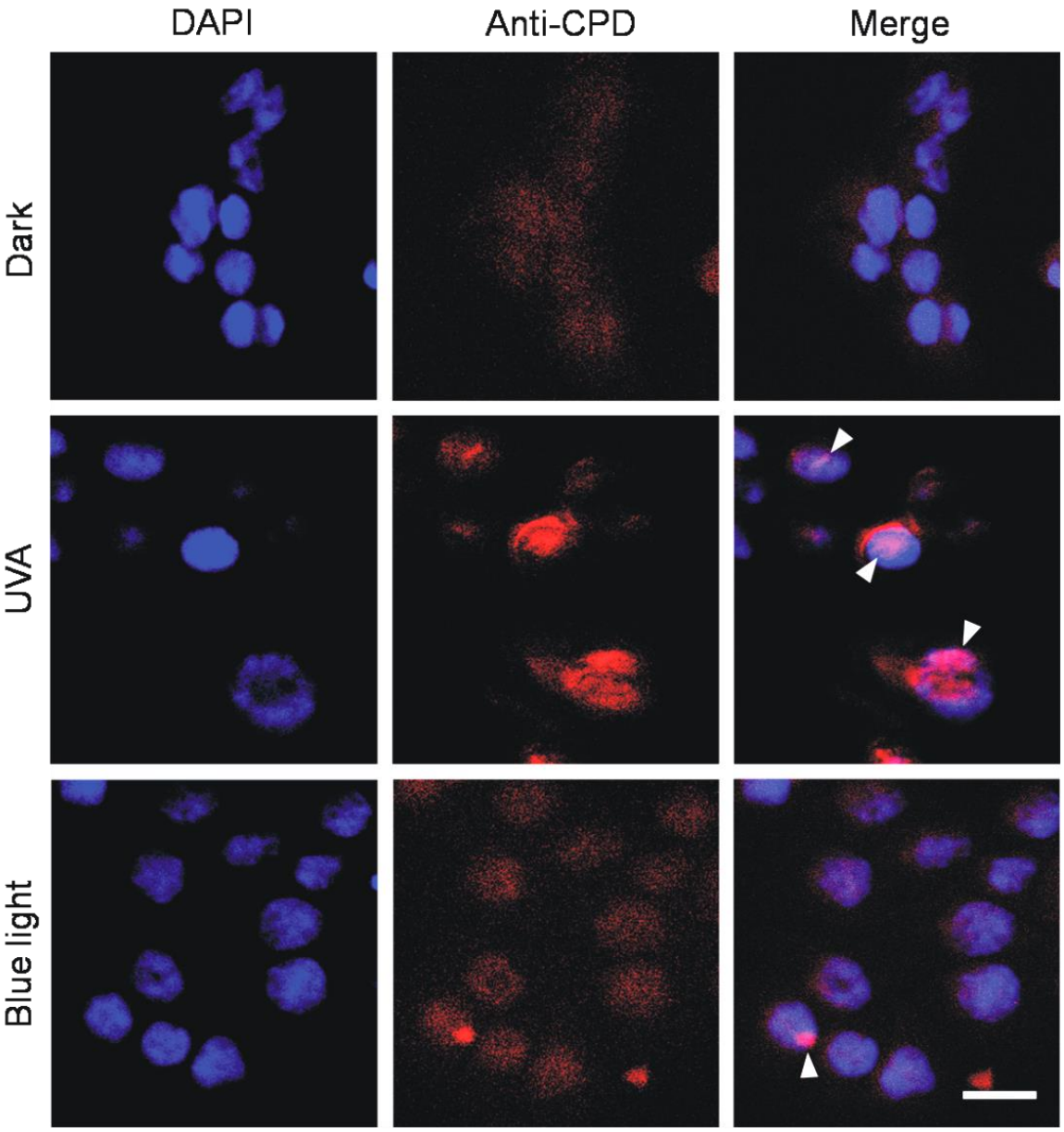

Figure 5.4. HaCaT cells chronically irradiated with blue light (λ = 408 nm, 50 J.cm^{-2}, three times/week) accumulated cyclobutane pyrimidine dimers (CPDs), indicated by white arrows, detected by immunofluorescence (anti-CPD labeled with anti-mouse Alexa Fluor 633) in nuclear DNA (labeled with DAPI). Cells exposed to UVA radiation (λ = 365 nm, 12 J.cm^{-2}), after 1 hour, were used as positive control to CPDs. Dark is a control of cells which were chronically irradiated with blue light. Scale bar = 20 µm.

In figure 5.5, we checked the colocalization between DAPI and anti-CPD labeling using the Mander's method, which gives two coefficients (M1 and M2) that represent the fraction of colocalizing objects in each component of a dual-labeling image (Manders, Verbeek and Aten, 1993). We observed the

significant colocalization correlation between anti-CPD labeled with *AlexaFluor* 633 and nucleus labeled with DAPI, with M1 = 0.7 (anti-CPD over DAPI channel) (Figure 5.5 a). Moreover, we used the scatterplots to verify overlapped pixels (Figure 5.5 b). Overlapped pixels are located toward the origin of graph, where the brighter pixels are located farther from this. Non-overlapped pixels (red or blue) usually are clustered near the axes of plot (red in y-axes and blue in x-axes).

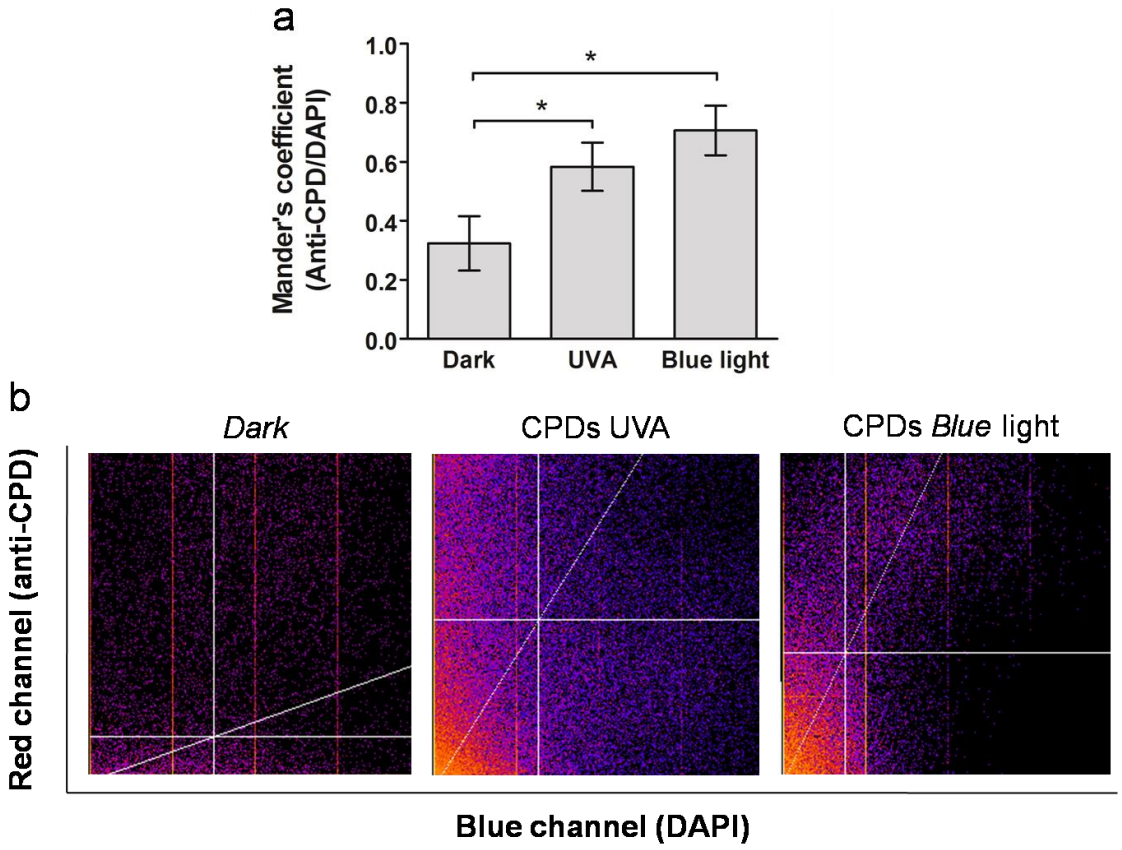

Figure 5.5. Colocalization analysis of anti-CPD labeled with AlexaFluor 633 (Red channel) overlapping in DAPI (Blue channel), the M1 Mander's coefficient. (a) Graph of colocalization correlation from four different confocal micrographs, calculating mean of Mander's coefficient ± standard deviation. Statistical analysis was performed using *SigmaStat* v.3.5., running one-way ANOVA test, and statistical differences determined by Holm-Sidak post-test, considering statistically significant at $p<0.05$ (*). (b) Scatterplots showing the colocalization and pixels intensity in representative images for each sample using the plugin "Colocalization threshold" of *Fiji ImageJ* software.

Morphological differences were observed between blue-light chronically exposed (*Blue*) and dark control (*Dark*) cells after 19th irradiation. The *Dark* cells presented epithelial-like morphology, showing uniformity in size and shape (Figure 5.6 a,c). The *Blue*-treated cells (λ= 408 nm, 50 J.cm^{-2}, three times/week) exhibited morphological alterations, giant cells with a clumped chromatin, giant and multiple nuclei and nucleoli with irregular shape (Figure 5.6 b,d), as have been reported during malignant transformation in HaCaT cells (He *et al.*, 2006; Pi *et al.*, 2008). Indeed, the morphologic changes of nucleus and cell have been commonly used to recognize malignant transformation and differentiation process (Hughes et al. 2013; Dey 2005).

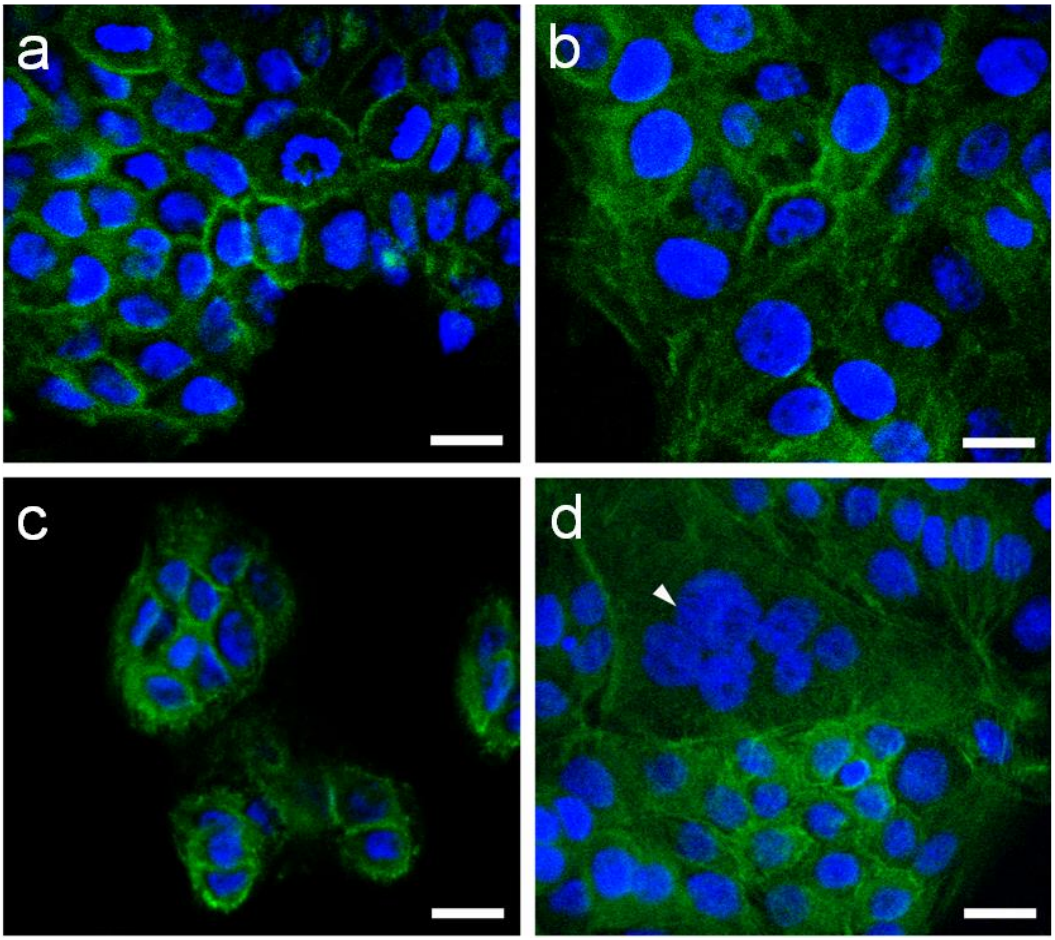

Figure 5.6. Morphological changes in nuclei (labeled with DAPI) and cell (F-actin labeled with 488-phalloidin in green) after chronic blue light irradiation in HaCaT cells. (a) *Dark* control, with a typical compacted organization. (b) *Blue*- treated cells, showing giant cells and increasing in nuclei size. (c) *Dark* control with mononucleated cells. (d) *Blue*-treated cells showing multinucleated cells (white arrows). Scale bar = 20 µm.

The nuclei in malignant cells are much larger than those in normal cells, usually in multiples, displaying irregular shape, chromatin clumping and/or rising in amount of DNA (Sørensen, 1996). In fact, these changes may reflect a new gene expression profile, which involves the chromatin reorganization and histone modification status, important to replication, recombination, and DNA repair (Hughes et al. 2013; Wolffe 2001). Here, the *Blue* and *Dark* cells had nuclei stained with DAPI, analyzed by fluorescence microscopy, allowing the quantification of nucleus size (Figure 5.7). Thus, we observed a two-fold increase of the nucleus size in *Blue* cells compared to *Dark* (Figure 5.7).

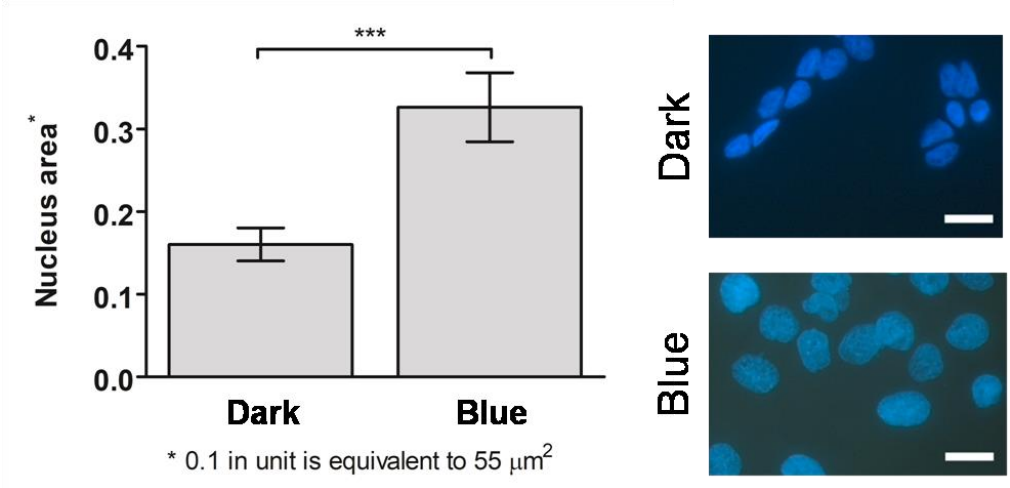

Figure 5.7. Nucleus area in cells chronically irradiated with blue light (*Blue*) are almost two times bigger than dark control cells (*Dark*). Bars indicate mean (n=100) ± standard deviation obtained from ten different micrographs. Statistical analysis was performed using t-test, considering statistically significant at $p<0.05$ (*** $p<0.001$). Scale bar = 20 μm.

Chromatin is divided into euchromatin and heterochromatin, which have different localization inside the nucleus. Heterochromatin is highly compacted, which makes it difficult to transcribe, and found on the nuclear membrane. Heterochromatin shows a low gene density and many repetitive sequences, being considered usually inactive. On the other hand, euchromatin is genetically

active, showing a higher transcription rate and is situated in the center of the nucleus (Dey, 2005).

In normal nuclei, usually, on light microscopy, chromatin is fine and uniformly distributed, while malignant cells show coarse or clumped chromatin with irregular distribution, forming clear regions in the central region of the nucleus (Figure 5.8) (Dey, 2005).

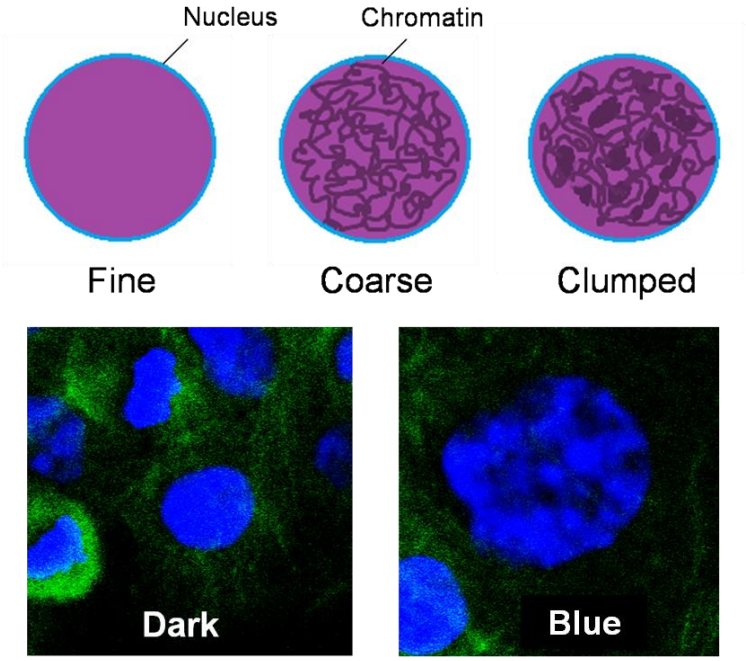

Figure 5.8. Chromatin pattern in *Blue*-treated and *Dark* cells. Clumped chromatin is usually observed in malignant cells, as showed by *Blue*-treated cells, indicating a new gene expression profile and/or genomic instability.

A significant increase (~20%) was observed in cell proliferation rate compared to dark control, starting in the sixth week after the irradiation (Figure 5.9, Table 1). The cell proliferation rate was increased from ten to twenty percent in *Blue* cells compared to *Dark* control (Figure 5.9 a). This enhancement of the cell proliferation rate was verified using others methodologies (counting cells and BrDU incorporation), proving once again a higher significant cell proliferation rate in *Blue* cells compared to both *Dark* and normal HaCaT cells, which show similar proliferation rates (Figure 5.9 c,d).

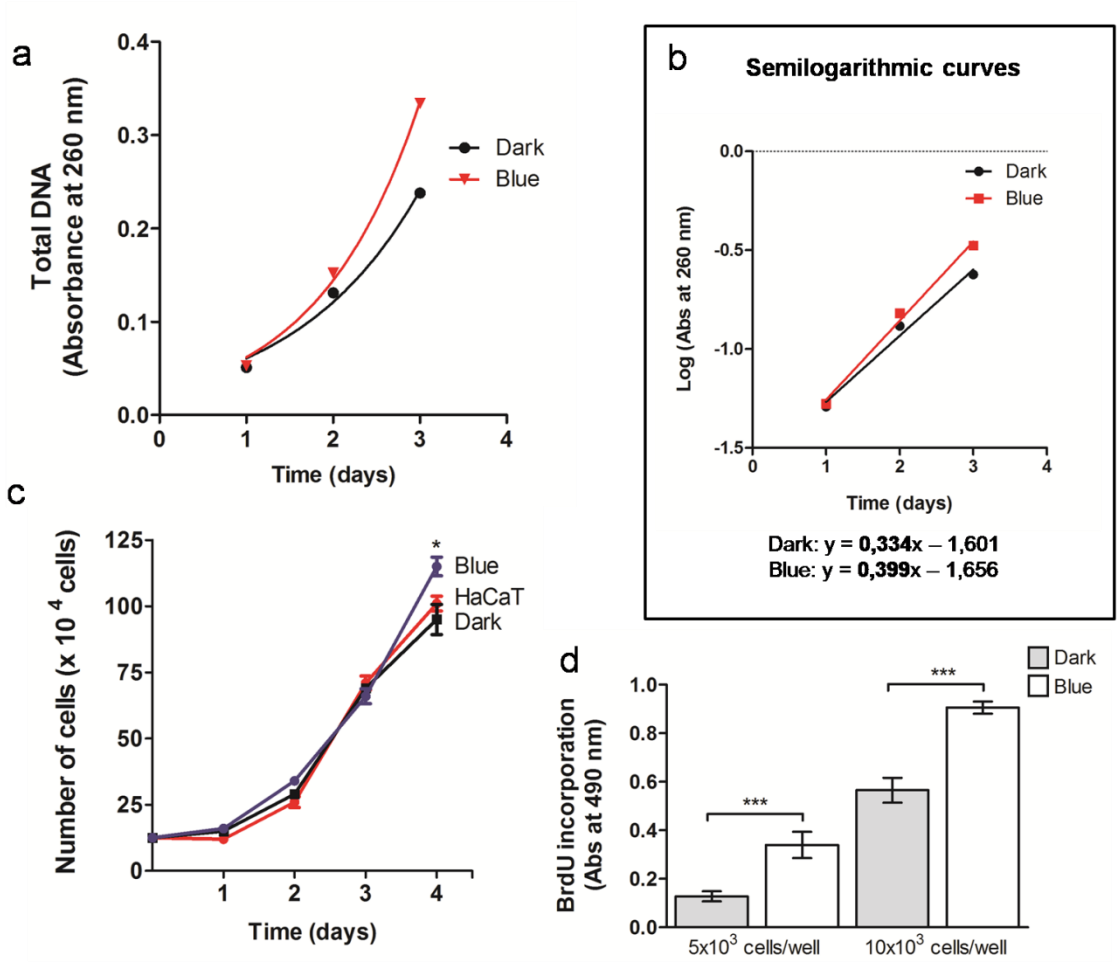

Figure 5.9. HaCaT cells chronically irradiated with blue light (λ= 408 nm, 50 J.cm^{-2}, 3x/week) showed higher cell proliferation rate than dark control. **(a)** Growth curve obtained from absorbance of total DNA from HaCaT irradiated seventeen times with blue light. **(b)** Semilogarithmic curves used to calculate cell proliferation rate showed in Table 1. **(c)** Number of cells counted during four days. On 4th day, there is a statistical difference among *Blue* cells in relation to *Dark* and normal HaCaT cells. **(d)** BrdU incorporation by ELISA assay, in HaCaT chronically irradiated with blue light (36 times irradiated) (*Blue*) and dark control (*Dark*).

Table 1. Cell proliferation rate of HaCaT cells chronically irradiated with blue light (λ= 408 nm, 50 J.cm^{-2}, 3x/week)

Serie	Proliferation rate [a]	Blue/Dark ratio
Dark p17S8	0.288	0.931
Blue p17S8	0.268	
Dark p18S11	0.327	1.009
Blue p18S11	0.330	
Dark p19S14	0.349	0.977
Blue p19S14	0.341	
Dark p20S17	0.334	1.195
Blue p20S17	0.399	
Dark p21S20	0.285	1.151
Blue p21S20	0.328	
Dark p26S25	0.146	1.110
Blue p25S25	0.162	

a angular coefficient obtained from slope of semilogarithm graph

In order to investigate changes in the protein levels of some cell proliferation markers, especially for human skin keratinocytes, we performed Western blots to detect PCNA, E2F2, and p16^{INK4a} (Figure 5.10).

Analyzing the protein expression of p16^{INK4a}, an important regulator of the cell cycle (p53 and RB pathway), a tumor suppression gene and inductor of senescence, we observed a higher level of protein expression (26%) in *Dark* control compared to *Blue*-treated cells (Figure 5.10). A higher level of p16^{INK4a} expression has been reported during aging of most cell types (Ressler *et al.*, 2006). Besides, the somatic mutation, deletion or methylation of the p16^{INK4a} gene were detected in many cancers, such as melanoma, where 96% of all cell lines showed these alterations in this gene (Walker *et al.*, 1998). Additionally, the inactivation of p16^{INK4a}, by promoter methylation, is involved in progression from pre-neoplastics lesions to squamous cell carcinoma of skin (SCC), which

represents 20% of the skin cancer cases, according to the American Cancer Society (Mortier *et al.*, 2002; Brown *et al.*, 2004). Thus, *Blue*-treated cells showed a common alteration as in cutaneous SCC, a neoplasia of epidermal skin keratinocytes. It will be interesting to investigate in the future which mechanism is involved in the reduction of the $p16^{INK4a}$ gene expression in *Blue*-treated cells.

We also observed a subtle increase in the protein expression level of the proliferating cell nuclear antigen (PCNA), a known marker for proliferating cells; there was no change in the level of transcription factor E2F2, both involved in cell cycle regulation and DNA replication (Figure 5.10).

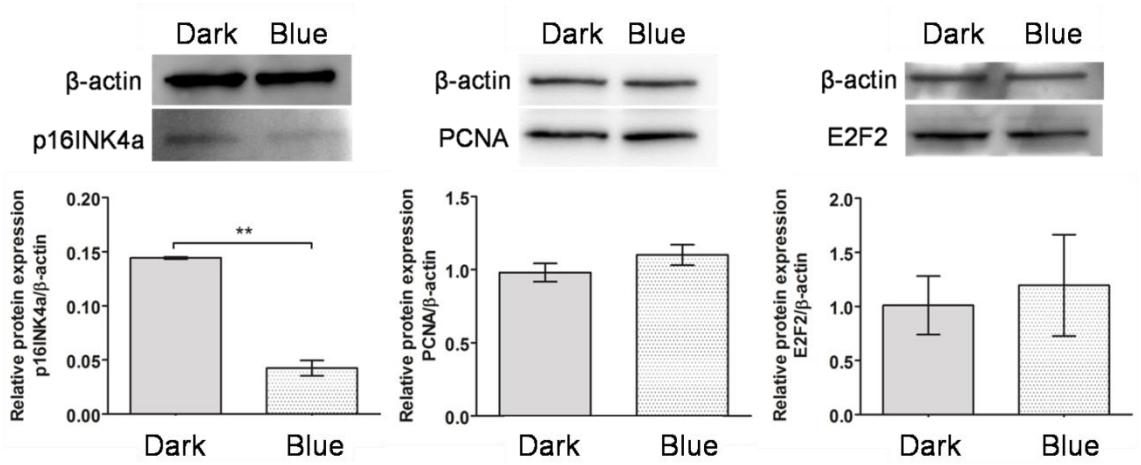

Figure 5.10. Relative protein expression of p16INK4a, PCNA and E2F2 in IR cells showed significant reduction compared to dark control. Statistical analysis was performed using t-test, considering statistically significant at $p<0.05$ (** $p<0.01$).

To engage in more replicative division, cancer cells require an elevation in uptake of nutrients, mainly glucose, as a source of carbon intermediates for anabolic reactions and ATP synthesis, to synthesize proteins and lipids and to form daughter cells (Frezza and Gottlieb, 2009). So, we verified the protein level of important regulatory enzymes in cell metabolism, glyceraldehyde 3-phosphate dehydrogenase (GAPDH) and cytochrome oxidase IV (COXIV),

which showed similar protein expression level in both *Blue*-treated and *Dark* control cells (Figure 5.11). Indeed, cells were grown in high glucose (4.5 g/L) medium in order to allow constant levels of metabolic enzymes. Interestingly, we did not observe any significant alteration in protein level of these enzymes, indicating that metabolism in both chronic irradiated and control cells is similar.

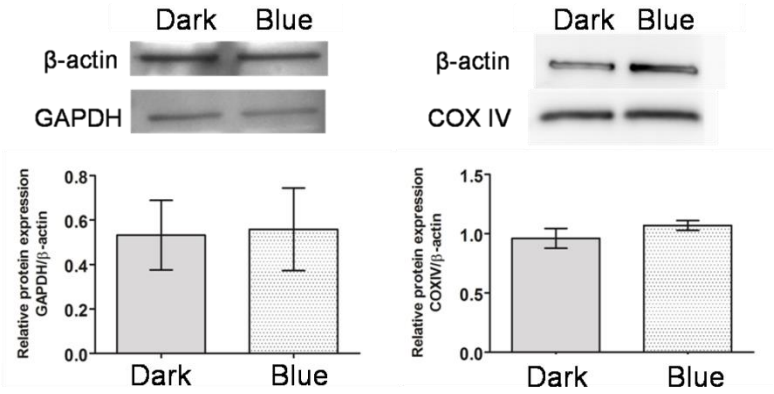

Figure 5.11. Relative protein expression of metabolic enzymes GAPDH (glycolysis) and COX IV in *Dark* and *Blue*-treated cells.

We investigated the resistance to UVA-induced apoptosis in *Blue*-treated and *Dark* control cells, using a dose of 24 J.cm^{-2}, which is known to induce apoptosis in HaCaT cells (He et al. 2006). For this purpose, the apoptotic cells were detected and quantified using a FACS analysis, co-staining cells with Annexin V and propidium iodide (PI) (Crowley *et al.*, 2016). As positive control for apoptosis, we treated cells with staurosporine, which is a typical inducer of this cell death (Figure 5.12) (McKeague, Wilson and Nelson, 2003).

Blue-treated cells, eighteen hours after exposure to UVA radiation (λ= 365 nm, 24 J.cm^{-2}), showed a significant decrease in total percentage of apoptotic cells (Annexin V$^+$/PI$^+$ + Annexin V$^+$/PI$^-$ quadrants): 30.71% compared to normal HaCaT (45.31%) and *Dark* control (37.15%) (Figure 5.12). The non-irradiated cells with UVA (HaCaT dark, *Dark* dark, and *Blue* dark cells), showed no significant increase in total percentage of apoptosis, as expected (Figure

5.12). These data were corroborated by a clonogenic assay, where *Blue*-treated cells showed a higher level of the surviving fraction in relation to the *Dark* control: *Blue*-treated cells showed 20% more colonies, in the clonogenic assay, than the dark control, one week after exposure to UVA (Figure 5.12). We have proposed that constant selective pressure involving the photoinduced stress by chronic exposure to high-energy blue light turns the *Blue*-treated cells more tolerant to oxidative stress, raising the cytotoxic threshold to drive cells to apoptosis.

Apoptosis is a natural barrier against the malignant transformation process, eliminating damaged cells by mechanisms of programmed cell death. Evasion of apoptosis is a common strategy used by cancer cells, which can be promoted by a reduction of death receptor/signals; defects/mutations in p53; reduced expression of caspases; increased expression of apoptosis inhibitors; and a misbalance between pro-apoptotic and anti-apoptotic proteins (Hanahan and Weinberg, 2011; Wong, 2011). Thus, evasion of apoptosis by *Blue*-treated cells is an additional evidence of carcinogenic potential of blue light on human skin keratinocytes.

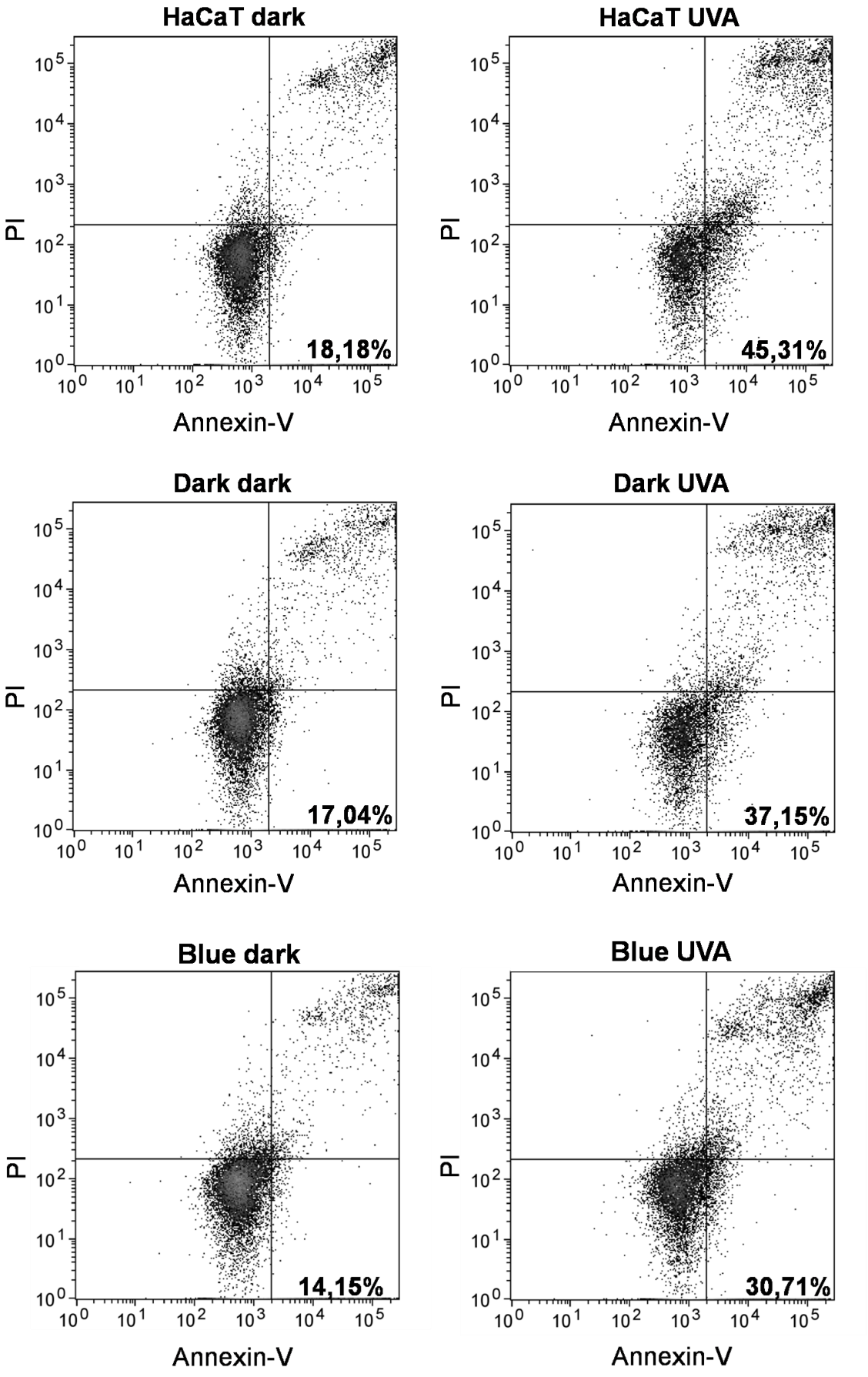
HaCaT dark
18,18%
HaCaT UVA
45,31%
Dark dark
17,04%
Dark UVA
37,15%
Blue dark
14,15%
Blue UVA
30,71%
PI
Annexin-V

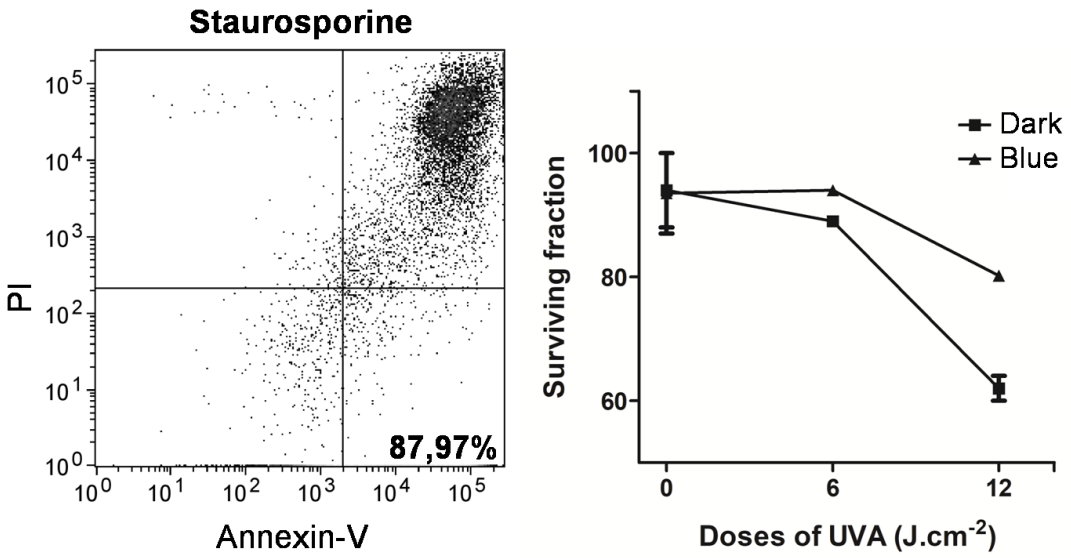

Figure 5.12. HaCaT cells chronically irradiated with high-energy blue light acquire a subtle resistance to apoptosis induced by UVA radiation at dose of 24 J.cm^{-2}. Eighteen hours after UVA treatment, cells were analyzed by flow cytometry after annexin-V and propidium iodide staining. The number in the lower right quadrant corresponds to total percentage apoptosis. Positive control was done with staurosporine. Clonogenic assay of *Dark* and *Blue*-treated cells after UVA-treatment using different doses (6 and 12 J.cm^{-2}).

In figure 5.13, we summarize the main results of this work, based on the classical illustration done in “Hallmarks of cancer”, by Hanahan & Weinberg (2011). These conditions comprise four out of ten biological capabilities acquired for multistep development of tumor in human cells, defined by Hanahan & Weinberg (2011) in “Hallmarks of Cancer: The Next Generation”.

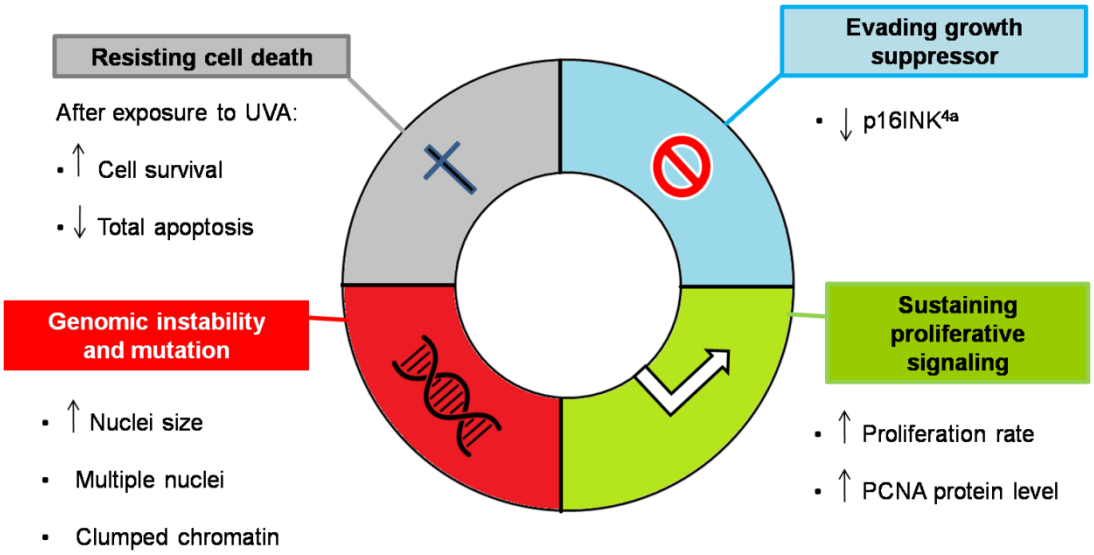

Figure 5.13. Four out of ten hallmarks of cancer defined by Hanahan & Weinberg (2011) were partially reached in *Blue*-treated cells, showing the potential of blue light to induce malignant transformation in human skin keratinocytes.

5.4. CONCLUSIONS

Ours results have shown the potential that high-energy blue light has in terms of leading to malignant transformation of human skin keratinocytes, including alteration in gene expression, changes in nucleus morphology and cell size, proliferation rate, and increasing resistance to UVA-induced apoptosis. Furthermore, we showed for the first time in literature that blue light can generate cyclobutane pyrimidine dimers (CPDs), shortly after or along the chronic exposure. CPDs are well-known to be generated by UVA and UVB radiation, being the major mutagenic lesions in mammalian cells, and the mostly involved in induction of melanoma (Pfeifer and Besaratinia, 2012). Moreover, the blue light can be an additional carcinogenic fraction of the sunlight involved in non-melanoma skin cancer (SCC and BCC), besides the UV, pointing to the need of being considered in sun protection.

5.5. SUPPLEMENTARY MATERIAL

Soft agar

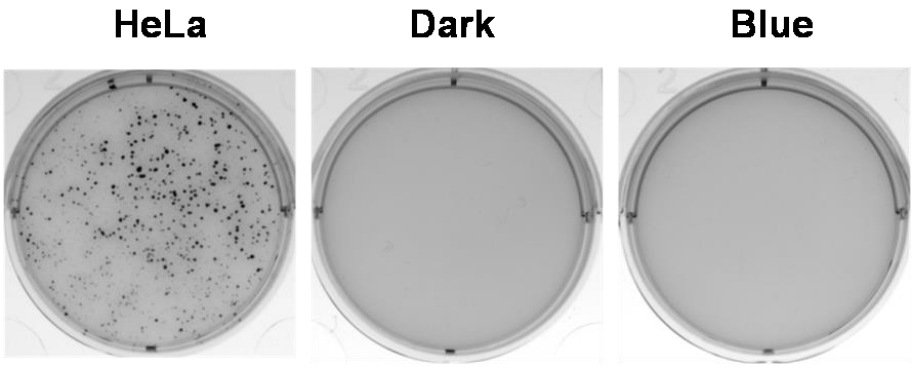

Figure S1. HaCaT cells chronically irradiated in Blue (*Blue*-treated cells) and *Dark* control did not establish colonies in Soft Agar, after 3 weeks. In this experiment, HeLa cells were used as positive control.

Chapter 6 – Conclusions and Final Remarks

We investigated the photoinduced accumulation of the age pigment lipofuscin in skin keratinocytes and how the photosensitization of this pigment augments the effects of light exposure. Lipofuscin absorbs in the visible region, and so we have focused on the effect of visible light on the viability of lipofuscin-loaded skin cells, on the generation of premutagenic lesions, as well as mutagenic transformation induced by blue light. We have used physiologically relevant light doses, observing that keratinocytes, after lipofuscin accumulation, become more sensitive to visible light, generating ROS and forming premutagenic lesions, which if not repaired, can lead to the accumulation of DNA mutations and cancer. So, the accumulation of lipofuscin is clearly an important factor for carcinogenesis in skin cells. The proof of this concept is undoubtedly one of the most important contributions of this work, because lipofuscin can be used as a marker of photoinduced skin aging and can allow the development of novel strategies of sun protection.

Although, skin keratinocytes are constantly renewed in the epidermis, because they are constantly under differentiation to form the *stratum corneum* (see ***Chapter 1***), migration of keratinocytes to outer layers of skin takes enough time to progenitor cells accumulate lipofuscin, accelerating the aging, and can likely be a link between skin aging and cancer. Besides, we detected that 48 hours after UVA exposure (***Chapter 2***), and after the DMMB-treatment (***Chapter 3***) and blue light exposure (***Chapter 4***), a maximal amount of lipofuscin is accumulated in keratinocytes. Therefore, if lipofuscin-loaded keratinocytes are exposed to visible light, photosensitization and amplification of the damage in biomolecules and organelles will occur.

To better characterize the accumulation of lipofuscin and its photosensitization properties, we established a protocol to efficiently induce lipofuscinogenesis (***Chapter 3***). This was based on the knowledge that lipofuscin generation is maximized if both mitochondria and lysosomes are damaged, because mitophagy and autophagy inhibition are stimulated in parallel (Martins *et al.*, 2017). In effect, we used 1,9-dimethylmethylene blue (DMMB) to induce an efficient lipofuscinogenesis in keratinocytes. By using this experimental model, we observed that lipofuscin in keratinocytes absorbs blue light and emits red light, having a fluorescence lifetime close to what can be found in lipofuscin from RPE cells. Thus, lipofuscin-loaded keratinocytes can be more sensitive to blue light than a normal cell.

Keratinocytes correspond to 90% of the cells found in the epidermis and also the main cell type involved in skin cancer (basal and squamous carcinoma) (see ***Chapter 1***). Besides, skin keratinocytes receive melanin from the melanocytes, and consequently can also carry melanin granules, which is also a photosensitizer in the visible light, generating ROS and premutagenic lesions in DNA (Chiarelli-Neto et al. 2014). Thus, in *in vivo* conditions, both keratinocytes and melanocytes can be exposed to mutual effects of lipofuscin and melanin photosensitization by visible light, therefore, amplifying the probability of a malignant transformation. To avoid the accumulation of lipofuscin due to oxidative stress induced by UVA and visible light (blue and green light, especially, as we showed in ***Chapter 4***) may be a fundamental way to prevent skin cancer and, therefore, an important target for development in the area of sun care.

At last, we aimed to answer whether visible light can induce HaCaT cell to engage in malignant transformation. For this, we chose the high-energy blue light (λ=408 nm) to induce direct oxidative stress, DNA damage, as well as damage in mitochondria and lysosomes, leading to malignant transformation. Indeed, as we showed in ***Chapter 5***, HaCaT cells chronically exposed to blue light reach at least four signs expected for a malignant cell, including the reduction in expression of the tumor suppressor $p16^{INK4a}$, commonly mutated and silenced in carcinoma and melanoma, an increase in cell proliferation, and a resistance to apoptosis. This work is now continuing in the tentative determination of the mutations accumulated in those cells by using genomic and transcriptomic techniques.

We expect that this thesis will contribute to change the current status of sun protection, which just considers protection against UVA and UVB. Our results clearly showed the carcinogenic potential of visible light, specifically of blue light in human skin keratinocytes. We hypothesize that much of the increase in skin cancer, reported nowadays, is a consequence of irresponsible use of sun protection agents. These products are clearly protecting only partially against the sunlight, but are advertised as high protection products that misleadingly guarantee that sun exposure is safe to their users. The challenge for the scientific community and for companies working in sun care area is clearly the development of more robust agents that protects our skin from the whole sunlight spectrum.

REFERENCES

Abrahamse, H. et al., 2016. **New photosensitizers for photodynamic therapy**. *Biochem J*, 473(4), pp.347–64.

Adamskaya, N. et al., 2011. **Light therapy by blue LED improves wound healing in an excision model in rats**. *Injury*, 42(9), pp.917–921.

Agar, N.S. et al., 2004. **The basal layer in human squamous tumors harbors more UVA than UVB fingerprint mutations: a role for UVA in human skin carcinogenesis**. *Proc Natl Acad Sci USA*, 101(14), pp.4954–4959.

Agnez-Lima, L.F. et al., 2012. **DNA damage by singlet oxygen and cellular protective mechanisms**. *Mutat Res*, 751(1), pp.15–28.

Anderson, S. et al., 1981. **Sequence and organization of the human mitochondrial genome**. *Nature*, 290(5806), pp.457–465.

Apalla, Z. et al., 2017. **Epidemiological trends in skin cancer**. *Dermatol Pract Concept*, 7(2), pp.1–6.

Bacellar, I. et al., 2014. **Membrane damage efficiency of phenothiazinium photosensitizers**. *Photochem Photobiol*, 90, pp.801–813.

Baier, J. et al., 2006. **Singlet oxygen generation by UVA light exposure of endogenous photosensitizers**. *Biophys J*, 91(4), pp.1452–1459.

Battie, C. et al., 2014. **New insights in photoaging, UVA induced damage and skin types**. *Exp Dermatol*, 23, pp.7–12.

Becker, D. et al., 2011. **Clinical efficacy of blue light full body irradiation as treatment option for severe atopic dermatitis**. *PLoS ONE*, 6(6).

Begum, R. et al., 2013. **Treatment with 670 nm Light Up Regulates Cytochrome C Oxidase Expression and Reduces Inflammation in an Age-Related Macular Degeneration Model**. *PLoS ONE*, 8(2).

Behar-Cohen, F. et al., 2014. **Ultraviolet damage to the eye revisited: Eye-sun protection factor (E-SPF®), a new ultraviolet protection label for eyewear**. *Clin Ophthalmol*, 8(1), pp.87–104.

Bernard, A. & Klionsky, D.J., 2013. **Autophagosome Formation: Tracing the Source**. *Dev Cell*, 25(2), pp.116–117.

Besaratinia, A. et al., 2007. **Riboflavin activated by ultraviolet A1 irradiation induces oxidative DNA damage-mediated mutations inhibited by vitamin C**. *Proc Natl Acad Sci USA*, 104(14), pp.5953–5958.

Betteridge, D.J., 2000. **What is oxidative stress?** *Metabolism: clinical and experimental*, 49(2 Suppl 1), pp.3–8.

Biesemeier, A. et al., 2010. **The classical pathway of melanogenesis is not essential for melanin synthesis in the adult retinal pigment epithelium**. *Cell Tissue Res*, 339(3), pp.551–560.

Bikle, D.D., Xie, Z. & Tu, C.-L., 2012. **Calcium regulation of keratinocyte differentiation**. *Expert Rev Endocrinol Metab*, 7(4), pp.461–472.

Boukamp, P. et al., 1988. **Normal keratinization in a spontaneously immortalized aneuploid human keratinocyte cell line**. *J Cell Biol*, 106(3), pp.761–771.

Boulton, M. et al., 1990. **Age-related changes in the morphology, absorption and fluorescence of melanosomes and lipofuscin granules of the retinal pigment epithelium**. *Vision Res*, 30(9), pp.1291–1303.

Boulton, M. & Marshall, J., 1985. **Repigmentation of human retinal pigment epithelial cells in vitro**. *Exp Eye Res*, 41(2), pp.209–218.

Boulton, M.E., 2014. **Studying melanin and lipofuscin in RPE cell culture models**. *Exp Eye Res*, 126, pp.61–67.

Brash, D.E., 2015. **UV signature mutations**. *Photochem Photobiol*, 91(1), pp.15–26.

Brodie, A.E. & Reed, D.J., 1987. **Reversible oxidation of glyceraldehyde 3-phosphate dehydrogenase thiols in human lung carcinoma cells by hydrogen peroxide**. *Biochem Biophys Res Commun*, 148(1), pp.120–125.

Brown, V.L. et al., 2004. **p16INK4a and p14ARF tumor suppressor genes are commonly inactivated in cutaneous squamous cell carcinoma**. *J Invest Dermatol*, 122(5), pp.1284–1292.

Brunk, U.T., Jones, C.B. & Sohal, R.S., 1992. **A novel hypothesis of lipofuscinogenesis and cellular aging based on interactions between oxidative stress and autophagocytosis**. *Mutat Res DNAging*, 275(3–6), pp.395–403.

Brunk, U.T. & Terman, A., 2002a. **Lipofuscin: Mechanisms of age-related accumulation and influence on cell function**. *Free Radic Biol Med*, 33(5), pp.611–619.

Brunk, U.T. & Terman, A., 2002b. **The mitochondrial-lysosomal axis theory of aging: Accumulation of damaged mitochondria as a result of imperfect autophagocytosis**. *Eur J Biochem*, 269(8), pp.1996–2002.

Cadenas, E. et al., 1977. **Production of superoxide radicals and hydrogen peroxide by NADH-ubiquinone reductase and ubiquinol-cytochrome c reductase from beef-heart mitochondria**. *Arch Biochem Biophys*, 180(2), pp.248–257.

Cadet, J. & Richard Wagner, J., 2013. **DNA base damage by reactive oxygen species, oxidizing agents, and UV radiation**. *CSH Perspect Biol*, 5(2).

Chial, H., 2008. **mtDNA and mitochondrial diseases**. *Nature Education*, 1(1), pp.1–6.

Chiarelli-Neto, O. et al., 2011. **Generation and suppression of singlet oxygen in hair by photosensitization of melanin**. *Free Radic Biol Med*, 51(6), pp.1195–1202.

Chiarelli-Neto, O. et al., 2014. **Melanin photosensitization and the effect of visible light on epithelial cells**. *PLoS ONE*, 9(11).

Cichorek, M. et al., 2013. **Skin melanocytes: Biology and development**. *Postepy Dermatol Alergol*, 30(1), pp.30–41.

Cohen, D. & Lee, P., 2016. **Photodynamic Therapy for Non-Melanoma Skin Cancers**. *Cancers*, 8(12), p.90.

Collins, A.R., Duthie, S.J. & Dobson, V.L., 1993. **Direct enzymic detection of endogenous oxidative base damage in human lymphocyte DNA**. *Carcinogenesis*, 14(9), pp.1733–1735.

Colombo, I. et al., 2017. **HaCaT Cells as a Reliable In Vitro Differentiation Model to Dissect the Inflammatory/Repair Response of Human Keratinocytes**. *Mediators Inflamm*, 2017, pp.1–12.

Croteau, D.L. et al., 1997. **An oxidative damage-specific endonuclease from rat liver mitochondria**. *J Biol Chem*, 272(43), pp.27338–44.

Crowley, L.C. et al., 2016. **Quantitation of apoptosis and necrosis by annexin V binding, propidium iodide uptake, and flow cytometry**. *Cold Spring Harbor Protocols*, 2016(11), pp.953–957.

Cuervo, A.M. & Wong, E., 2014. **Chaperone-mediated autophagy: Roles in disease and aging**. *Cell Research*, 24(1), pp.92–104.

Czarnecki, D., 2016. **The Relentless Rise in the Incidence of Melanoma in Susceptible Australians**. *J Invest Dermatol*, 136(9), pp.1912–1913.

Deaton, A. & Bird, A., 2011. **CpG islands and the regulation of transcription**. *Genes & development*, 25(10), pp.1010–1022.

Delinasios, G.J. et al., 2018. **Vitamin E inhibits the UVAI induction of "light" and "dark" cyclobutane pyrimidine dimers, and oxidatively generated DNA damage, in keratinocytes**. *Sci Rep*, 8(1).

Dey, P., 2010. **Cancer nucleus: Morphology and beyond**. *Diagnostic Cytopathol*, 38(5), pp.382–390.

Dey, P., 2005. **Chromatin pattern alteration in malignant cells: An enigma**. *Diagn Cytopathol*, 32(1), pp.25–30.

Dizdaroglu, M., 2005. **Base-excision repair of oxidative DNA damage by DNA glycosylases**. *Mutat Res*, 591(1–2), pp.45–59.

Douki, T. et al., 2003. **Bipyrimidine photoproducts rather than oxidative lesions are the main type of DNA damage involved in the genotoxic effect of solar UVA radiation**. *Biochemistry*, 42(30), pp.9221–9226.

Eckert, R.L. & Rorke, E.A., 1989. **Molecular biology of keratinocyte differentiation**. *Environ Health Perspect,* 80, pp.109–116.

Eichner, R., Sun, T.T. & Aebi, U., 1986. **The role of keratin subfamilies and keratin pairs in the formation of human epidermal intermediate filaments**. *J Cell Biol*, 102(5), pp.1767–1777.

Eide, M.J. et al., 2010. **Identification of patients with nonmelanoma skin cancer using health maintenance organization claims data**. *Am J Epidemiol*, 171(1), pp.123–128.

Eldred, G.E. et al., 1982. **Lipofuscin: resolution of discrepant fluorescence data**. *Science*, 216(4547), pp.757–759.

Eldred, G.E. & Katz, M.L., 1988. **Fluorophores of the human retinal pigment epithelium: separation and spectral characterization**. *Exp Eye Res*, 47(1), pp.71–86.

Elias, P.M. & Choi, E.H., 2005. **Interactions among stratum corneum defensive functions**. *Exp Dermatol*, 14(10), pp.719–726.

Evans, M.D., Dizdaroglu, M. & Cooke, M.S., 2004. **Oxidative DNA damage and disease: Induction, repair and significance**. *Mutat Res*, 567(1), pp.1–61.

Everett, M.A. et al., 1966. **Penetration of epidermis by ultraviolet rays**. *Photochem Photobiol*, 5(7), pp.533–542.

Feng, Y. et al., 2014. **The machinery of macroautophagy**. *Cell Research*, 24(1), pp.24–41.

Filomeni, G., De Zio, D. & Cecconi, F., 2015. **Oxidative stress and autophagy: The clash between damage and metabolic needs**. *Cell Death Differ*, 22(3), pp.377–388.

Floor, S.L. et al., 2012. **Hallmarks of cancer: Of all cancer cells, all the time?** *Trends Mol Med*, 18(9), pp.509–515.

Freeman, S.E. et al., 1989. **Wavelength dependence of pyrimidine dimer formation in DNA of human skin irradiated in situ with ultraviolet light**. *Proc Natl Acad Sci USA*, 86(14), pp.5605–5609.

Frezza, C. & Gottlieb, E., 2009. **Mitochondria in cancer: Not just innocent bystanders**. *Semin Cancer Biol*, 19(1), pp.4–11.

Fuchs, E., 1998. **Beauty is skin deep: the fascinating biology of the epidermis and its appendages**. *Harvey Lect*, 94, pp.47–77.

Furda, A.M. et al., 2012. **Analysis of DNA damage and repair in nuclear and mitochondrial DNA of animal cells using quantitative PCR**. *Methods Mol Biol*, 920, pp.111-32.

Fusenig, N.E. & Boukamp, P., 1998. **Multiple stages and genetic alterations in immortalization, malignant transformation, and tumor progression of human skin keratinocytes**. *Mol Carcinog*, 23(3), pp.144–58.

Gaillard, E.R. et al., 1995. **Photophysical studies on human retinal lipofuscin**. *Photochem Photobiol*, 61(5), pp.448–453.

Georgakopoulou, E.A. et al., 2013. **Specific lipofuscin staining as a novel biomarker to detect replicative and stress-induced senescence. A method applicable in cryo-preserved and archival tissues**. *Aging*, 5(1), pp.37–50.

Godley, B.F. et al., 2005. **Blue light induces mitochondrial DNA damage and free radical production in epithelial cells**. *J Biol Chem*, 280(22), pp.21061–6.

Gray, D. a & Woulfe, J., 2005. **Lipofuscin and aging: a matter of toxic waste**. *Sci Aging Knowledge Environ*, 2005(5), p.re1.

Green, D.R. & Reed, J.C., 1998. **Mitochondria and apoptosis**. *Science*, 281(5381), pp.1309–1312.

de Gruijl, F.R., 1999. **Skin cancer and solar UV radiation**. *Eur J Cancer*, 35(14), pp.2003–9.

Gunther, M., 2011. **Advanced CSP Teaching Materials** - Linear Fresnel Technology. *Advanced CSP teaching materials*, pp.1–43.

Guo, C. et al., 2017. **Transversions have larger regulatory effects than transitions**. *BMC Genomics*, 18(1), p.1.

Hackbarth, S. et al., 2010. **New insights to primary photodynamic effects - Singlet oxygen kinetics in living cells**. *Journal of Photochemistry and Photobiology B: Biology*, 98(3), pp.173–179.

Halliwell, B. & Gutteridge, J.M.C., 2015. **Free Radicals in Biology and Medicine**. *Free Radic Biol Med*, 24(10), p.764.

Hanafi, A., Gharbi, T. & Cornu, J.-Y., 2005. **In vivo measurement of lower back deformations with Fourier-transform profilometry**. *Applied optics*, 44(12), pp.2266–73.

Hanahan, D. & Weinberg, R.A., 2011. **Hallmarks of cancer: The next generation**. *Cell*, 144(5), pp.646–674.

Hanahan, D. & Weinberg, R.A., 2000. **The hallmarks of cancer**. *Cell*, 100(1), pp.57–70.

Hanasoge, S. & Ljungman, M., 2007. **H2AX phosphorylation after UV irradiation is triggered by DNA repair intermediates and is mediated by the ATR kinase**. *Carcinogenesis*, 28(11), pp.2298–2304.

Haralampus-Grynaviski, N.M. et al., 2003. **Spectroscopic and morphological studies of human retinal lipofuscin granules**. *Proc Natl Acad Sci USA*, 100(6), pp.3179–3184.

Hatahet, Z. et al., 1994. **New substrates for old enzymes. 5-Hydroxy-2'-deoxycytidine and 5-hydroxy- 2'-deoxyuridine are substrates for Escherichia coli endonuclease III and formamidopyrimidine DNA N-glycosylase, while 5-hydroxy-2'-deoxyuridine is a substrate for uracil DNA N-glyco**. *J Biol Chem*, 269(29), pp.18814–18820.

He, Y.Y. et al., 2006. **Chronic UVA irradiation of human HaCaT keratinocytes induces malignant transformation associated with acquired apoptotic resistance**. *Oncogene*, 25(26), pp.3680-8.

Höhn, A. et al., 2010. **Lipofuscin-bound iron is a major intracellular source of oxidants: Role in senescent cells**. *Free Radic Biol Med*, 48(8), pp.1100–1108.

Höhn, A. et al., 2011. **Lipofuscin inhibits the proteasome by binding to surface motifs**. *Free Radic Biol Med*, 50(5), pp.585–591.

Höhn, A., König, J. & Grune, T., 2013. **Protein oxidation in aging and the removal of oxidized proteins**. *J Proteomics*, 92, pp.132–159.

Holick, M.F., 2016. **Biological effects of sunlight, ultraviolet radiation, visible light, infrared radiation and Vitamin D for health**. *Anticancer Research*, 36(3), pp.1345–1356.

House, R.L. et al., 2015. **Artificial photosynthesis: Where are we now? Where can we go?** *Journal of Photochemistry and Photobiology C: Photochemistry Reviews*.

Hughes, M.W., Lu, W. & Chuong, C.-M., 2013. **Nuclear Topology, Epigenetics, and Keratinocyte Differentiation**. *J Invest Dermatol*, 133(9), pp.2130–2133.

Hulstrom C & Riordan R, 1990. **What Is an Air Mass 1.5 Spectrum?** *Ieee*, pp.1085–1088.

Ishida-Yamamoto, A. & Iizuka, H., 1998. **Structural organization of cornified cell envelopes and alterations in inherited skin disorders**. *Exp Dermatol*, 7(1), pp.1–10.

Jeanmougin, M. & Civatte, J., 1987. **Dosimetry of solar ultraviolet radiation. Daily and monthly changes in Paris**. *Ann Dermatol Venereol*, 114(5), pp.671–6.

Jiang, Y. et al., 2009. **UVA generates pyrimidine dimers in DNA directly**. *Biophys J*, 96(3), pp.1151–1158.

Jung, T., Höhn, A. & Grune, T., 2010. **Lipofuscin: Detection and quantification by microscopic techniques**. *Methods Mol Biol*, 594, pp.173–193.

Kanofsky, J.R., 2011. **Measurement of singlet-oxygen in vivo: Progress and pitfalls**. *Photochemistry and Photobiology*, 87(1), pp.14–17.

Kaur, J. & Debnath, J., 2015. **Autophagy at the crossroads of catabolism and anabolism**. *Nat Rev Mol Cell Biol*, 16(8), pp.461–472.

Kim, M., Jung, H.Y. & Park, H.J., 2015. **Topical PDT in the treatment of benign skin diseases: Principles and new applications**. *International Journal of Molecular Sciences*, 16(10), pp.23259–23278.

King, A. et al., 2004. **Mitochondria-derived Reactive Oxygen Species Mediate Blue Light-induced Death of Retinal Pigment Epithelial Cells**. *Photochem Photobiol*, 79(5), pp.470–475.

Kino, K. & Sugiyama, H., 2001. **Possible cause of G·C→C·G transversion mutation by guanine oxidation product, imidazolone**. *Chem Biol*, 8(4), pp.369–378.

Klionsky, D.J. et al., 2008. **Guidelines for the use and interpretation of assays for monitoring autophagy in higher eukaryotes**. *Autophagy*, 4(2), pp.151–175.

König, J. et al., 2017. **Mitochondrial contribution to lipofuscin formation**. *Redox Biology*, 11, pp.673–681.

Kovalenko, O. & Santos, J.H., 2009. **Analysis of oxidative damage by gene-specific quantitative PCR**. *Curr Protoc Hum Genet*, Editorial board, Jonathan L. Haines et al., Chapter 19: p.Unit 19.1.

Kowaltowski, A.J. et al., 2009. **Mitochondria and reactive oxygen species**. *Free Radic Biol Med*, 47(4), pp.333–43.

Kuluncsics, Z. et al., 1999. **Wavelength dependence of ultraviolet-induced DNA damage distribution: Involvement of direct or indirect mechanisms and possible artefacts**. *Photochem Photobiol B: Biology*, 49(1), pp.71–80.

Kuo, L.J. & Yang, L.X., 2008. **Gamma-H2AX - a novel biomarker for DNA double-strand breaks**. *In Vivo*, 22(3), pp.305–309.

Labi, V. & Erlacher, M., 2015. **How cell death shapes cancer**. *Cell Death Dis*, 6(3), 6:e1675.

Lamore, S.D. et al., 2010. **Proteomic identification of cathepsin B and nucleophosmin as novel UVA-targets in human skin fibroblasts**. *Photochem Photobiol*, 86(6), pp.1307–1317.

Lamore, S.D. & Wondrak, G.T., 2012. **Autophagic-lysosomal dysregulation downstream of cathepsin B inactivation in human skin fibroblasts exposed to UVA**. *Photochem. Photobiol. Sci.*, 11(1), pp.163–172.

Lamore, S.D. & Wondrak, G.T., 2013. **UVA causes dual inactivation of cathepsin B and L underlying lysosomal dysfunction in human dermal fibroblasts**. *Photochem Photobiol B: Biology*, 123, pp.1–12.

Lawrence, K. P. *et al.*, 2018. **The UV/Visible Radiation Boundary Region (385–405 nm) Damages Skin Cells and Induces "dark" Cyclobutane Pyrimidine Dimers in Human Skin in vivo**. *Sci Rep*, 8(1):12722.

Lee, H.C. & Wei, Y.H., 2009. **Mitochondrial DNA instability and metabolic shift in human cancers**. *Int J Mol Sci*, 10(2), pp.674–701.

Lhiaubet, V., Paillous, N. & Chouini-Lalanne, N., 2001. **Comparison of DNA damage photoinduced by ketoprofen, fenofibric acid and benzophenone via electron and energy transfer**. *Photochem Photobiol*, 74(5), pp.670–678.

Li, J. et al., 2006. **Similarities and differences between cyclobutane pyrimidine dimer photolyase and (6-4) photolyase as revealed by resonance raman spectroscopy: Electron transfer from the FAD cofactor to ultraviolet-damaged DNA**. *J Biol Chem*, 281(35), pp.25551–25559.

Li, W.W., Li, J. & Bao, J.K., 2012. **Microautophagy: Lesser-known self-eating**. *Cell Mol Life Sci*., 69(7), pp.1125–1136.

Li, Y. et al., 2016. **The lysosomal membrane protein SCAV-3 maintains lysosome integrity and adult longevity**. *J Cell Biol*, 215(2), pp.167–185.

Liebel, F. et al., 2012. **Irradiation of skin with visible light induces reactive oxygen species and matrix-degrading enzymes**. *J Invest Dermatol*, 132(7), pp.1901–1907.

Liebmann, J., Born, M. & Kolb-Bachofen, V., 2010. **Blue-light irradiation regulates proliferation and differentiation in human skin cells**. *J Invest Dermatol*, 130(1), pp.259–269.

Lleonart, M.E., Artero-Castro, A. & Kondoh, H., 2009. **Senescence induction; a possible cancer therapy**. *Mol Cancer*, 8, p.3.

Loeb, L.A., Loeb, K.R. & Anderson, J.P., 2003. **Multiple mutations and cancer**. *Proc Natl Acad Sci USA*, 100(3), pp.776–81.

Mahmoud, B.H. et al., 2008. **Effects of visible light on the skin**. *Photochem Photobiol*, 84(2), pp.450–462.

Mahmoud, B.H. et al., 2010. **Impact of long-wavelength UVA and visible light on melanocompetent skin**. *J Invest Dermatol*, 130(8), pp.2092–2097.

Manders, E.M.M., Verbeek, F.J. & Aten, J.A., 1993. **Measurement of co-localization of objects in dual colour confocal images**. *J Microscopy*, 169(3), pp.375–382.

Marian, C.M. et al., 2014. **Photophysics of flavin derivatives absorbing in the blue-green region: thioflavins as potential cofactors of photoswitches**. *J Phys Chem B*, 118(7), pp.1743–1753.

Martins, W.K. et al., 2018. **Parallel damage in mitochondria and lysosomes is an efficient way to photoinduce cell death**. *Autophagy*, accepted.

Martins, W.K. et al., 2017. **Membrane damage by betulinic acid provides insights into cellular aging**. *Biochim Biophys Acta*, 1861(1), pp. 3129-43.

Martins, W.K. et al., 2015. **Parallel damage in mitochondrial and lysosomal compartments promotes efficient cell death with autophagy: The case of the pentacyclic triterpenoids.** *Sci Rep,* 12425(5).

McKeague, A.L., Wilson, D.J. & Nelson, J., 2003. **Staurosporine-induced apoptosis and hydrogen peroxide-induced necrosis in two human breast cell lines**. *British Journal of Cancer*, 88(1), pp.125–131.

McNeilly, A.D. et al., 2012. **Characterization of a human keratinocyte HaCaT cell line model to study the regulation of CYP2S1**. *Drug Metab Dispos*, 40(2), pp.283–289.

Montecino, M. et al., 2008. **Vitamin D control of gene expression: Temporal and spatial parameters for organization of the regulatory machinery**. *Crit Rev Euk Gene Exp*, 18(2), pp.163–172.

Mortier, L. et al., 2002. **Progression of actinic keratosis to squamous cell carcinoma of the skin correlates with deletion of the 9p21 region encoding the p16INK4atumor suppressor**. *Cancer Lett.*, 176(2), pp.205–214.

Mouret, S. et al., 2010. **UVA-induced cyclobutane pyrimidine dimers in DNA: a direct photochemical mechanism?** *Org Biomol Chem*, 8, pp.1706–1711.

Nakashima, Y., Ohta, S. & Wolf, A.M., 2017. **Blue light-induced oxidative stress in live skin**. *Free Radic Biol Med*, 108, pp.300–310.

Neumann, N.J. et al., 2005. **Evaluation of phototoxic and photoallergic potentials of 13 compounds by different in vitro and in vivo methods**. *Journal of Photochemistry and Photobiology B: Biology*, 79(1), pp.25–34.

Nishigori, C., Hattori, Y. & Toyokuni, S., 2004. **Role of reactive oxygen species in skin carcinogenesis**. *Antioxid Redox Signal*, 6(3), pp.561–570.

Noomnarm, U. & Clegg, R.M., 2009. **Fluorescence lifetimes: Fundamentals and interpretations**. *Photosynthesis Research*, 101(2–3), pp.181–194.

del Olmo-Aguado, S., Núñez-Álvarez, C. & Osborne, N.N., 2016. **Blue Light Action on Mitochondria Leads to Cell Death by Necroptosis**. *Neurochem Res*, 41(9), pp.2324–2335.

Opländer, C. et al., 2013. **Mechanism and biological relevance of blue-light (420-453 nm)-induced nonenzymatic nitric oxide generation from photolabile nitric oxide derivates in human skin in vitro and in vivo**. *Free Radic Biol Med*, 65, pp.1363–1377.

Osborne, N.N., Núñez-Álvarez, C. & del Olmo-Aguado, S., 2014. **The effect of visual blue light on mitochondrial function associated with retinal ganglions cells**. *Exp Eye Res*, 128, pp.8–14.

Pfeifer, G.P., 1997. **Formation and processing of UV photoproducts: effects of DNA sequence and chromatin environment**. *Photochem Photobiol*, 65(2), pp.270–283.

Pfeifer, G.P. & Besaratinia, A., 2012. **UV wavelength-dependent DNA damage and human non-melanoma and melanoma skin cancer**. *Photochem. Photobiol. Sci.*, 11(1), pp.90–97.

Pfeifer, G.P., You, Y.-H. & Besaratinia, A., 2005. **Mutations induced by ultraviolet light**. *Mutat Res*, 571(1–2), pp.19–31.

Pfeiffer, P., 1998. **The mutagenic potential of DNA double-strand break repair.** *Toxicol Lett*, 96–97(1–2), pp.119–129.

Pi, J. et al., 2008. **Arsenic-induced malignant transformation of human keratinocytes: Involvement of Nrf2**. *Free Radic Biol Med*, 45(5), pp.651–658.

Premi, S., Wallisch, S., Mano, C.M., et al., 2015. **Chemiexcitation of melanin derivatives induces DNA photoproducts long after UV exposure**. *Science*, 347(6224), pp.842–847.

Randhawa, M. et al., 2015. **Visible light induces melanogenesis in human skin through a photoadaptive response**. *PLoS ONE*, 10(6).

Repnik, U., Česen, M.H. & Turk, B., 2016. **The use of lysosomotropic dyes to exclude lysosomal membrane permeabilization**. *CSH Protocols*, 2016(5), pp.447–452.

Ressler, S. et al., 2006. **p16^{INK4A} is a robust in vivo biomarker of cellular aging in human skin**. *Aging Cell*, 5(5), pp.379–389.

Reszka, K. et al., 1995. **The photochemistry of human retinal lipofuscin as studied by EPR**. *Photochem Photobiol*, 62(6), pp.1005–1008.

Reuter, S. et al., 2010. **Oxidative stress, inflammation, and cancer: How are they linked?** *Free Radic Biol Med*, 49(11), pp.1603–1616.

Rigel, D.S., 2008. **Cutaneous ultraviolet exposure and its relationship to the development of skin cancer**. *J Am Acad Dermatol*, 58(5 Suppl. 2):S129-32.

Rochette, P.J. et al., 2003. **UVA-induced cyclobutane pyrimidine dimers form predominantly at thymine-thymine dipyrimidines and correlate with the mutation spectrum in rodent cells**. *Nucleic Acids Res*, 31(11), pp.2786–2794.

Rodgers, K. & Mcvey, M., 2016. **Error-Prone Repair of DNA Double-Strand Breaks**. *J Cell Physiol*, 231(1), pp.15–24.

Romani, N., Brunner, P.M. & Stingl, G., 2012. **Changing views of the role of langerhans cells**. *J Invest Dermatol*, 132(3 PART 2), pp.872–881.

Rózanowska, M. et al., 1998. **Blue light-induced singlet oxygen generation by retinal lipofuscin in non-polar media**. *Free Radic Biol Med*, 24(7–8), pp.1107–1112.

Rubin, H., 2011. **Fields and field cancerization: The preneoplastic origins of cancer: Asymptomatic hyperplastic fields are precursors of neoplasia, and their progression to tumors can be tracked by saturation density in culture**. *BioEssays*, 33(3), pp.224–231.

Santos, N.F, 2014. **Relação entre o estresse oxidativo fotoinduzido e morte celular autofágica**. Dissertação de Mestrado - Programa de Pós-graduação em Ciências Biológicas (Bioquímica) - IQ-USP, São Paulo, 100p.

Santos, F.S. et al., 2011. **Synthesis, characterization, and spectroscopic investigation of benzoxazole conjugated Schiff bases**. *J Phys Chem A*, 115(46), pp.13390–13398.

Schieke, S.M., Schroeder, P. & Krutmann, J., 2003. **Cutaneous effects of infrared radiation: from clinical observations to molecular response mechanisms**. *Photodermatol Photoimmunol Photomed*, 19(5), pp.228–234.

Schraermeyer, U. & Heimann, K., 1999. **Current understanding on the role of retinal pigment epithelium and its pigmentation**. *Pigment Cell Res*. 12(4), pp.219–236.

Schuch, A.P. et al., 2009. **Development of a DNA-dosimeter system for monitoring the effects of solar-ultraviolet radiation**. *Photochem. Photobiol. Sci.*, 8(1), pp.111–120.

Schweitzer, D., Hammer, M. & Schweitzer, F., 2005. **Limits of the confocal laser-scanning technique in measurements of time-resolved autofluorescence of the eye-ground**. *Biomed Tech (Berl)*, 50(9), pp.263–267.

Serrano-Puebla, A. & Boya, P., 2016. **Lysosomal membrane permeabilization in cell death: new evidence and implications for health and disease**. *Ann N Y Acad Sci*, 1371(1):30-44.

Setlow, R.B. et al., 1993. **Wavelengths effective in induction of malignant melanoma**. *Proc Natl Acad Sci USA*, 90(14), pp.6666–70.

Shamsi, F.A. & Boulton, M., 2001. **Inhibition of RPE lysosomal and antioxidant activity by the age pigment lipofuscin**. *Invest Ophthalmol Vis Sci*, 42(12), pp.3041–3046.

Shrestha, T.B. et al., 2012. **Stem cell-based photodynamic therapy**. *Photochem. Photobiol. Sci.*, 11(7), p.1251.

Sies, H. & Menck, C.F.M.C., 1992. **Singlet oxygen induced DNA damage**. *Mutat Res DNAging*, 275(3–6), pp.367–375.

Sitte, N. et al., 2001. **Lipofuscin accumulation in proliferating fibroblasts in vitro: An indicator of oxidative stress**. *Exp Gerontol*, 36(3), pp.475–486.

Skoczyńska, A. et al., 2017. **Melanin and lipofuscin as hallmarks of skin aging**. *Postepy Dermatol Alergol*, 34(2), pp.97–103.

Sonnenschein, C. & Soto, A.M., 2013. **The aging of the 2000 and 2011 Hallmarks of Cancer reviews: A critique**. *J Biosci*, 38(3), pp.651–663.

Sonnenschein, C. & Soto, A.M., 2011. **The death of the cancer cell**. *Cancer Res*, 71(13), pp.4334–4337.

Sørensen, F.B., 1996. **Quantitative analysis of nuclear size for prognosis-related malignancy grading**. *Adv Oncobiol*, Chapter 11,1, pp.221–255.

Soroka, Y. et al., 2008. **Aged keratinocyte phenotyping: Morphology, biochemical markers and effects of Dead Sea minerals**. *Exp Gerontol*, 43(10), pp.947–957.

Sparrow, J.R. & Boulton, M., 2005. **RPE lipofuscin and its role in retinal pathobiology**. *Exp Eye Res*, 80(5), pp.595–606.

Stamatas, G.N. et al., 2004. **Non-Invasive Measurements of Skin Pigmentation**. *Pigment Cell Res*, 17(6), pp.618–626.

Steenken, S. & Jovanovic, S. V., 1997. **How easily oxidizable is DNA? One-electron reduction potentials of adenosine and guanosine radicals in aqueous solution**. *JACS*, 119(3), pp.617–618.

Stepanenko, A.A. & Kavsan, V.M., 2012. **Immortalization and malignant transformation of Eukaryotic cells**. *Tsitol Genet*, 46(2), pp.96–129.

Steven, A.C. et al., 1990. **Biosynthetic pathways of filaggrin and loricrin-two major proteins expressed by terminally differentiated epidermal keratinocytes**. *J Struct Biol*, 104(1–3), pp.150–162.

Suzuki, T. & Kamiya, H., 2017. **Mutations induced by 8-hydroxyguanine (8-oxo-7,8-dihydroguanine), a representative oxidized base, in mammalian cells**. *Genes Environ*, 39(2).

Terman, A. et al., 2010. **Mitochondrial Turnover and Aging of Long-Lived Postmitotic Cells: The Mitochondrial–Lysosomal Axis Theory of Aging**. *Antioxid Redox Signal*, 12(4), pp.503–535.

Terman, A., Abrahamsson, N. & Brunk, U.T., 1999. **Ceroid/Lipofuscin-loaded human fibroblasts show increased susceptibility to oxidative stress**. *Exp Gerontol*, 34(6), pp.755–770.

Terman, A., Gustafsson, B. & Brunk, U.T., 2006a. **Mitochondrial damage and intralysosomal degradation in cellular aging**. *Mol Aspects Med*, 27(5–6), pp.471–482.

Terman, A., Gustafsson, B. & Brunk, U.T., 2006b. **The lysosomal-mitochondrial axis theory of postmitotic aging and cell death**. *Chem Biol Interact*, 163(1–2), pp.29–37.

Thacher, T.D., Fischer, P.R. & Pettifor, J.M., 2014. **Vitamin D treatment in calcium-deficiency rickets: a randomised controlled trial**. *Archives of disease in childhood*, 99(9), pp.807–11.

Tonolli, P.N., et al., 2017. **Lipofuscin Generated by UVA Turns Keratinocytes Photosensitive to Visible Light**. *J Invest Dermatol*, 137(11), pp.2447–2450.

Trautmann, Susanne Buschmann, V., 2013. **Fluorescence Lifetime Imaging (FLIM) in Confocal Microscopy Applications: An Overview**. *Picoquant*, pp.1–14.

Tsubone, T.M. et al., 2017. **Enhanced efficiency of cell death by lysosome-specific photodamage**. *Sci Rep*, 7(1), pp.6734.

Tubbs, A. & Nussenzweig, A., 2017. **Endogenous DNA Damage as a Source of Genomic Instability in Cancer**. *Cell*, 168(4), pp.644–656.

Turrens, J.F. & Boveris, A., 1980. **Generation of superoxide anion by the NADH dehydrogenase of bovine heart mitochondria**. *Biochem J*, 191(2), pp.421–427.

Vandersee, S. et al., 2015. **Blue-violet light irradiation dose dependently decreases carotenoids in human skin, which indicates the generation of free radicals**. *Oxid Med Cell Longev*, 2015.

Visconti, R. & Grieco, D., 2009. **New insights on oxidative stress in cancer**. *Curr Opin Drug Discov Devel*, 12(2), pp.240–245.

Walker, G.J. et al., 1998. **Virtually 100% of melanoma cell lines harbor alterations at the DNA level within CDKN2A, CDKN2B, or one of their downstream targets**. *Genes Chromosomes Cancer*, 22(2), pp.157–163.

Wang, H. & Joseph, J.A., 1999. **Quantifying cellular oxidative stress by dichlorofluorescein assay using microplate reader**. *Free Radic Biol Med*, 27(5–6), pp.612–616.

Wang, S. et al., 2013. **Mitochondrial DNA mutations in diabetes mellitus patients in Chinese Han population**. *Gene*, 531(2), pp.472–475.

Watanabe, I. & Yamada, E., 1983. **The fine structure of lamellated nerve endings found in the rat gingiva**. *Arch Histol Jap. Nippon soshikigaku kiroku*, 46(2), pp.173–182.

Weinstabl, A. et al., 2011. **Prospective randomized study on the efficacy of blue light in the treatment of psoriasis vulgaris**. *Dermatol*, 223(3), pp.251–259.

Weisiger, R.A. & Fridovich, I., 1973. **Superoxide dismutase. Organelle specificity**. *J Biol Chem*, 248(10), pp.3582–3592.

Wheeland, R.G. & Dhawan, S., 2011. **Evaluation of self-treatment of mild-to-moderate facial acne with a blue light treatment system**. *J Drugs Dermatol*, 10(6), pp.596–602.

Wolffe, A.P., 2001. **Chromatin remodeling: Why it is important in cancer**. *Oncogene*, 20(24 Rev. ISS. 3), pp.2988–2990.

Wondrak, G.T., Jacobson, M.K. & Jacobson, E.L., 2006. **Endogenous UVA-photosensitizers: mediators of skin photodamage and novel targets for skin photoprotection**. *Photochem. Photobiol. Sci.*, 5(2), pp.215–237.

Wong, R.S.Y., 2011. **Apoptosis in cancer: from pathogenesis to treatment**. *J Exp Clin Cancer Res*, 30(1), p.87.

Wood, S.R. et al., 2006. **UV causation of melanoma in Xiphophorus is dominated by melanin photosensitized oxidant production**. *Proc Natl Acad Sci USA*, 103(11), pp.4111–4115.

Xiao, B. et al., 2016. **Flow Cytometry-Based Assessment of Mitophagy Using MitoTracker**. *Front Cell Neurosci*, 10:76.

Yakovleva, M.A. et al., 2017. **Estimation of fluorescence lifetime of lipofuscin fluorophores contained in lipofuscin granules of retinal pigment epithelium of human cadaver eyes without signs of pathology**. *Dokl Biochem Biophys*, 472(1), pp.19–22.

Yin, D., 1996. **Biochemical basis of lipofuscin, ceroid, and age pigment-like fluorophores**. *Free Radic Biol Med*, 21(6), pp.871–888.

Young, A.R. et al., 1998. **Human melanocytes and keratinocytes exposed to UVB or UVA in vivo show comparable levels of thymine dimers**. *J Invest Dermatol*, 111(6), pp.936–940.

Zhang, L. et al., 2009. **Effects of red light emitting diode on apoptosis of HeLa cells and suppression of implanted HeLa cells growth in mice**. *J Radiat Res*, 50(2), pp.109–117.

Zhou, R. et al., 2011. **A role for mitochondria in NLRP3 inflammasome activation**. *Nature*, 469(7329), pp.221–225.

Ziegler, A. et al., 1994. **Sunburn and p53 in the onset of skin cancer**. *Nature*, 372(6508), pp.773–776.

Curriculum Vitae

Personal data

Name: Paulo Newton Tonolli

Birth date and place: March 15th 1989, in São José do Rio Preto, SP, Brazil.

E-mail: paulontonolli@yahoo.com.br

Current occupation: PhD student in Biological Sciences (Biochemistry), Universidade de São Paulo (São Paulo, SP), with scholarship from Conselho Nacional de Desenvolvimento Científico e Tecnológico (CNPq). Advisor: Prof. Dr. Maurício da Silva Baptista.

Education

2004 – Ensino Médio E.E. “Major Juvenal Alvim”, Atibaia, SP, Brazil.

2005-2006 – Ensino Médio Colégio Interativo Atibaia, Atibaia, SP, Brazil.

2007-2010 – Graduation in Biological Sciences in Universidade Federal de São Carlos, Sorocaba, SP, Brazil.

2011-2014 – Master student – Biological Sciences (Biochemistry), Universidade de São Paulo, SP, Brazil. Advisor: Prof. Dr. Nadja C. Souza-Pinto.

Complementary education

2015 – Instrumentação Científica: Citometria de Fluxo, Universidade Federal do ABC, Santo André, Brazil.

2010 – Summer School of Molecular Biophysics, Universidade Estadual Paulista “Júlio de Mesquita Filho” (IBILCE-UNESP), Brazil.

2010 – Oxygen and Redox Processes – Sociedade Brasileira de Bioquímica e Biologia Molecular (SBBq), Foz do Iguaçu, Brazil.

Teaching experience

2018 – Aula “Fotossensibilização de Lipofuscina em Queratinócitos da Pele Humana: Efeitos da Luz Visível na Pele” proferida para alunos do Curso de Pós-Graduação na disciplina *Basic Research Seminar Series II*, Fundação Antônio Prudente, área de Oncologia. A.C. Camargo Cancer Center – Centro Integrado de Diagnóstico, Tratamento, Ensino e Pesquisa – São Paulo, Brazil.

2014 - QBQ0250: Bioquímica: Estrutura de Biomoléculas e Metabolismo. Teaching assistant for the Biochemistry Department, Ciências Biomédicas, USP. Supervisor: Profa. Dra. Flávia Meotti; Profa. Dra. Regina Baldini.

2013 - QBQ0317: Biologia Molecular. Teaching assistant for the Biochemistry Department, Curso de Graduação em Farmácia-Bioquímica, USP. Supervisor: Profa. Dra. Suely Gomes; Prof. Dr. Sergio Verjovski-Almeida.

2013 - QBQ0316: Bioquímica Experimental. Teaching assistant for the Biochemistry Department, Ciências Farmacêuticas e Bioquímica, USP. Supervisor: Profa. Dra. Sayuri Miyamoto; Profa. Dra. Ohara Augusto.

2013 - Organizing and teacher in *Summer School of Biochemistry and Molecular Biology*, in Department of Biochemistry, IQ-USP. Supervisors: Prof. Dr. Fábio Forti; Profa. Dra. Letícia Labriola; Profa. Dra. Nadja C. Souza-Pinto.

2012 - QBQ0215: Bioquímica: Estrutura de Biomoléculas e Metabolismo. Graduate teaching assistant for the Biochemistry Department, Curso de Graduação em Farmácia-Bioquímica, USP. Supervisor: Prof. Dr. Bayardo Baptista Torres; Profa. Dra. Clélia Ferreira; Profa. Dra. Iolanda Cuccovia.

Research experience

2008 Internship in the Laboratório de Biologia Estrutural e Funcional, under supervision of Prof. Dr. Fábio Camargo Abdalla, Universidade Federal de São Carlos, Sorocaba, Brazil.

2008-2010 Scientific Initiation – Project: **"**Origem anatômica e bioquímica da bioluminescência em larvas de Elateroidea: expressão de luciferina-luciferase". Laboratório de Bioquímica e Biotecnologia de Sistemas Bioluminescentes. Advisor: Prof. Dr. Vadim Viviani.

2011-2014 Master Degree. Project: "O Papel do Fator de Transcrição Mitocondrial A na Proteção do DNA Mitocondrial Contra Lesões Oxidativas". Laboratório de Genética Mitocôndria. Advisor: Prof. Dr. Nadja C. Souza Pinto.

PhD Degree, Laboratório de Processos Fotoinduzidos e Interfaces. Project: "Photosensitization of Lipofuscin in Skin Keratinocytes: Effect of Visible Light on Human Skin". Advisor: Prof. Dr. Maurício da Silva Baptista.

Scholarships

2009-2010 Fundação de Amparo à Pesquisa do Estado de São Paulo (FAPESP) – Process number: 2009/06645-8.

2011 Conselho Nacional de Desenvolvimento Científico e Tecnológico (CNPq)

2011-2013 Fundação de Amparo à Pesquisa do Estado de São Paulo (FAPESP) – Process number: 2011/16188-3

2014-2018 Conselho Nacional de Desenvolvimento Científico e Tecnológico (CNPq)

Awards

2018 - Travel Award of Institute of Chemistry, Universidade de São Paulo

2017 - Best Poster at the European Society for Photobiology Congress, Royal Society of Chemistry

Publications

TONOLLI, P.N.; CHIARELLI-NETO, O.; SANTACRUZ-PEREZ, C.; JUNQUEIRA, H.C.; WATANABE, I.S.; RAVAGNANI, F.G; MARTINS, W.K.; BAPTISTA, M.S. *Lipofuscin Generated by UVA Turns Keratinocytes Photosensitive to Visible Light*. Journal of Investigative Dermatology, v. 137, p. 2447-2450, 2017.

TONOLLI, P.N.; OKAWACHI, F.M.; ABDALLA, F.C.; VIVIANI, V.R. *Bioluminescent Fat Body of Larval A. lineatum (Coleoptera: Lampyridae) Firefly: Ontogenic Precursor of Lantern's Photogenic Tissue*. Ann. Entomol. Soc. Am., v.104, p.761-7, 2011.

Work presentations in conferences (2014-2018)

Oral presentation

TONOLLI, P.N.; CHIARELLI NETO, O.; SANTACRUZ-PEREZ, C.; JUNQUEIRA, H.C.; WATANABE, I.S.; SEVERINO, D.; MARTINS, W.K.; BAPTISTA, M.S*. Lipofuscin accumulates in skin cells turning keratinocytes photosensitive to visible light.* 39th American Society for Photobiology Biennal Meeting, Tampa, Florida, USA. 2018.

TONOLLI, P.N.; CHIARELLI NETO, O.; SANTACRUZ-PEREZ, C.; JUNQUEIRA, H.C.; WATANABE, I.; SEVERINO, D.; MARTINS, W..; BAPTISTA, M.S*. Fotossensibilização de queratinócitos da pele humana por luz visível e transformação maligna.* Seminários dos Pós-Graduandos e Pós-Doutorandos do Departamento de Bioquímica, IQ-USP. 2018.

TONOLLI, P.N.; CHIARELLI NETO, O.; SANTACRUZ-PEREZ, C.; JUNQUEIRA, H.C.; WATANABE, I.; SEVERINO, D.; MARTINS, W..; BAPTISTA, M.S*. O Lado Escuro da Luz Visível*. Palestra conferida aos alunos do Curso de Graduação em Biomedicina da Universidade Santo Amaro (UNISA), São Paulo, 2017.

TONOLLI, P.N.; MARTINS, W.K.; SEVERINO, D.; SANTACRUZ-PEREZ, C.; WATANABE, I.S.; BAPTISTA, M.S. *Visible-light photosensitization of lipofuscin in human keratinocytes: can visible light be mutagenic to human skin cells?* 5th Human Biology Symposium, Tsukuba Global Science Week, Tsukuba, Japan. 2016.

Poster

TONOLLI, P. N.; CHIARELLI NETO, O.; SANTACRUZ-PEREZ, C.; JUNQUEIRA, H.C.; WATANABE, I.S.; RAVAGNANI, F.G.; MARTINS, W.K.; BAPTISTA, M.S. *Human skin keratinocytes exposed to UVA turn photosensitive to visible light*. 17th European Society for Photobiology Congress (Pisa, Italy). 2017.

TONOLLI, P.N.; MARTINS, W.K.; SEVERINO, D.; SANTACRUZ-PEREZ, C.; WATANABE, I.S.; BAPTISTA, M.S. XLV Annual Meeting of Brazilian Society for Biochemistry and Molecular Biology (Natal, RN). Photosensitization of Lipofuscin from Human Skin Keratinocytes by Visible Light and Malignant Transformation. 2016.

GOUVEA, A.F.; **TONOLLI, P.N.**; FRANCO, F. *The historical construction of enzymes concept and its use in the biology teaching*. In: International Society for History, Philosophy, Social Studies of Biology, São Paulo. International Society for History, Philosophy, Social Studies of Biology, 2017.

TONOLLI, P.N.; MARTINS, W.K.; SEVERINO, D.; SANTACRUZ-PEREZ, C.; WATANABE, I.S.; BAPTISTA, M.S. Photosensitization of Lipofuscin from Human Skin Keratinocytes by Visible Light and Malignant Transformation. II Reunião Anual do CEPID-Redoxoma (São Paulo, SP). 2016.